AN ENERGY DISPERSIVE METHOD FOR RESONANCE NEUTRON CAPTURE GAMMA RAY SPECTROSCOPY

AN ENERGY DISPERSIVE METHOD FOR RESONANCE NEUTRON CAPTURE GAMMA RAY SPECTROSCOPY

by

Vincent J. Thomson

A Thesis

Submitted to the Faculty of Graduate Studies

in Partial Fulfilment of the Requirements

for the Degree

Doctor of Philosophy

McMaster University

October, 1975

DOCTOR OF PHILOSOPHY (1975)
(Physics)

McMASTER UNIVERSITY
Hamilton, Ontario

TITLE: An Energy Dispersive Method for Resonance Neutron Capture Gamma Ray Spectroscopy

AUTHOR: Vincent J. Thomson, B.Sc. (University of Windsor)

SUPERVISOR: Professor T.J. Kennett

NUMBER OF PAGES: x, 93

ABSTRACT:

A method for the determination of partial radiation cross sections based on the energy dispersion of the capture process was undertaken. A description of the experimental reactor facility and details of the method has been presented. Measurements of gamma rays following neutron capture in isotopes of silicon, chromium and nickel revealed resonances which were analyzed for resonance parameters. The characteristics of the resonance decay properties for the different isotopes were discussed.

ACKNOWLEDGEMENTS

I wish to express my appreciation to my Research Director, Dr. T.J. Kennett, for his advice and assistance. His insight and direction during my research at McMaster have resulted in a valuable educational experience. I am also indebted to Dr. W.V. Prestwich for his interest and aid in the pursuit of this research project. Numerous members of the research group at the McMaster Reactor have provided assistance and support at various times during the course of this work.

I am grateful to Mr. John McDougall, Mr. Peter Ernst and the other members of the Reactor staff for their help and cooperation, and to Mrs. Dorothy Matthews for her efficiency in preparing this manuscript.

A special word of thanks to my wife, Claudia, and my family for their support during my work at McMaster University.

This work has been financially supported by the National Research Council and the Provincial Government of Ontario.

TABLE OF CONTENTS

SUMMARY OF TABLES

A LIST OF FIGURES

CHAPTER 1

INTRODUCTION

In 1911 Marsden, Geiger and Rutherford discovered that an atom was composed of electrons orbiting about a small positively charged nucleus in which almost all the atomic mass was concentrated (Ru 11). From that time onwards there has been an intense interest in understanding the strong forces displayed within the nucleus and the properties resulting from its complex structure.

Nuclear properties have been difficult to observe because of the size of the nucleus; consequently, experiments designed to investigate such properties use projectiles of approximately nuclear dimensions to interact with the nucleus. Experiments involving scattering, stripping, pick up and capture have produced data which have helped in forming theories about nuclear forces and have provided understanding of some properties of nuclear structure.

Most frequently particles projected at nuclei are charged, since control of energy is readily achieved, but they do experience Coulomb repulsion. Reaction rates are therefore often inhibited by the requirement that the projectiles be sufficiently energetic to overcome the Coulomb barrier. The use of the uncharged neutron as a projectile has the

advantage that significant reaction rates can occur even at low bombardment energies.

NEUTRON REACTIONS

A typical reaction may be represented by A(a,b)B, where the target nucleus is represented by A, the residual nucleus by B, the incident particle by a and the emitted particle by b. When, for example, a neutron is captured it results in a highly excited nucleus which then deexcites by emission of gamma radiation or another particle such as a neutron or proton. When the emitted particle is a neutron elastic scattering may occur, in which instance the residual nucleus is left in the same state as the original target.

For neutron reactions one can write

$$M_A + m_n + T_n \rightarrow (\text{Intermediate Nucleus}) \rightleftharpoons \begin{matrix} M_{A+1}+E_x \\ M_B+m_b+T_b \end{matrix} \qquad 1\cdot1$$

where M_A, m_n, M_{A+1}, M_B respectively represent the masses of the target nucleus, the incident neutron, the residual nucleus following radiative deexcitation and the residual nucleus formed when a particle with mass m_b is emitted. For elastic scattering m_b is equivalent to m_n. If one neglects nuclear recoil, the kinetic energy of the incident neutron and the emitted particle are given as T_n and T_b respectively, while E_x stands for the excitation energy

given off in the form of gamma radiation. For a radiative transition, the neutron separation energy is given by

$$Q_n = M_A + m_n - M_{A+1}$$

which, from equation 1.1, leads to

$$E_x = Q_n + T_n .$$

Radiative decay may involve the emission of a single gamma ray of energy E_x or a cascade of gamma rays whose summed energy is E_x.

For a particular reaction induced by a flux of incident particles a cross section can be defined as

$$\sigma = \frac{\text{no. of particular events per unit time per nucleus}}{\text{no. of incident particles per unit area per unit time}} .$$

Quantitatively it is the effective area which a nucleus presents to an incoming particle. Early measurements revealed that when the total neutron capture cross section is examined, as a function of neutron energy, structure is observed (Mo 36, Ra 36). In the low energy region this takes the form of narrow peaks at definite, but non-uniformly spaced energies. These maxima are called resonances and correspond to unbound neutron states.

The widths and spacings of resonances vary greatly from nucleus to nucleus. However, for nuclei of medium mass ($A \sim 50$) resonance widths are generally the order of electron volts to a few keV and the spacings are several keV. In

more massive nuclei the spacings are substantially smaller being the order of a few eV. In general, the number of resonances per unit energy increases with mass number and excitation energy.

For a given nuclide resonance widths tend to increase with neutron energy. At low energy the resonance width Γ is usually less than the level spacing D but, with increasing energy, widths become comparable to spacings. At very high energies widths become greater than spacings and so overlapping occurs. In this continuum region the fine structure of the resonances cannot be observed. This effect of resonance broadening can be expected since the penetrability increases with energy above the barrier of a potential.

REACTOR NEUTRONS

The present study makes use of a nuclear reactor as a neutron source and consequently knowledge of the associated neutron spectrum is necessary if the method used is to be understood and evaluated. Neutrons produced in the fission reaction initially have an evaporation spectrum given analytically (Wa 52) by

$$N(E) = 0.484\, e^{-E} \sinh \sqrt{2E} \,. \qquad 1\cdot2$$

This spectrum has a most probable energy of 500 keV and an average energy of 1·5 MeV.

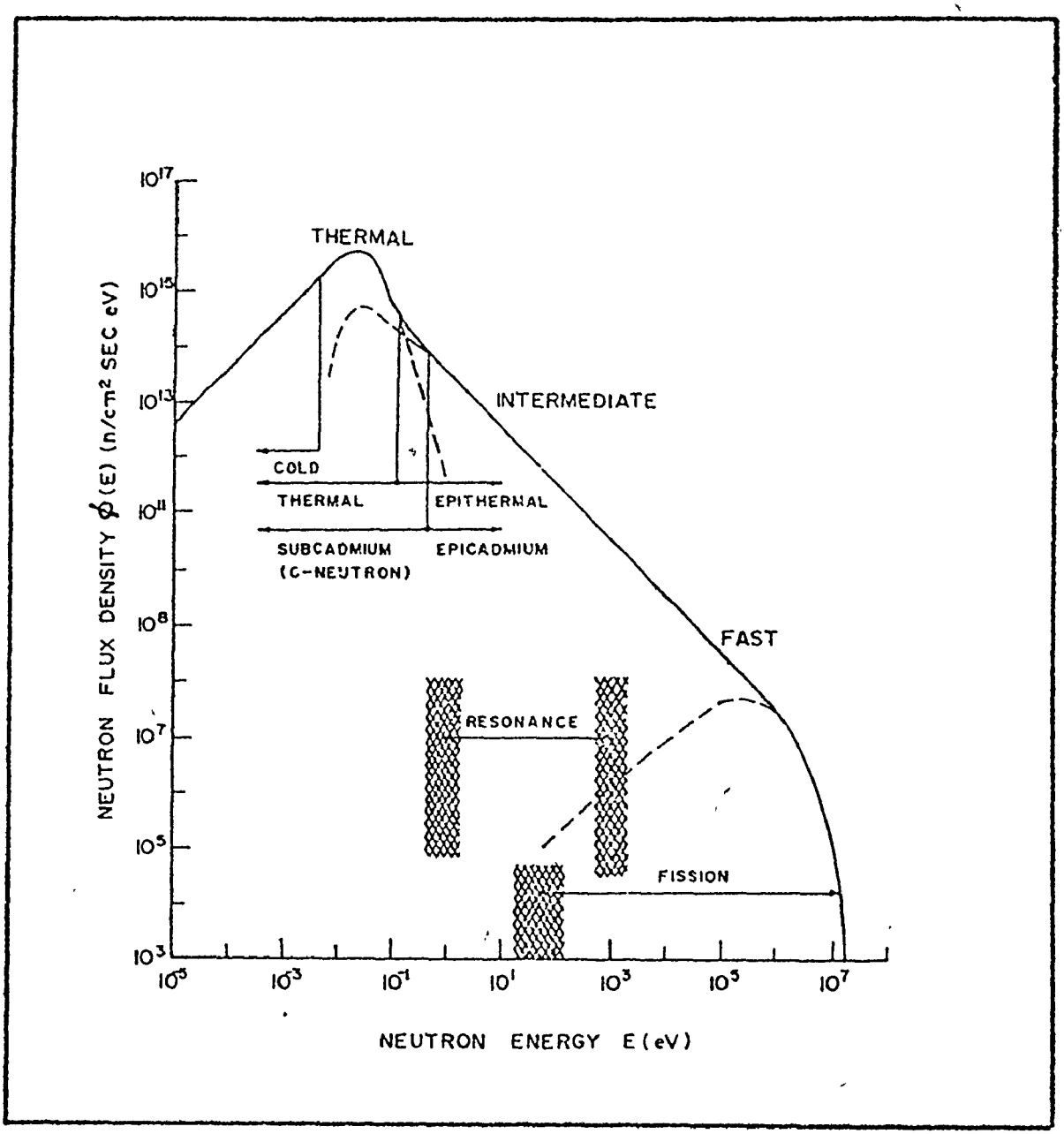

Figure 1.1 Neutron spectrum from a water moderated nuclear reactor.

These neutrons undergo elastic collisions with the moderator and are slowed down until they reach thermal equilibrium with the moderator. A typical reactor neutron spectrum is shown in figure 1·1 (IA 70a). For convenience the spectrum is divided into three regions, viz. thermal, intermediate and fast. Thermal neutrons are those in thermal equilibrium with the moderator; intermediate or resonance neutrons are those which are losing energy while undergoing collisions with the moderator; fast neutrons refer to those produced immediately from the fission process. In figure 1·1 these regions respectively are the large contribution at low energy, the straight line mid-energy region and the high energy region shown by a dotted curve. In a typical nuclear reactor neutrons are present which have energies from a fraction of a meV to 14 MeV.

NEUTRON RADIATIVE CAPTURE

Neutron capture gamma radiation was first detected by Lea in 1934 (Le 34). Little information was added in the next 15 years except for some maximum energy determinations. In the early 1950's Kinsey and Bartholomew at Chalk River (Ki 53) contributed greatly to our knowledge of the capture process through the use of a magnetic pair spectrometer. A little later in 1955 Groshev (Gr 56) developed a high resolution Compton spectrometer and greatly expanded radiative capture

studies. Also about this time a considerable amount of study, particularly of time correlation, was conducted with NaI(Tℓ) scintillation spectrometers (Re 54, Se 58). Until 1957 detailed spectra were obtained only for thermal neutron capture and, while measurement of total radiative yield was conducted for a wide range of neutron energies, no information regarding decay modes of particular resonances was obtained. Two reasons for this were that the thermal neutron flux available for irradiations from research reactors far exceeded that provided by fast neutron sources within the narrow energy region necessary for isolated resonance study, and that the average capture cross section decreases with increasing energy while competing elastic and inelastic scattering cross sections increase.

In 1957 Landon and Rae (La 57) used a linear accelerator to produce a pulsed neutron source with which they studied the high energy gamma ray spectrum from neutron capture in the 34 eV resonance in ^{199}Hg. Following closely upon this work detailed study of the spectra arising from resonance capture was undertaken through the use of fast choppers at nuclear reactor sites (Fo 58, Ke 58). This work revealed a wide variation in the spectra associated with each resonance in accord with the fluctuations observed for single channel scattering (Ha 55, Po 56). Targets for such studies were generally limited to medium or high

atomic number in order that several resonances occurred below ∿ 2 keV. Such nuclei have correspondingly high level density and complex spectra which are not amenable to scintillation spectroscopy. This limitation was obviated with the development of the Ge(Li) spectrometer by Ewan and Tavendale (1964). Since that time very active study of the resonance capture process has been conducted at the Brookhaven high flux reactor by Chrien and coworkers (Ch 67) who employ a fast chopper and Kane and coworkers (IA 69) who employ a neutron diffraction spectrometer. The work of these investigators did not include many nuclides of lower atomic weight because of low resonance density. To date this mass region has been mainly explored through the use of pulsed linear accelerators from which suitable neutron spectra can be produced.

The feasibility of capture measurements with neutrons in the energy range 10-300 keV was first demonstrated in 1960 with NaI detectors and neutrons from pulsed Van de Graaf accelerators (Be 61). These experiments led to two programs: one in Sweden where the shape of gamma ray spectra for various neutron energies was investigated and the other at Oak Ridge, Tenn. where gamma ray intensities for capture of 10 to 100 keV neutrons were studied (ND 73). More recent measurements gave gamma ray intensities for resolved

resonances in 2s - 1d shell nuclei (Lu 70). With the advent of Ge(Li) detectors, measurements at Lucas Heights, Australia, have produced much more detailed results (Al 69). All the previous mentioned keV capture measurements have used time of flight techniques to select the neutron energy of interest. Normally, two parameter investigations are conducted and digital windows used following the experiment to sort the regions of interest. When a Ge(Li) detector is used, the shift in energy of primary gamma rays with neutron energy can be observed particularly when the resonance spacing is large. (ND 73)

The Australian data has been the most detailed to date for elements with complex resonance capture cross sections in the keV region. However, it is limited because of the complex response of the Ge(Li) to high energy photons, the poor resolution of the Ge(Li) detectors used ($\geq$ 20 keV) and the large spread in neutron energies as a result of short flight paths ($\sim$ 30 keV).

THE PRESENT EXPERIMENT

As just pointed out keV neutron capture experiments have mainly been performed using pulsed accelerators and a time of flight arrangement. Gamma ray spectra are obtained as a function of time of flight which is subsequently translated into neutron energy. This technique is effective

for widely spaced resonances, in that, precise knowledge of neutron energies defines a specific capture state. The spectra of emitted gamma rays corresponding to this capture state can be measured and this leads to values of partial radiation widths, the probabilities of gamma ray decay from the capture state to particular final states, and of the total radiation width, the probability of gamma decay to all final states. However, in most cases time of flight energy resolution is greater than resonance separations with the result that measurements are obtained for an average over many resonances. The present technique allows the spectral dispersion of gamma rays to be that inherent in the capture process and the resolution of gamma ray peaks to be that of the detector.

The method presented here is based on the direct observation of neutron kinetic energy as an energy shift of primary photons emitted following capture (Th 75a). The capture process is dispersive as indicated in figure 1·2 where aspects of the technique are presented. Here an isotope is shown to undergo the reaction $^{A}_{Z}(n,\gamma)^{A+1}_{Z}$ absorbing neutrons of resonance energies E_{R1} and E_{R2} and yielding radiative emission to the ground state and an excited state E_1. Also in figure 1·2 diagrams of the neutron capture cross section of the isotope, with its two resonances, and a

Figure 1.2

This figure illustrates the salient features of the energy dispersive method. At the top right, two states at neutron energy E_{R1} and E_{R2} are shown as part of a decay scheme. Adjacent to these is shown the neutron cross section, the transmitted neutron spectrum and the expected reaction rate as functions of incident neutron energy. Below these graphs is depicted the gamma ray spectrum arising from the decay of the resonance states to the ground and first excited state. The resonance E_{R2} is indicated to have a significant breadth which in turn leads to noticeable width increase of the corresponding radiative transition in the gamma ray spectrum.

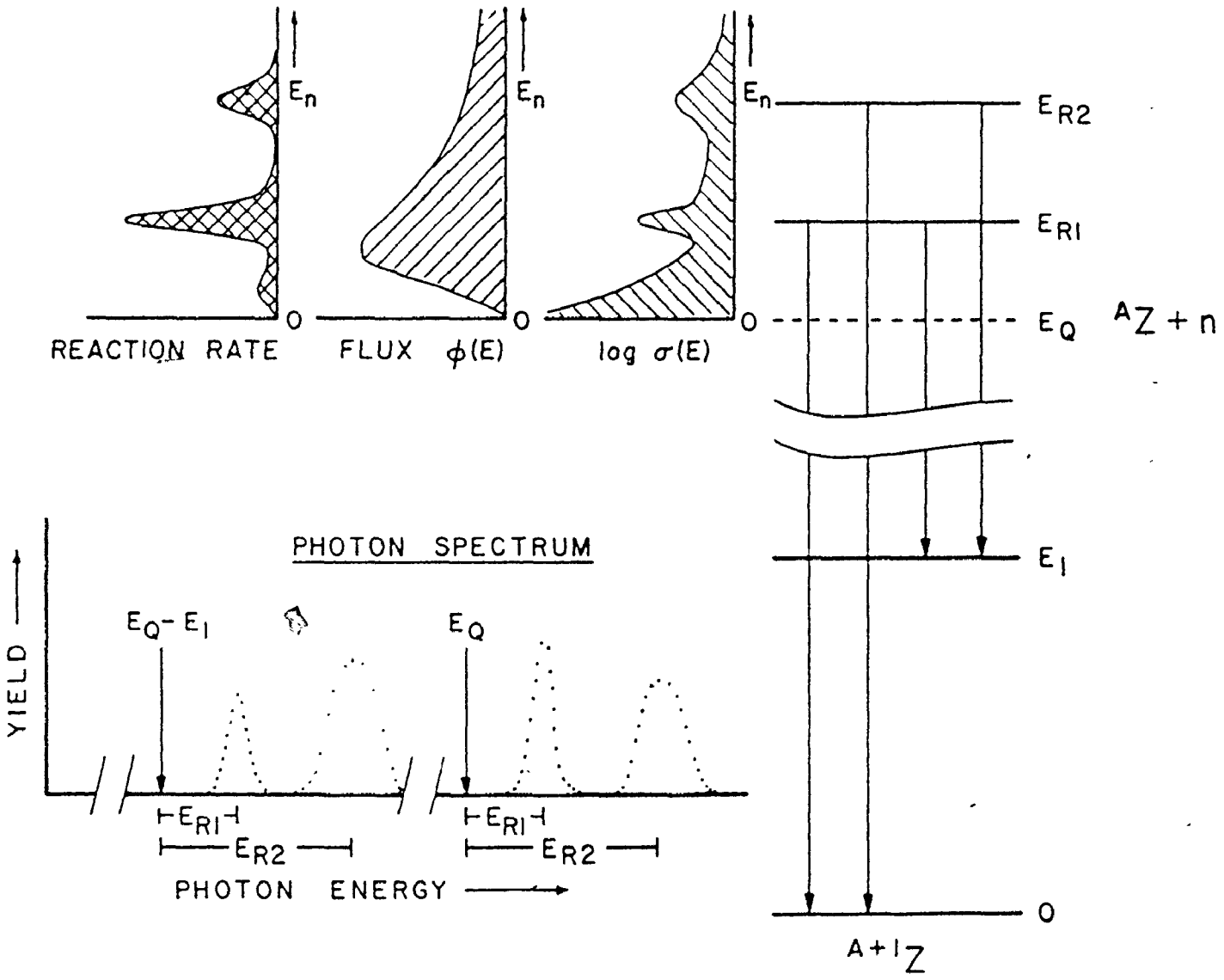
E_n
0
REACTION RATE
FLUX $\phi(E)$
log $\sigma(E)$
E_{R2}
E_{R1}
E_Q
$^{A}Z + n$
E_1
0
^{A+1}Z
PHOTON SPECTRUM
YIELD
$E_Q - E_1$
E_Q
E_{R1}
E_{R2}
PHOTON ENERGY

neutron flux distribution are shown as a function of neutron energy. In addition a graph of reaction rate versus neutron energy, obtained as the product of the cross section and neutron flux distribution, is shown. The result of this reaction rate is the emission of a spectrum of photons, such that, gamma ray peaks are detectable at energies $E_Q + E_{R1}$, $E_Q + E_{R2}$ and $(E_Q - E_1) + E_{R1}$, $(E_Q - E_1) + E_{R2}$. The photon spectra above energies E_Q and $E_Q - E_1$ mirror the reaction rate but are governed by the probabilities of each energy state E_{R1} and E_{R2} decaying to the energy levels 0 and E_1.

The use of a typical nuclear reactor spectrum of neutrons to illuminate targets (figure 1·1) would result in a high reaction rate from thermal neutrons and consequently dominant peaks, at the unshifted energies, orders of magnitude greater in intensity than those arising from neutron resonance capture in the keV energy range. The region immediately above such a large peak is always distorted by pulse pile up effects resulting in interference with the resonance capture components. Thus it is essential to reduce the contribution from thermal neutrons by reshaping the neutron spectrum through the use of a filter (Bo 70, Lo 73). Several filters capable of high neutron absorption at low energies would be suitable but some have an absorption 'cut off' at such a low

energy as to transmit a substantial portion of the thermal contribution in the reactor spectrum. A filter with a $1/\sqrt{E}$ cross section and no positive energy resonances in the region below 200 keV has suitable characteristics. A filter composed of ^{10}B was found to be ideal for the current investigation.

An example of the reshaped neutron distribution is shown in figure 1·3 (dotted line) as well as a typical reactor neutron spectrum (solid line). The neutron spectrum shown in figure 1·2 is that observed within a ^{10}B filter. If a large thermal contribution were present in the neutron spectrum, large photon peaks would be observable at energies E_Q and $E_Q - E_1$ in the photon spectrum. The reaction diagram in the same figure shows little thermal contribution and thus little or no contribution is observable in the photon spectrum.

In the present work samples were irradiated with a ^{10}B shaped spectrum of reactor neutrons and capture gamma ray spectra were acquired through use of a Ge(Li) diode device. Spectral peaks attributable to resonance capture gamma rays were readily discernible due to the energy dispersion of the capture process. Spectra were then analyzed for resonance parameters.

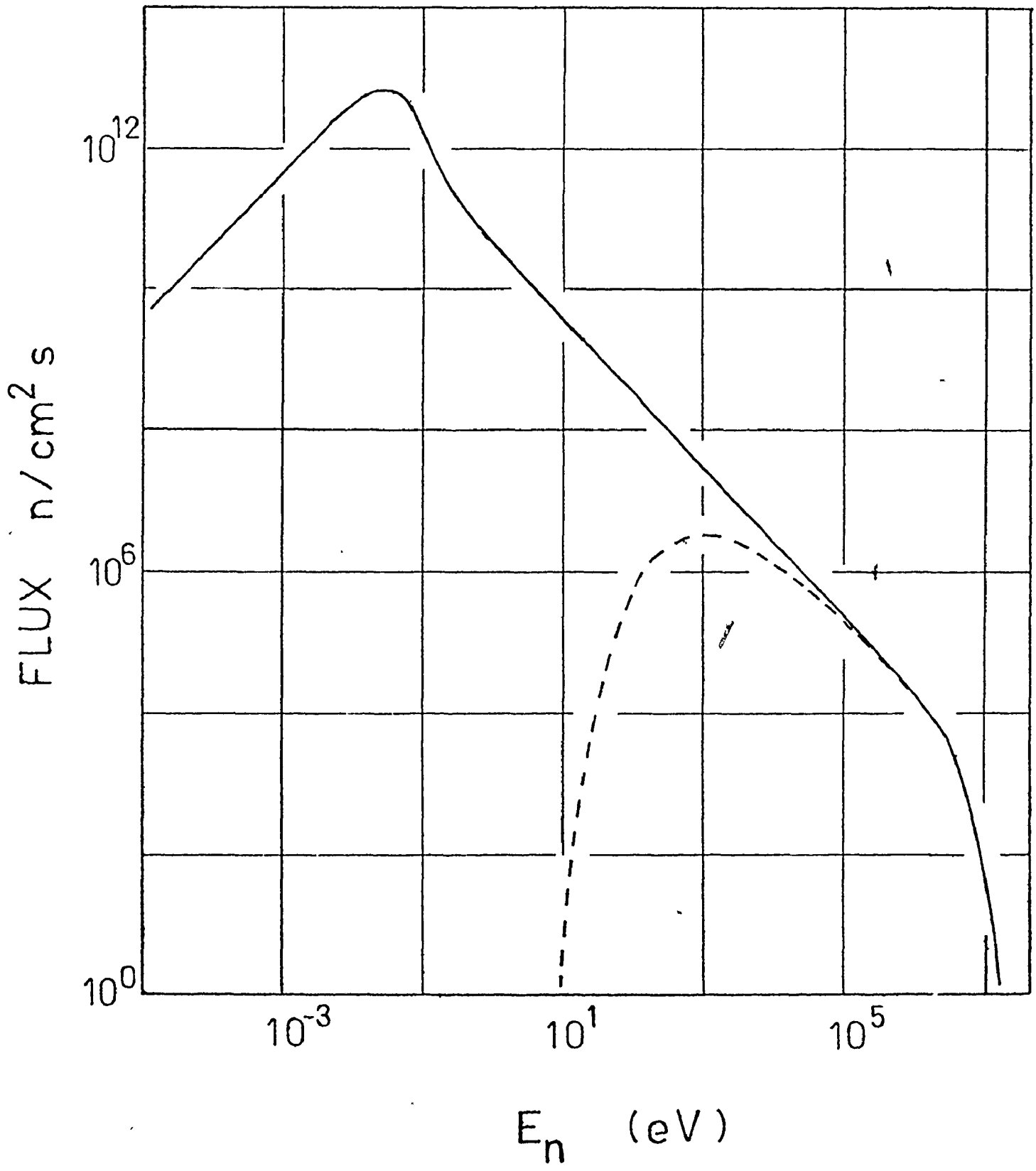

Figure 1.3 The solid curve indicates the nature of the neutron flux characteristic of a nuclear reactor. The dashed curve shows the flux within a 1·2gm/cm^2 ^{10}B shield.

CHAPTER 2

NEUTRON REACTIONS

The present experiment is designed to measure partial radiation widths of gamma transitions in various nuclei. By this we mean the probability of radiative emission to a certain final state after neutron capture into an initial state. This is done through examination of keV neutron capture gamma ray spectra. In order to analyze these spectra for resonance parameters, several factors in the neutron capture process must be examined. These include: the neutron flux distribution impingent upon the target nuclei, capture cross section parameters, the neutron interaction and deexcitation processes and the properties of radiation widths.

THE $^{1}/_{E}$ NEUTRON DISTRIBUTION

As previously mentioned neutrons produced in the fission process are slowed down through collision with the moderator until they reach thermal equilibrium. The fission neutron distribution, which represents the primary source of neutrons, was described previously and is given by equation 1·2. The intermediate or resonance region of the reactor neutron spectrum is the component used in the current study.

The general form of this component can be derived by considering the case in which high energy neutrons are scattered by the moderator, specifically hydrogen, and neutron absorption is negligible. The collision density C(E) can be determined by considering the scattering of neutrons into and out of an energy interval dE at energy E. Neutrons arrive in dE as a result of scattering collisions that occur at higher energies. Since a collision can drop the energy of a neutron to a lower value, some of the source neutrons may acquire an energy in dE as the result of only one collision. Neutrons that have had one or more collisions but whose energy E' is still above E may also fall into dE with their next collision.

Consider first the source neutrons. In the steady state if S of these neutrons are produced per cm^3/sec, exactly this number of neutrons must be scattered per cm^3/sec at this energy. If this were not so, there would be an accumulation of neutrons at E_o. The probability that one of these neutrons will be scattered into dE is dE/E_o. It follows that a total of SdE/E_o source neutrons are scattered directly into dE per cm^3/sec.

Turning to the neutrons having energies between E and E_o, there are, by definition, C(E')dE' scattering collisions per cm^3/sec in the energy interval dE' at E'.

The probability that one of these neutrons is scattered into dE is dE/E', so that C(E')dE'dE/E' neutrons are scattered per second from dE' to dE. The number of neutrons arriving in dE from all dE' above E is

$$\int_{E}^{E_o} \frac{C(E')\ dE'\ dE}{E'} \quad .$$

Since in the steady state the number of neutrons scattered into dE must be equal to the number scattered out, it follows that

$$C(E)dE = \frac{S\ dE}{E_o} + \int_{E}^{E_o} \frac{C(E')\ dE'\ dE}{E} \quad . \qquad 2\cdot1$$

After cancellation of dE from both sides in equation 2·1, the following integral equation for C(E) is obtained:

$$C(E) = \frac{S}{E_o} + \int_{E}^{E_o} \frac{C(E')\ dE'}{E'} \quad . \qquad 2\cdot2$$

Equation 2·2 can be solved by differentiating both sides of the equation with respect to E. This gives

$$\frac{d\ C(E)}{d\ E} = -\ \frac{C(E)}{E} \quad , \qquad 2\cdot3$$

where the minus sign appears because the variable E occurs in the lower limit of the integral. The general solution of equation 2·3 is

$$C(E) = \frac{K}{E} \quad , \qquad 2\cdot4$$

where K is a constant that must be determined. The value of K can be found by placing $E=E_o$ in equation 2·2; this gives

$$C(E_o) = \frac{S}{E_o} \quad . \qquad 2\cdot5$$

Comparing equations 2·4 and 2·5, it is seen that K = S, so that

$$C(E) = \frac{S}{E} \quad . \qquad 2\cdot6$$

If S neutrons are produced per cm^3/sec throughout a medium and none are absorbed, exactly S neutrons must be slowing down at every energy in a steady state situation. If this were not the case, there would be an accumulation of neutrons somewhere between E=0 and $E=E_o$. (La 66) It follows that

$$S = q(E)$$

where q(E) is the slowing down density, i.e. the number of neutrons slowing down past energy E per cm^3/sec. Then equation 2·6 becomes

$$C(E) = \frac{q(E)}{E} \quad . \qquad 2\cdot7$$

The number of collisions per cm^3/sec at energy E can be expressed as

$$C(E) = \Phi(E)\ \Sigma_s\ (E) \quad , \qquad 2\cdot8$$

where $\Phi(E)$ is the flux density per unit energy interval and $\Sigma_s(E)$ is the macroscopic scattering cross section of the moderator. From equations 2·7 and 2·8 it follows that

$$\phi(E) = \frac{q(E)}{\Sigma_s(E)} \cdot \frac{1}{E} \cdot \qquad 2\cdot9$$

If there is no absorption, $q(E)$ equals the total source density q_o. Provided the scattering cross section is a constant, as is the case over the energy range being considered, then, equation 2·9 becomes

$$\phi(E) = \frac{q_o}{\Sigma_o} \cdot \frac{1}{E}$$

$$= \frac{\text{constant}}{E}$$

$$= \frac{K}{E} \cdot \qquad 2\cdot10$$

The result is the same, i.e. the flux in the intermediate region is proportional to $1/E$, for moderators with mass larger than 1.

While resonances associated with the light water moderator give rise to some structure, it is restricted to the highest energy or fission neutron portion of the spectrum (IA 70b). The slowing down or resonance region is devoid of structure and the neutron flux here is well approximated by an inverse energy dependence.

For those neutrons slowed down further into the thermal region, the flux energy distribution is described

by the Maxwellian

$$\Phi_{th}(E) = E/(kT)^2 \exp(-E/kT) .$$

This is normalized for unit flux area with T the moderator temperature and k the Boltzman constant.

NEUTRON CROSS SECTION

The total cross section σ_T at energy E for an isolated resonance at energy E_R can be written as

$$\sigma_T = \sigma \text{ (resonance)} + \sigma \text{ (interference)} + \sigma \text{ (potential)}$$

$$= \sigma_n + \sigma_\gamma + \sigma \text{ (interference)} + \sigma \text{ (potential)} .$$

The latter equation is composed of, in order, the resonance scattering cross section, the resonance capture cross section, the cross section for interference between resonance and potential scattering, and the potential scattering cross section. If it is assumed that the interaction of the neutron is limited to elastic scattering and radiative capture, one may write the Breit-Wigner formulation of the cross section as

$$\sigma_T = \frac{\pi \lambda\!\!\!^{-2}_R g \Gamma_n^2}{(E-E_R)^2+(\Gamma/2)^2} + \left(\frac{E}{E_R}\right)^{1/2} \frac{\pi \lambda\!\!\!^{-2}_R g \Gamma_n \Gamma_\gamma}{(E-E_R)^2+(\Gamma/2)^2} + \frac{4\pi \lambda\!\!\!^{-2}_R g \Gamma_n R(E-E_R)}{(E-E_R)^2+(\Gamma/2)^2} + 4\pi R^2 \qquad 2.11$$

Here $2\pi\ \lambda\!\!\!^{-}_R$ is the neutron wavelength of resonance energy, Γ is the total probability per unit time interval for the

compound nucleus to emit a photon or a particle, and Γ_n and Γ_γ are the probabilities for the emission of a neutron and a photon respectively. A statistical factor, which is represented by g, may be expressed as

$$g = {}^1/_2 \ (2\ J + 1)/(2\ I + 1) \ ,$$

where J stands for the angular momentum of the compound nucleus and I the angular momentum of the original nucleus. Further R is the radius of a sphere at which scattering is possible but penetration impossible.

The probability amplitude corresponding to the Breit Wigner formula can be derived by taking the Fourier transform of an exponentially decaying state. This decaying state corresponds to the'long-lived' state comprised of the incident neutron and the target nucleus. The lifetime of the quasi-stationary state, which decays by particle or gamma ray emission, is related to the resonance width by means of the uncertainty principle ($\Gamma\tau=h$). A virtual state 1 eV wide would have a mean lifetime $\tau \sim 10^{-15}$sec. This is long compared to the nuclear transit time $\sim 10^{-21}$sec.

When more than one resonance contributes significantly to the cross section, two other interference terms should be examined. The first is the interference between resonances in neutron scattering. This term is small when the resonances are widely separated (Ha 70a). The second is the interference

of resonances decaying to the same final state. The sign of the interference terms fluctuate randomly between resonances and, if a significant number of resonances are included, this term may be neglected. Furthermore, this term is small if the resonances are widely separated (Ha 70b).

When determining relative partial radiation widths, the total cross section is a factor in the calculation. This calculation utilizes only those energy terms close to the resonance energy. Therefore, the σ (interference) term in the total cross section may be neglected since it is only appreciable far from the resonance energy. In addition, the approximation can be made that $\Gamma \sim \Gamma_n$, since $\Gamma_\gamma << \Gamma_n$ for the nuclei to be studied here. Following the above simplifications, the equation for the total cross section reduces to

$$\sigma_T(E) \simeq \frac{\pi \lambda_R^2 g \Gamma_n^2}{(E-E_R)^2+(\Gamma_n/2)^2} + 4\pi R^2 . \qquad 2\cdot12$$

In the case of a nuclear deexcitation by gamma ray emission to a given final state, a neutron of energy E is captured and a gamma ray of energy,

$$E_{\gamma i} = E + (E_Q - E_{xi}) , \qquad 2\cdot13$$

is emitted. Here, E_{xi} is the excitation energy of the final state and E_Q the neutron separation energy. In this expression recoil energy is neglected since it is small for

the nuclei of concern. The intensity of the gamma ray of energy $E_{\gamma i}$ is given by

$$I_{\gamma i}(E) = (1 - T(E))\,\Phi(E)\,\frac{\sigma_{\gamma i}(E)}{\sigma_T(E)} \quad , \qquad 2\cdot14$$

where $T(E)$ represents the transmission averaged over the sample geometry; $\Phi(E)$ is the flux impingent upon the sample; $\sigma_T(E)$ is defined by equation 2·12; $\sigma_{\gamma i}(E)$ may be obtained from the second term in equation 2·11 and written as

$$\sigma_{\gamma i}(E) = \left(\frac{E_R}{E}\right)^{1/2} \frac{\pi \lambda\!\!\!^{-}_R{}^2\, g\, \Gamma_n \Gamma_{\gamma i}}{(E-E_R)^2 + (\Gamma_n/2)^2} \quad . \qquad 2\cdot15$$

From this equation it can be seen that spectroscopic examination of gamma rays to a particular final state gives information towards the evaluation of $\Gamma_{\gamma i}$, the partial radiation width. However, before one can interpret radiation width properties a knowledge of relevant nuclear theories is required.

COMPOUND REACTIONS

To explain the observed slow neutron cross section Bohr (1936) introduced the compound nucleus model of nuclear reactions. According to this theory the incident particle upon absorption by the nucleus interacts very strongly with the nucleons. The interaction is so strong that the energy of the observed neutron is immediately shared by many nucleons. Thus, many particles participate in the compound

nucleus formation resulting in a large number of virtual states. By random processes one of the nucleons may acquire sufficient energy to escape or radiative deexcitation may occur.

As a result of the participation of many nucleons following neutron capture the mode of decay is independent of the manner in which the compound nucleus is formed. The reaction cross section can therefore be expressed as

$$\sigma(a,b) = \sigma_c(a)\ \sigma(b) \ ,$$

where $\sigma_c(a)$ is indicative of the probability of forming a compound nucleus by capture of the incident particle, a, and $\sigma(b)$ the probability of decay by emission of particle b. Often a and b are referred to as the incident and exit channels respectively. A channel is more properly defined as the configuration which includes all the particles involved and their respective properties such as spins, parities and angular momenta.

The cross section for gamma ray emission following neutron capture is given by the Breit Wigner formula quoted in equations 2·15. It is related to the initial and final states through the partial width expressed as

$$\Gamma_{\gamma if} = \frac{2\pi}{\hbar} |\langle f|0|i\rangle|^2 \rho_f \ ,$$

where ρ_f is the density of final states of the system and

0 is either an electric or a magnetic multipole operator.

According to this model when a compound state of excitation E_x decays by photon emission, the spectrum of primary gamma rays is predominantly distributed as $E_\gamma^3 \rho\,(E_x - E_\gamma)$, where E_γ is the photon energy and $\rho(E_x - E_\gamma)$ is the level density of the residual nucleus with excitation energy equal to $E_x - E_\gamma$. This theoretical spectrum has a broad maximum around 2-3 MeV and then 'tails off' towards higher energies.

PORTER-THOMAS DISTRIBUTION

The present interpretation of the distribution that governs partial widths of neutron resonances supports the compound nucleus model. In a study on the fluctuations of nuclear reaction widths, Porter and Thomas (1956) analyzed the reduced neutron widths Γ_n^o (i.e. $\Gamma_n^o = \Gamma_n/\sqrt{E}$. $[E] = eV$) of intermediate and heavy nuclei using a statistical procedure based on the method of maximum likelihood. The results showed that the data were consistent with a chi-squared distribution of one degree of freedom. This distribution, which is of the form $x^{-1/2}\ e^{-x/2}$ where $x = \Gamma_n^o/\langle\Gamma_n^o\rangle$, is sometimes called the Porter-Thomas distribution.

Porter and Thomas point out that the reduced width amplitude for neutron emission from a compound state is proportional to an integral over a very complicated wave

function and that the wave functions for the different states may be expected to be essentially unrelated. Moreover, it is assumed that the wave function for a given state fluctuates in a random manner with equal probability of having positive and negative values. Under these assumptions the central limit theorem of statistics implies that the integral, and hence the amplitude, may be expected to have a Gaussian distribution with a mean value of zero. The square of the amplitude in a Gaussian distribution corresponds to the Porter-Thomas distribution for the width (Bo 60). By this reasoning the distribution of partial radiation widths corresponding to a single exit channel should be a chi-squared distribution with one degree of freedom. When many exit channels are available, as in the radiative deexcitation of a compound nucleus, the fluctuations that are present in the partial radiation width to a single exit channel are absent. The total radiation width Γ_γ is relatively constant corresponding to a sample from a chi-squared distribution with a large number of degrees of freedom. Many experiments have shown Γ_γ to be almost constant from resonance to resonance (Hu 54, La 55, Le 56).

COMPOUND MODEL ANOMALIES

Although Bohr's theory explained a large segment of reaction data, anomalies turned up which could not be explained by the simple compound nucleus model. The experimentally obtained distribution of El primary gamma rays from some nuclides disagrees with theoretical predictions. Although there appears to be agreement at low gamma ray energies, there are numerous isotopes which exhibit anomalously strong high energy transitions (Gr 58). The shape of the gamma ray spectrum depends not on the general distribution of levels, but on the position of the single particle p-levels. Furthermore, only those p-levels with a large single particle reduced width are most important. Strong evidence for single particle effects in neutron capture is indicated by the correlation between (n,γ) and (d,p) strengths for the same set of final states, i.e. the correspondence between the intensity of proton groups in a (d,p) reaction and the intensity of neutron capture gamma rays proceeding to the same final state (Gr 67).

There have been experimentally observed correlations between the reduced neutron and radiation widths in neutron resonance reactions (Be 68, Mu 70, St 71). As described earlier, the statistical distribution of partial radiation widths for resonances decaying via the same exit channel

is expected to have a Porter-Thomas distribution. Since each compound nuclear state is, in the compound model, composed of many components, a statistical model is favoured. This reduces the probability of correlations between neutron and partial radiation widths.

Large fluctuations have been observed in the total radiation widths for resonances in certain isotopes (St 71). As well, the ^{60}Ni capture cross section at the 12·5 keV resonance is asymmetric with a significantly slow varying cross section below the resonance. This is interpreted as being due to the interference between á channel and compound nucleus amplitude (Lu 74).

DIRECT REACTIONS

A simple mechanism has been sought to shed light on the anomalies previously indicated. Some of these are: (i) The direct potential or hard sphere capture in the off resonance region where an incident s-wave neutron is scattered by the nuclear surface and makes a radiative transition to a low lying p-state with the emission of E1 radiation. (ii) The channel capture, suggested by Lane and Lynn (1960), where an s- or p-wave neutron is scattered through a resonant state and makes a transition into a low lying orbit while radiating gamma rays.

(iii) The semi-direct process of Brown (1964) (doorway states (Fe 63)) where an incident neutron scatters in the target nucleus creating a 2p-1h state. In this process a gamma ray is emitted when the particle and hole combine. Channel capture is more probable for nuclear states which have a large single particle component. These nuclear reaction models are ones in which an s-wave neutron and the target nucleus undergo an El transition to a low lying single particle state without forming a compound nucleus. These reactions can be formulated in terms of R-matrix theory by considering the external region of configuration space to coincide with the channel region. (Lu 74)

The partial photon width $\Gamma_{\lambda\gamma c}$ for the λ_{th} resonance can be written as

$$\Gamma_{\lambda\gamma c} = (\gamma^{ch.}_{\lambda\gamma c} + \gamma^{c.n.}_{\lambda\Gamma c})^{2} , \qquad 2\cdot16$$

where $\gamma_{\lambda\gamma c}$ is the reduced amplitude of resonance λ for channel c, and $\gamma^{2}_{\lambda\gamma c}$ is equal to $\Gamma_{\lambda\gamma c}$. The value of $\gamma^{2\ ch.}_{\lambda\gamma c}$ is proportional to the initial and final state reduced neutron widths. The value of $\gamma^{2\ c.n.}_{\lambda\gamma c}$ is the compound nucleus contribution to the partial width. When the channel component is large one would expect a correlation

between the partial radiation and neutron widths, since $\Gamma_{\lambda\gamma c}$ would be approximately equal to $\gamma^{2ch.}_{\lambda\gamma c}$. In addition, amplitudes usually interfere constructively below and destructively above the resonance (Lu 74). These theories not only predict correlations between the radiation widths and the reduced neutron widths but also predict the anomalously strong high energy transitions found for certain isotopes. The level structure of the nuclei with the 'anomalous' spectra has low energy levels containing configurations in which large components of p-orbitals are expected. This should be favourable for channel capture.

The (d,p) reaction mechanism is primarily a direct process and is characterized by short reaction times. The picture associated with the (d,p) reaction is that a neutron is transferred into a shell model orbital of the target nucleus. Because this assumption is, in general, not strictly true, the experimental differential cross section is often written as

$$\frac{d\sigma}{d\omega}_{exp} = S \frac{d\sigma}{d\omega}_{TH} , \qquad 2\cdot17$$

where S is the spectroscopic factor and $\frac{d\sigma}{d\omega}_{TH}$ the theoretical result (En 66a). The spectroscopic factor expresses the degree to which the final state is composed

of the target state with a neutron bound in an orbit with quantum numbers ℓ and j . It is a measure of the reduced neutron width of the initial state.

In the Lane and Lynn theory the direct component of the radiative transition may dominate if the final state has a large p-orbit single particle component. The dependence of the direct component on the single particle reduced width is identical to the dependence of the (d,p) strength on the spectroscopic factor. Furthermore, for s-wave neutron capture followed by E1 decay the final states that will be preferentially populated will be the same as the final states for which $\ell_n = 1$ in the (d,p) reaction. It is therefore expected that in such situations a significant correlation should exist between the (n,γ) and (d,p) strengths.

CHAPTER 3

EXPERIMENTAL METHOD

As indicated in chapter 1, the feasibility of the method proposed here is based upon the nature of the neutron spectrum which prevails in a light water moderated nuclear reactor and the ability of ^{10}B with a $1/\sqrt{E}$ cross section to reshape this distribution into a near optimum form. For the present discussion we will assume a ^{10}B filter is used which is sufficiently thick as to exclude all thermal neutrons thereby requiring examination of only resonance and fission spectrum neutrons.

The dominant neutron reaction for ^{10}B is $^{10}B\ (n,\alpha)\ ^{7}Li$ and has a cross section in the region below 200 keV given by (BN 66)

$$\sigma_{n,\alpha}\ (E) = 611/\sqrt{E} \text{ barns} , \qquad 3\cdot1$$

where the neutron energy E is in eV. The form of the neutron flux after passage through an infinite plane of ^{10}B containing n atoms/barn is given by

$$\phi^{T}\ (E) = \phi\ (E) \exp\ (-\ n\ \sigma_{n,\alpha}(E)) \qquad 3.2$$

under the assumption of normal incidence. Using equation 2·10 developed earlier for the resonance flux, the

expression for the filtered flux becomes

$$\phi^T(E) = \frac{K}{E} \exp(-n\,611/\sqrt{E}) \quad . \qquad 3\cdot3$$

This function has a maximum which occurs at a neutron energy of

$$E_{max} = \frac{1}{4}(n\,611)^2 \text{ eV}$$

$$= \frac{a^2}{4}$$

where the flux is

$$\phi^T(E_{max}) = \frac{4K}{a^2} e^{-2} \quad .$$

A family of curves representing the transmitted flux for various boron thicknesses is shown in figure 3·1. In the present work a thickness of 1 gm/cm^2 was typical. From figure 3·1 it is seen that for such a filter the flux maximum occurs at a neutron energy of about 1 keV. In all cases it should be noted that the flux above the maximum approaches the $^1/_E$ form rapidly with increasing neutron energy. Ideally one should use a thickness which removes neutrons just below the energy of interest. However, experimental constraints in the current work limit the thickness to 1·5 gm/cm^2. The present study made use of an annular filter geometry in which a 1·5 cm diameter sample was surrounded by a 1 to 1·5 gm/cm^2 ^{10}B sleeve.

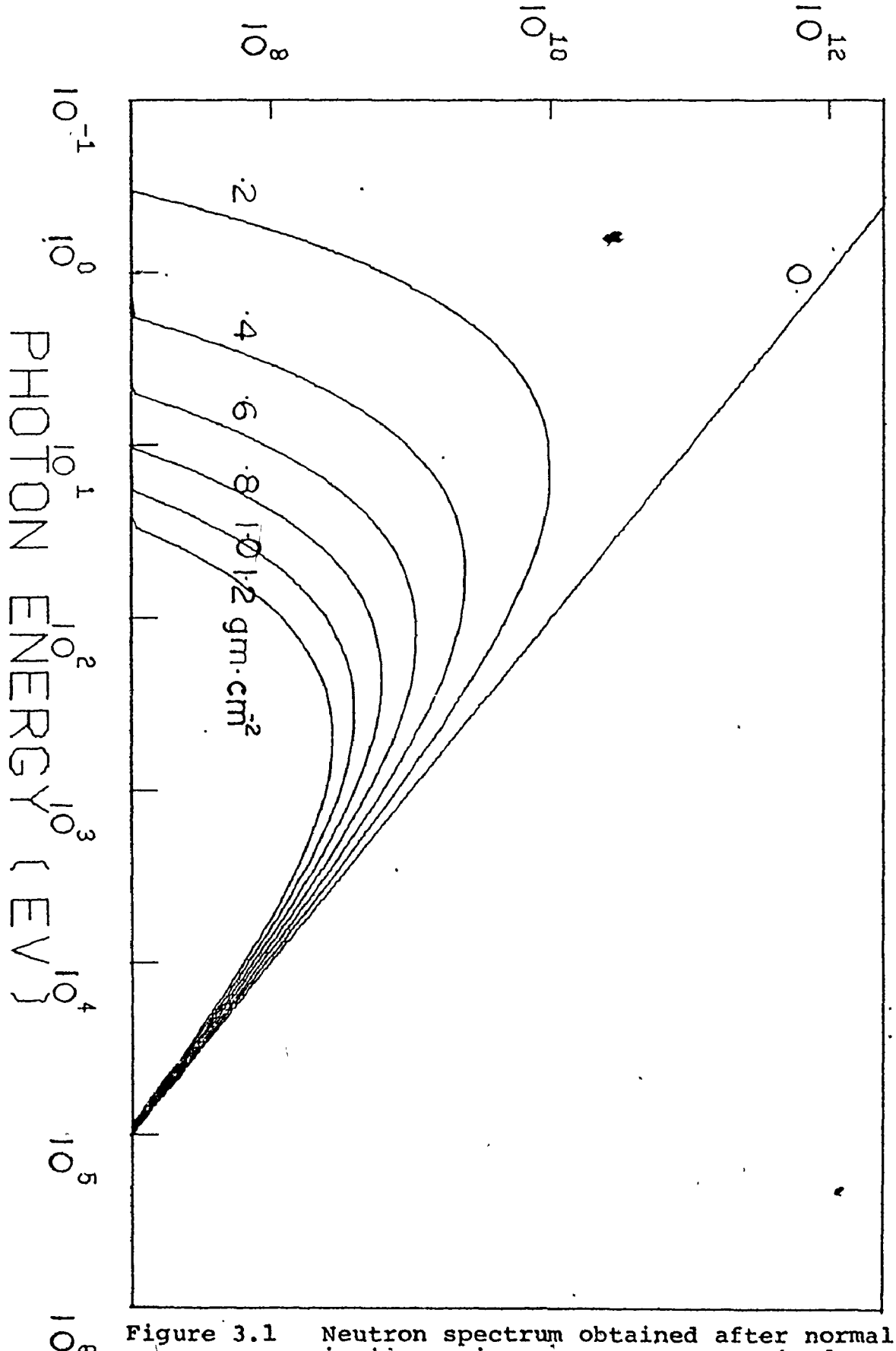

Figure 3.1 Neutron spectrum obtained after normal

ter

For such an arrangement the transmitted flux is not identical to the parallel beam assumed in the derivation of equation 3·3 but undergoes a minor modification because of the chord distribution. The effective radius of the annular ^{10}B sleeve is 20% larger (Lo 74) when calculating the mean chord for a transmitted neutron. This results in a small change in the distributions as shown in figure 3·1. The effect of multiple scattering in ^{10}B during neutron transmission increases the flux transmitted at a given energy. Thus, the effect of geometrical considerations is to increase the effective filter thickness and the effect of multiple scattering is to decrease it (Lo 73). Despite these small effects the flux distribution at energies above the maximum is not greatly disturbed from the $^{1}/E$ resonance neutron distribution.

The illumination of a target which possesses resonances by a range of neutron energies will result in the capture of neutrons at the resonance energies. By observing the corresponding radiative transitions with a high resolution Ge(Li) pair spectrometer, components will be seen provided the resonance width and the counter resolutions are less than the resonance spacing. Unlike most studies of this type the present arrangement operates in a continuous mode exhibiting a 100% duty cycle. To quantitatively evaluate the value of

this approach, comparison with more conventional methods is useful.

METHOD ADVANTAGES

Let us compare the present method with the time of flight technique under the assumption that the same reactor is to be used. For a quantitative assessment the flight path of the hypothetical chopper spectrometer is adjusted in order to achieve an energy resolution equal to that of the dispersive technique. For the figure of merit a comparison of counting rates will be made. It is important to remember that for the dispersive method the advantages of a pair spectrometer are realized rather than the simple Ge(Li) spectrometer assumed for the time of flight arrangement.

Proceeding with the assessment let us assume that the fast chopper is located 3m from the core, that it has 7 slits 0·038 cm x 5 cm, a radius of 15 cm and rotates at 20,000 rpm. For this arrangement the burst width Δt is 0·72 μsec (FWHM) and the duty cycle is ·05%.

The resolution of a time of flight spectrometer is given by $\Delta t/L$ (μsec/m) where L is the flight path. Converting to energy resolution we have

$$\Delta E = \frac{\Delta t}{L} \cdot \frac{E^{3/2}}{36.15} ,$$

where the neutron energy E is in eV. In comparing this

method with the dispersive technique the value for ΔE is selected to be equal to the resolution of the Ge(Li) spectrometer. Assuming this to be 10 keV the flight path required to achieve this resolution is

$$L \sim 2 \times 10^{-6} E^{3/2} .$$

The transmittance of the chopper is determined by the aperture, the solid angle with respect to the core and the duty cycle. For a flux ϕ_o adjacent to the core the transmitted intensity is

$$6 \times 10^{-10} \phi_o \text{ neutrons/sec.}$$

The pulsed beam diverges after passage through the slit of the chopper and as a consequence a large target may be required if the total beam intensity is to be intercepted. The dimension of such a target is linearly related to the flight path L. If such a target, having height h and width w, is observed by a detector of area A at a distance c, the detection efficiency is

$$\sim \frac{A}{w\,h} \ln \left[\frac{\sqrt{4(c+w)^2+h^2} - h}{\sqrt{4c^2 + h^2} - h} \cdot \frac{c}{c+w} \right] .$$

The actual counting rate will involve the detector efficiency per unit area, the transmission through the sample and the transmitted intensity.

For the dispersive system the solid angle subtended 3m from the core is the principal factor governing the efficiency. Assuming the same flux, detector efficiency and sample thickness, the ratio of the counting rates for the two methods is

$$\frac{R_{disp}}{R_{tof}} = \frac{L^2}{1\cdot 2\times 10^{-3}} \cdot \frac{1}{\ell n\left[\frac{\sqrt{4(c+w)^2+h^2}-h}{\sqrt{4c^2+h^2}-h}\cdot\frac{c}{c+w}\right]} .$$

If one assumes that the detector used in the time of flight spectrometer is 2 cm from the target, i.e. c=2, then, the efficiency ratio obtained for ΔE = 5, 10, 20 keV is shown in figure 3·2. The figure shows the present method to have a 10^5 to 10^8 increase in counting rate over the time of flight method for an energy resolution of 10 keV. It should be noted that this increase is improved with better detector resolution.

An interesting feature of distinction between the methods is that involving multiple scattering. In the time of flight method, the energy determined is not that of the neutron at the instant of capture but rather that measured by the flight period. This results in the well established spectral distortion as observed by Kennett and Bollinger (1959) when targets with a large degree of

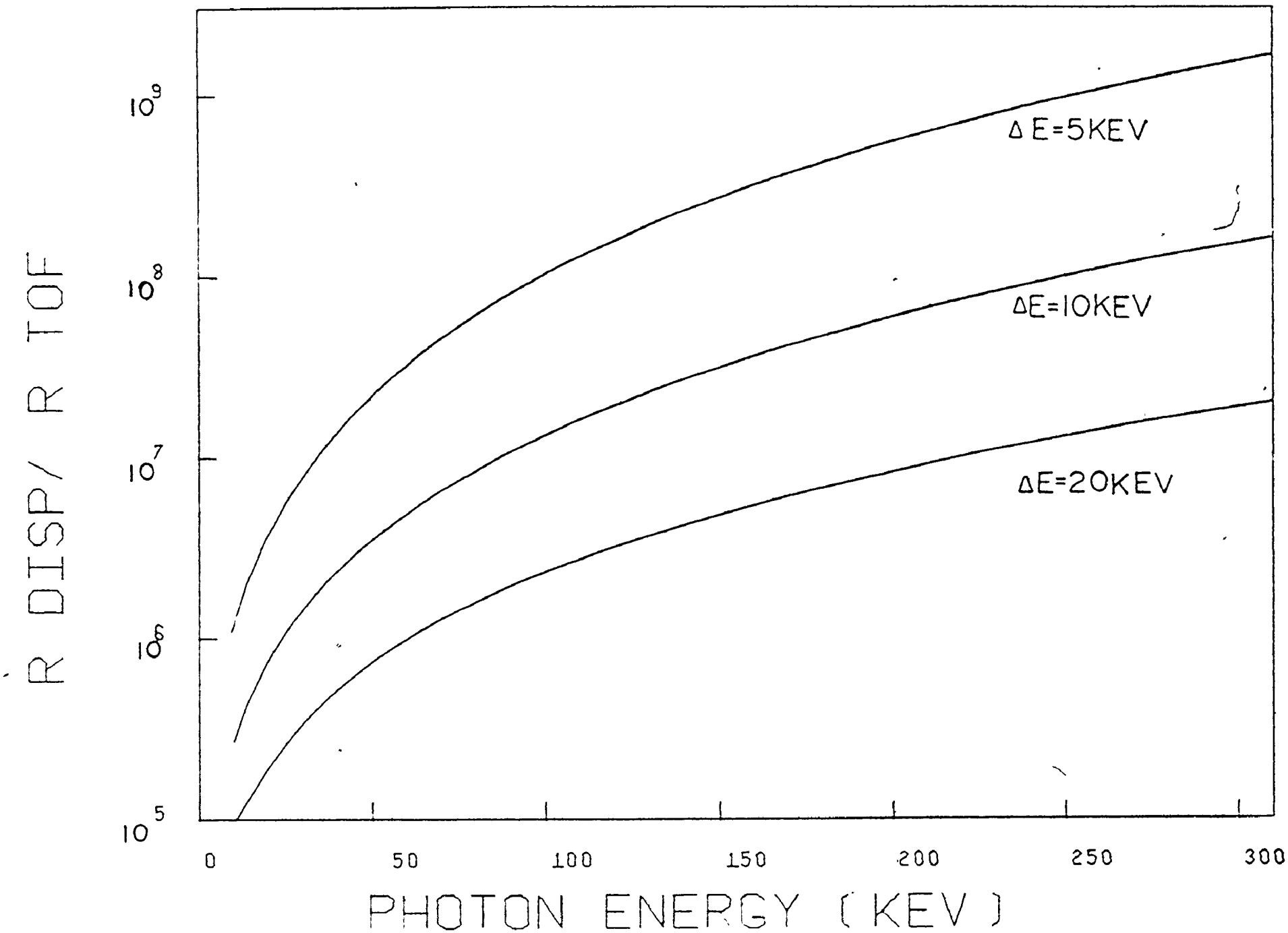

Fig. 3.2 The relative count rate for the energy dispersive technique to that of the time of flight method for the case of equal resolution is shown for resolution of ΔE=5,10,20

scattering are used. In the method used here the energy measured is that at the instant of capture so this effect does not occur (Th 75a).

In addition to the measurement of partial radiation widths the dispersive method yields isotopic identification of resonances, measurement of resonance neutron widths, when appreciable compared to detector resolution, and specification of primary transitions in gamma ray cascades.

CHAPTER 4

INSTRUMENTATION

NEUTRON SOURCE

The McMaster Nuclear Reactor was used as the source of neutrons for the current work. It is a 5 megawatt swimming pool reactor which employs ^{235}U enriched uranium as fuel with light water as moderator and coolant. A diagram showing the reactor facilities is given in figure 4.1.

There are six beam ports which extend radially from the reactor core, through the containment wall surrounding the pool into the experimental area. Beam ports used for neutron extraction are equipped with bismuth plugs to attenuate gamma radiation coming from the core since the radial configuration leads to high photon backgrounds. The neutron flux can be controlled and shaped by placing the appropriate filters in the beam. In an experimental irradiation position outside the containment wall, the neutron flux is typically 10^6 neutrons/cm^2/sec. Such facilities are suitable for experiments requiring external target configurations, such as γ-γ coincidence investigations, (n,γ) lifetime measurements and angular correlation studies.

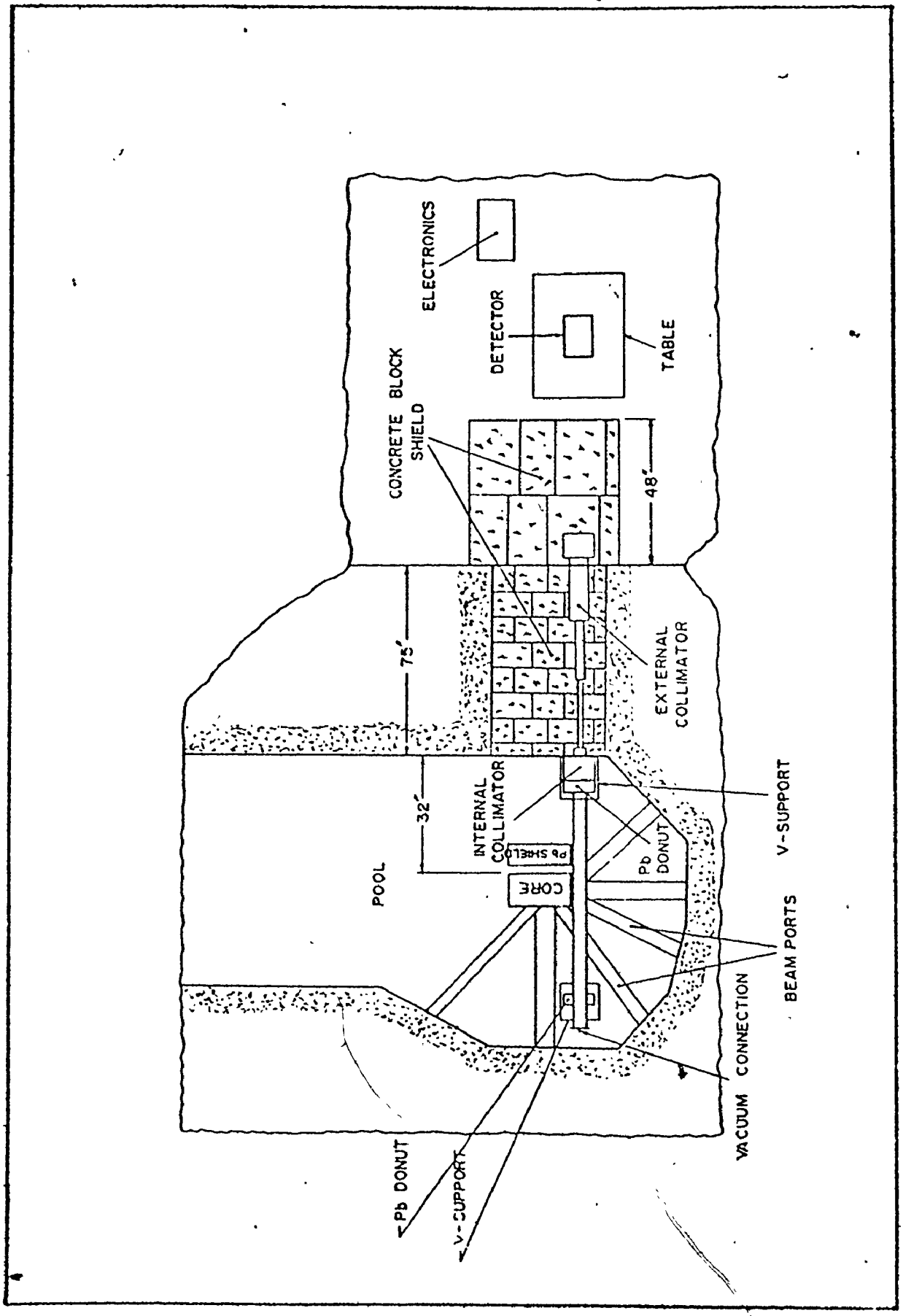

Figure 4.1 General Layout of the nuclear reactor facilities.

However, this arrangement does not permit in core target emplacements because of the intense gamma ray background associated with the radial configuration. Since resonance capture experiments, among others, need high sensitivity and low background, a tangential irradiation facility was developed (Ni 70). The facility was later adopted for convenient sample changing (Co 72) and large sample positioning (Lo 73).

TANGENTIAL THROUGH TUBE FACILITY

The through tube, shown in figure 4·1, is horizontal and is placed tangentially to the core. This ensures a high neutron flux incident upon the target and minimizes background radiation from the core. The capture gamma rays from the sample pass through a collimation system and are viewed by a detector in the experimental area external to the pool water.

The internal geometry offered by the through tube facility increases sensitivity for a given sample size compared to an external geometry. The ratio of internal to external sensitivity may be simply expressed as

$$R = \frac{\Omega n i \ \Omega \gamma i}{\Omega n e \ \Omega \gamma e} ,$$

where the subscripts i and e refer to internal and external geometry and the solid angles subtended by the

target relative to the neutron source and the detector are Ωn and $\Omega \gamma$ respectively. Typical values are:

$\Omega ni/4\pi \sim \cdot 75$ (one side of an isotropic neutron source plus 50% reflection from water)

$\Omega \gamma i/4\pi \sim 10^{-6}$ (beam 2·5 cm in diameter)

$\Omega ne/4\pi \sim 10^{-6}$ (beam 2·5 cm in diameter)

$\Omega \gamma e/4\pi \sim 3x10^{-2}$ (an 8 cm^2 faced Ge(Li) detector 5 cm from the target)

This gives rise to a ratio of R ∿ 25. In the determination of the ratio the small differences between internal and external geometry for the transmission of neutrons and gamma rays through materials along beam paths have been neglected. The neutron flux at the through tube irradiation position has been evaluated as 10^{13} neutrons/cm^2/sec.

THROUGH TUBE DESIGN

Schematic diagrams of the through tube are shown in figures 4·1, 4·2, and 4·3. The through tube is a closed system into which samples can be shuttled from the pool surface to the reactor core and the systems subsequently evacuated. The tube is a semi-permanent facility which can be surfaced and modified for the needs of different experiments. The design consists of a 7·6 cm O.D. 65 ST

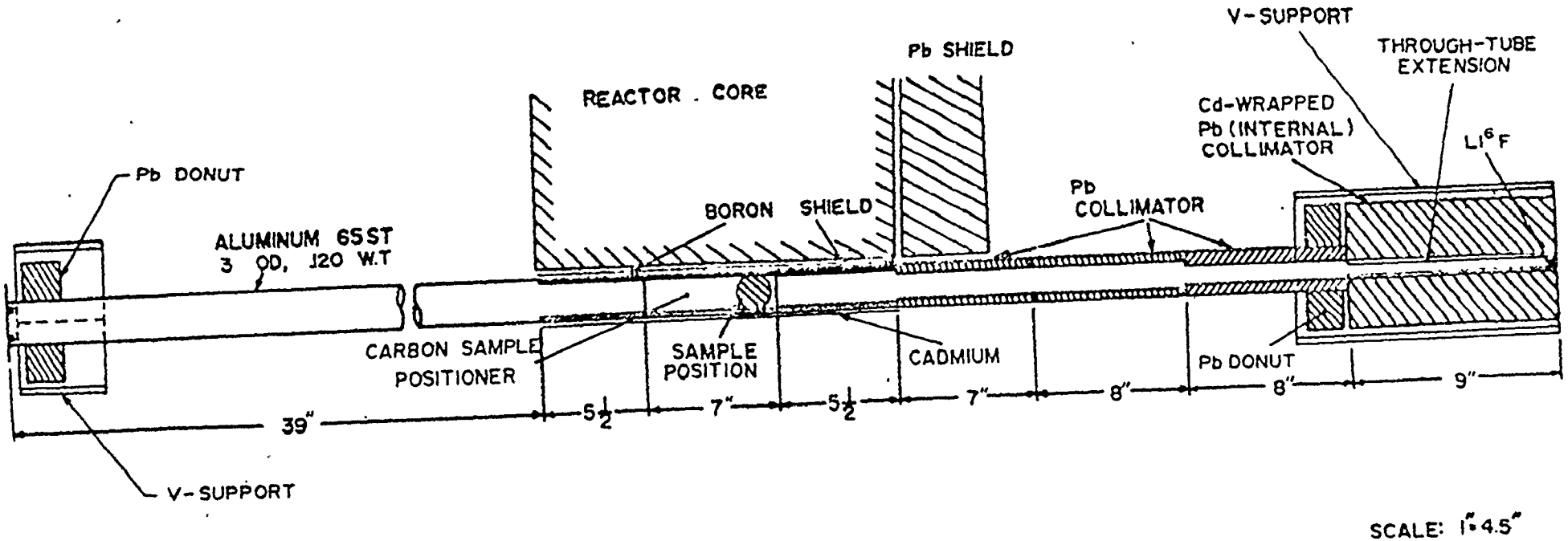

Figure 4.2 A plane view of the horizontal through tube showing shielding and collimation systems.

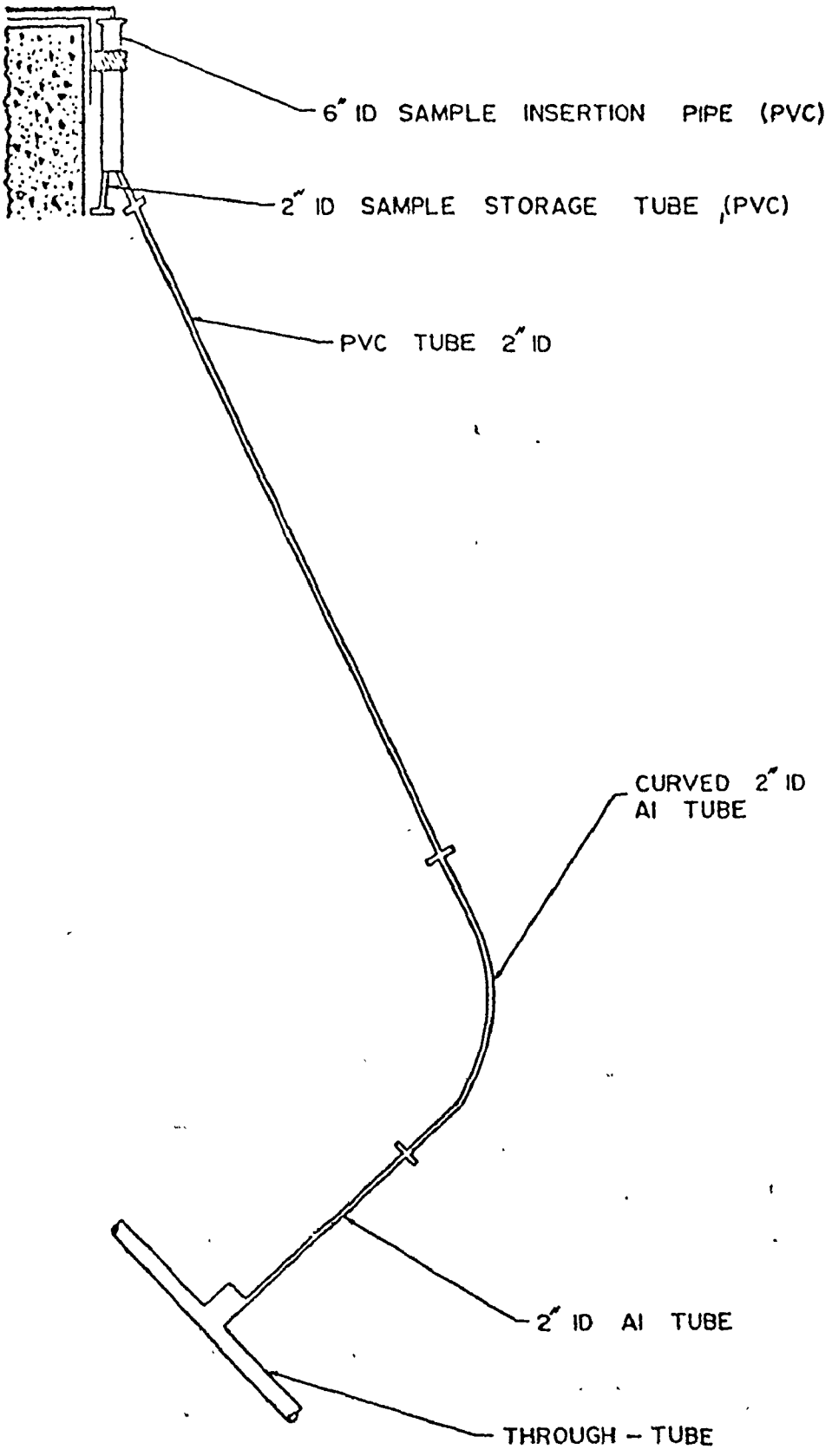

Figure 4.3 Arrangement of through tube sample delivery and storage system.

aluminum pipe 2m in length. To assure correct alignment (1-2 cm from the core) lead 'donut' spacers at each end of the tube rest on V-notched stands anchored to the pool floor.

The tube geometry is such that direct radiation from the core is excluded. To reduce scattered radiation from reaching the detector a 10 cm thick lead plate is positioned on the core framewith sufficient area to shadow the core face as seen by the detector (figure 4·2). Inside the pool a collimator consisting of a split cylindrical lead annulus, 15·2 cm O.D. and 22·9 cm long with a 2·5 cm diameter central hole, sits on a V-notched support stand at the detector end of the tube. The annulus shields the detector from capture gamma rays arising in the aluminum tube. The through tube has a 2·5 cm diameter, 22.9 cm long extension which fits into the annulus; the top of the annulus is removed to permit easy installation and to prevent damage to this extension.

A collimation system external to the pool wall attenuates any radiation other than from the sample. The only material between the split annulus and the external collimator is an aluminum window in the pool wall which consists of a 2·5 cm aluminum plate thinned to ·6 cm in the region where the beam is transmitted.

The external collimator is a ·83 cm diameter aluminum tube centred in a rectangular aluminum container which is stepped in the lateral dimension as the distance from the pool wall increases. The container is filled with polyethlene and lead shot. The collimator is 2·3 m long. The detector is placed 1·5m from the exit of this collimator. In the 1·5m between the collimator and the detector, barytes concrete blocks are placed to further attenuate radiation from the reactor pool. There is also 30 cm of wax placed in the beam to prevent fast neutrons, reflected down the collimation system by the target, from striking the detector.

Inside the tube the sample is positioned towards the back of the core to reduce the energy of photons scattered from the target. (The sample position shown in figure 4·2 is the entrance location to the tube at which point the sample is rotated and placed near the back of the core. See figure 4·4). From the sample to the beam emergent end of the tube there are lead collimators inside the tube positioned so that they do not appear in the line of sight of the detector. At each side of the sample position there are cylindrical sleeves filled with B_4C_3 to shadow the sample, thereby reducing the number of impinging thermal neutrons.

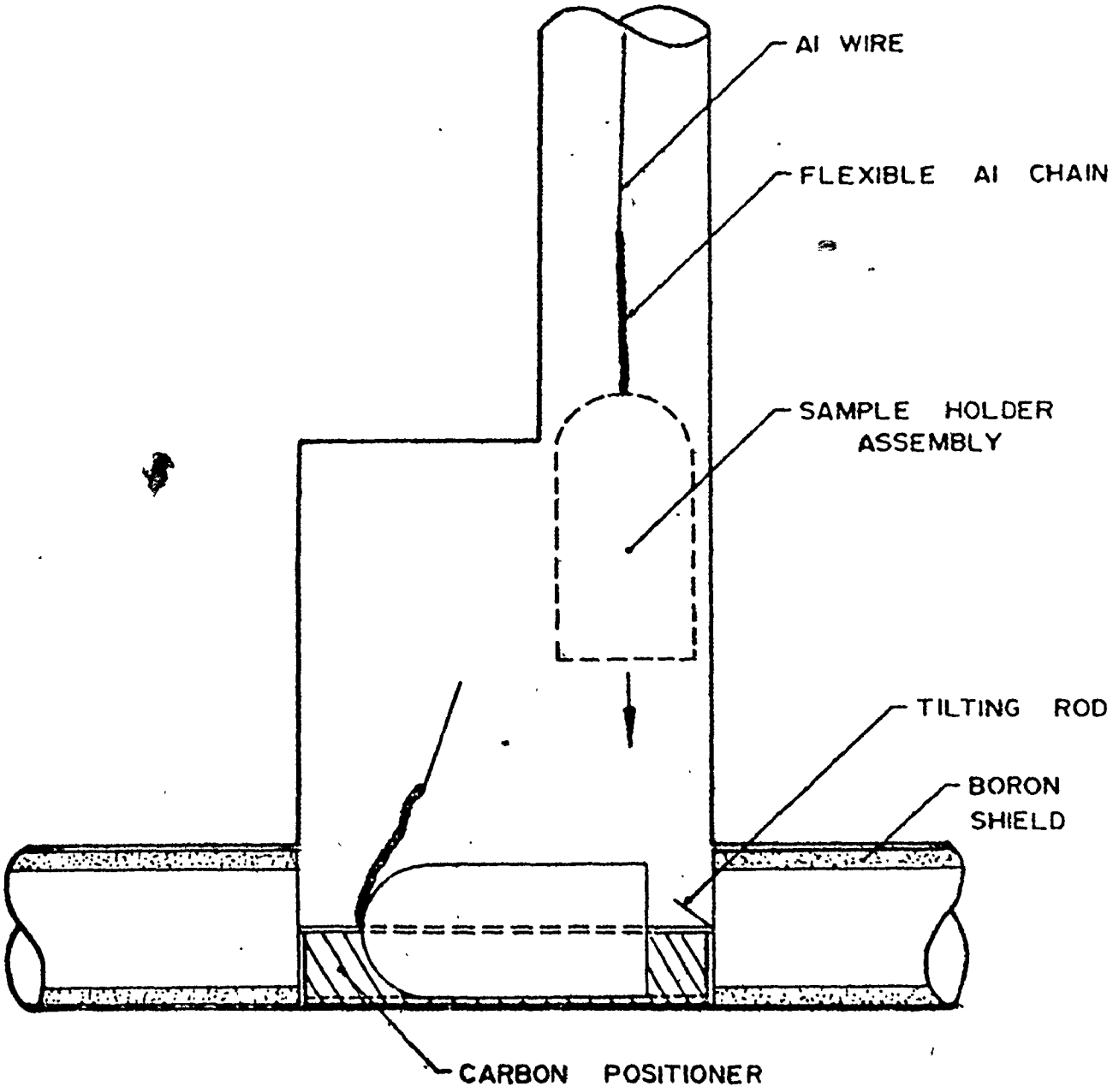

Figure 4.4 The facility for sample rotation and positioning in the horizontal through tube.

In order to prevent interference by capture gamma rays from the aluminum window, the split annulus at the pool wall is clad with cadmium sheet. In addition the end caps of the tube are coated with ^{6}LiF to protect them from the local flux.

As shown in figures 4·3 and 4·4, samples are lowered into position from the surface of the pool through the 5·6 cm I.D. tubing to the through tube. The system has a 15 cm I.D. by 2 m long polyvinylchloride enlargement at the pool surface with a 5·6 cm I.D. by ·5 m long storage tube to one side. The through tube and the enlarged tube at the surface are connected with 7m of tubing; the upper 4m is formed from polyvinylchloride and the lower 3m, aluminum since polyvinylchloride is highly susceptible to radiation damage. The aluminum tube is angled upwards and away from the core until it reaches the pool wall where it turns toward the entrance port at the surface.

Samples are lowered in cylindrical carbon containers to the core on a cotton line; 2m of aluminum wire and 30 cm of aluminum chain are attached to the carbon containers to guard against radiation damage to the cotton line. The chain is necessary for flexibility since the carbon holder at the irradiation position is turned onto its side into

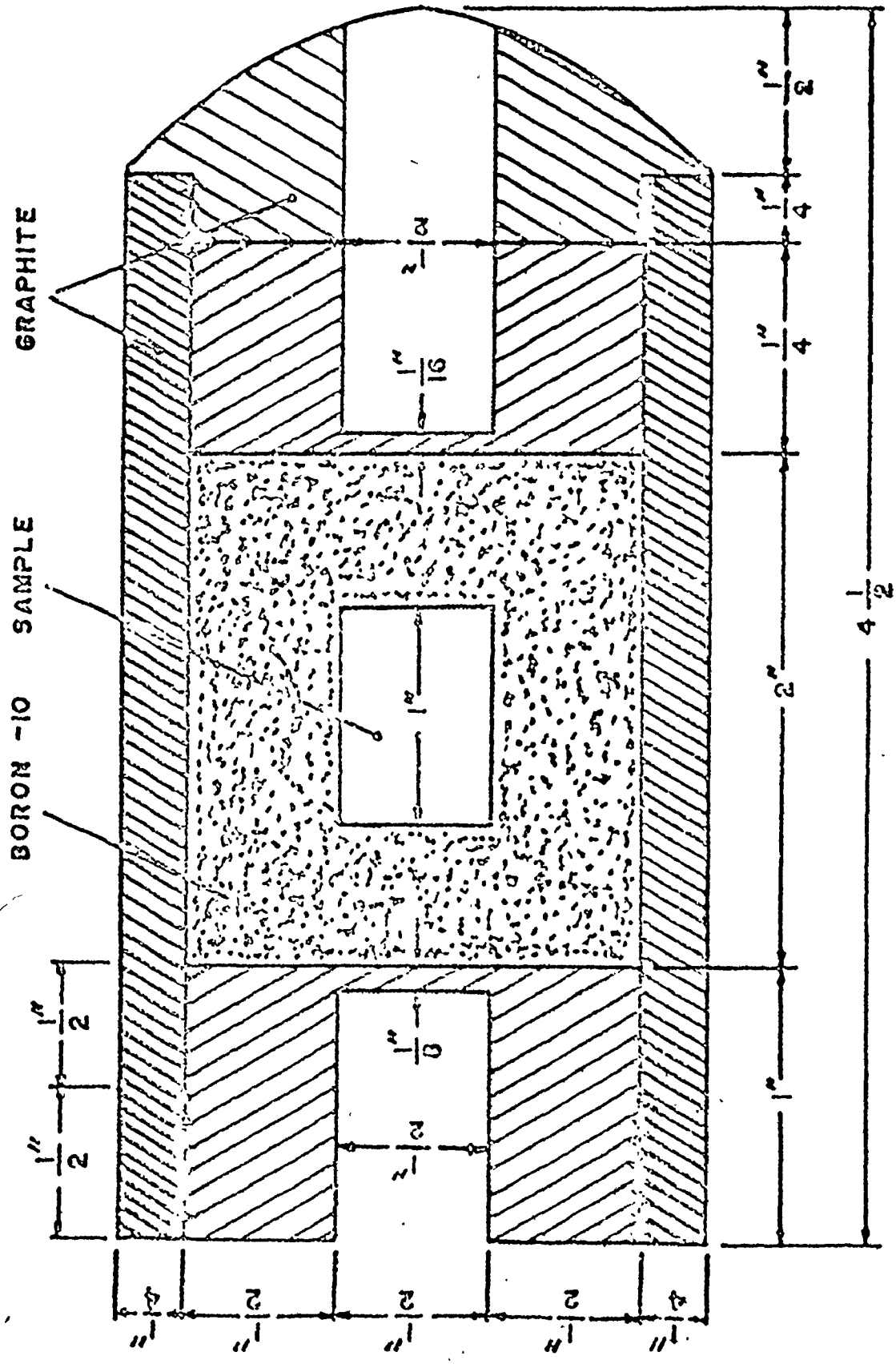

Figure 4.5 A typical sample assembly.

a carbon seat, as shown in figure 4·4. A horizontal placement along the cylinder axis allows the detector to view a larger sample than would be possible with a vertical arrangement. At the sample position the geometry permits the detector to view a 1 cm^2 area. Both sample and container have cylindrical symmetry (figure 4·5). The container is 5·0 cm O.D., 11·5 cm long and has ·5 cm thick walls. Samples are centrally located within the holder and surrounded by a uniform annulus of ^{10}B. There is a carbon spacer inside the holder cap to allow for varying sample sizes.

DETECTION SYSTEM

Gamma rays, following neutron capture, were detected with an annihilation pair spectrometer which consists of a Ge(Li) counter centrally located in an annulus of NaI(Tℓ) as shown in figure 4·6. The optically quadrisected annulus and the associated electronic circuitry select gamma rays which interact with the Ge(Li) detector by pair creation.

The Ge(Li) detector used in the work was fabricated using the techniques described by Fiedler et al. (1966) and Robertson (1972). A germanium ingot (gallium doped) was alloyed with lithium using an electroplating bath. The

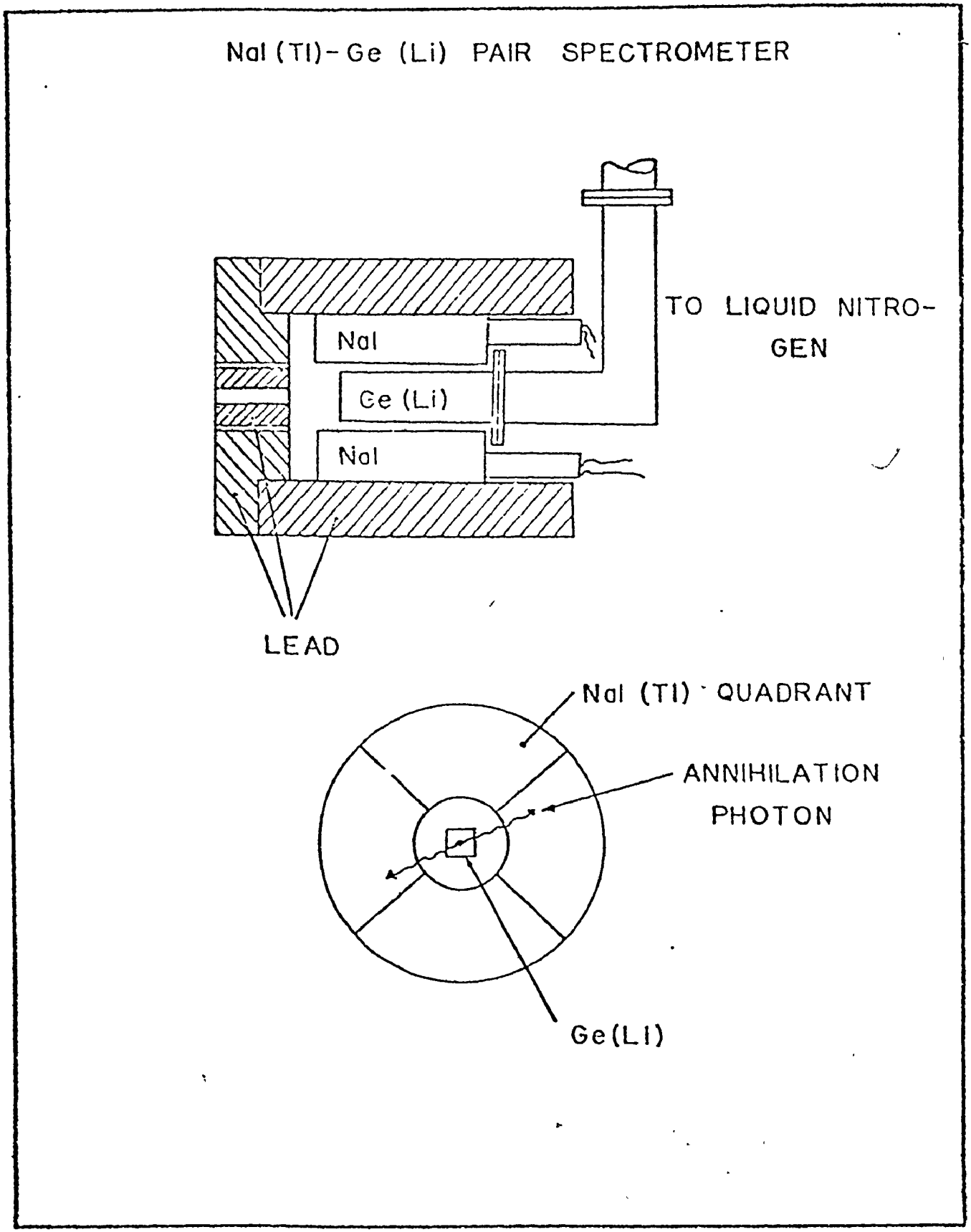

Figure 4.6 A schematic diagram of the Ge(Li) - NaI(Tℓ) pair spectrometer.

germanium from Hoboken, Belgium, was acquired through NPC Electronics Co., Los Angeles. The detector is coaxial, open at one end, with an active volume of 20 cm^3.

The NaI(Tℓ) crystal has an outside diameter of 23·0 cm, an inside diameter of 7·6 cm, and a length of 15·2 cm, and each of the optically isolated quadrants is coupled to a photomultiplier. A photon interacting with the NaI(Tℓ) crystal causes light to be emitted which is detected by the photocathode. The signal of photoelectrons produced at the photocathode is accelerated and amplified by a chain of dynodes with the output being taken at the anode.

Detection of gamma rays by the Ge(Li) detector is based on the interaction processes of photoelectric effect, Compton scattering and pair production. Each of these interactions results in energy transfer from gamma radiation to charge carriers, where the number of carriers liberated is proportional to the gamma ray energy. The energy dependence of the cross sections for each process is shown in figure 4·7. The cross sections show that above 2 MeV the photoelectric effect for gamma ray detection is much smaller than Compton scattering and pair production. Thus for efficiency one of the latter two processes would be preferred.

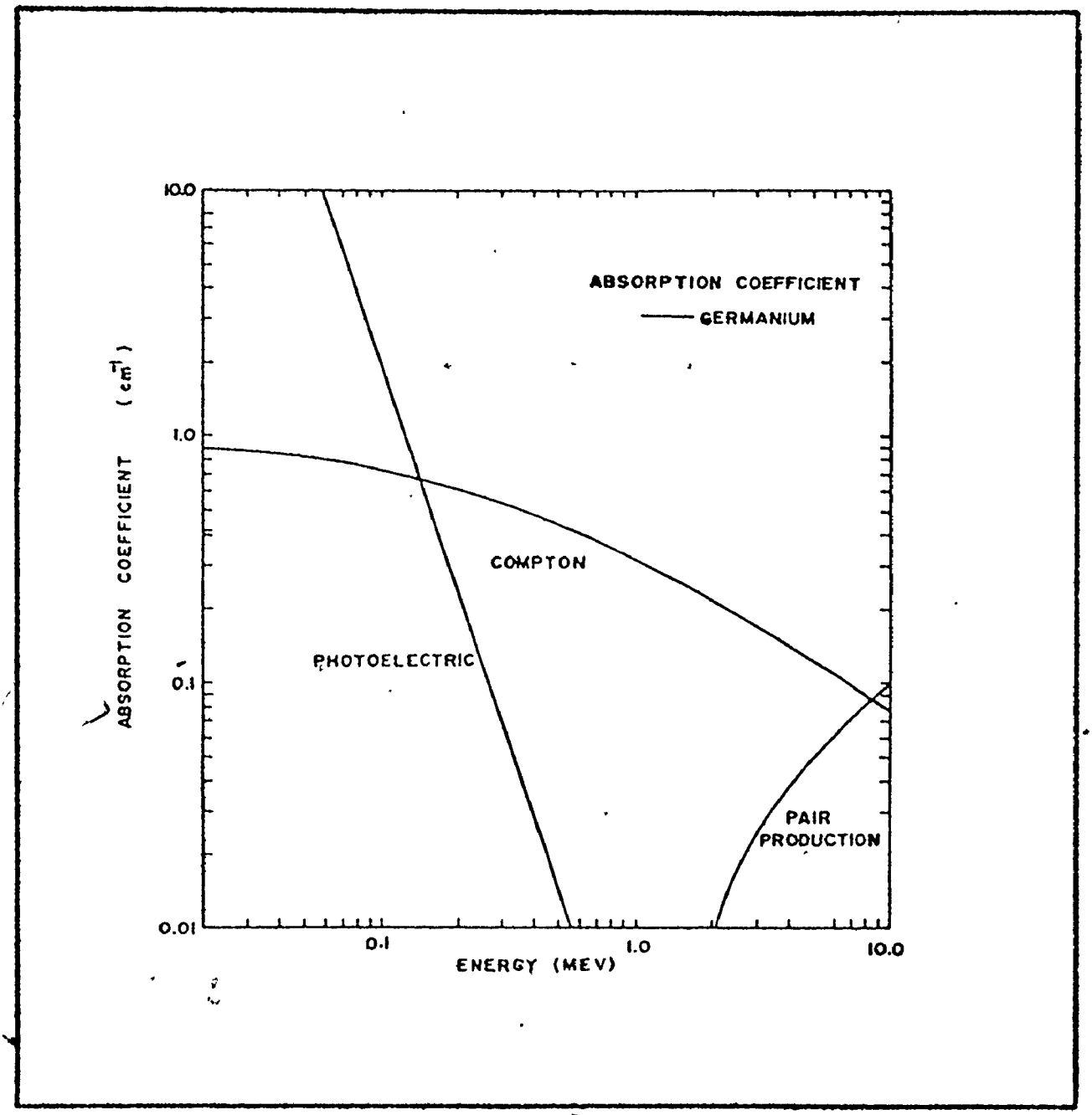

Figure 4.7 The energy dependence of the photoelectric, Compton effect and pair production cross sections in germanium.

One other consideration is to select events from one process only in order to reduce background in collected spectra. The properties of pair production in a Ge(Li) detector is used to select pair production events and discriminate against Compton scattering and photoelectric events.

In the pair production process a gamma ray with energy greater than $2\ m_o c^2$, where m_o is the election rest mass, interacts with a nucleus to form an electron positron pair. The energy in excess of $2\ m_o c^2$ is imparted as kinetic energy to the created pair. Only a small amount of the energy is lost to nuclear recoil. The positron, after being slowed down by multiple collisions, combines with an unbound electron to form positronium, a hydrogen-like atom composed of a positron and an electron. The positronium decays mainly through annihilation into two 511 keV photons. Since the mean lifetime of positronium is small compared to charge collection time, the annihilation photons can interact further and release more charge carriers. It is quite probable that one or both of the annihilation photons escape from the Ge(Li) detector. If one photon escapes the gamma ray energy E_γ absorbed is equivalent to $E_\gamma - m_o c^2$ and if both escape, $E_\gamma - 2m_o c^2$.

The resulting peaks which appear in the spectrum are referred to as 'single escape' and 'double escape' respectively.

Therefore gamma rays with energies above $2 m_o c^2$ will yield a spectrum exhibiting the photopeak, escape peaks and a continuous Compton distribution. Other partial energy transfer processes cause spectral distortion, some of these are: escape of high energy electrons or positrons through range effects, trapping of charge carriers in a 'dead' zone of the crystal and escape of bremsstrahlung radiation arising from deceleration of either member of the positron-electron pair.

The NaI(Tℓ) - Ge(Li) pair spectrometer selectively identifies events in which a gamma ray creates a pair in the Ge(Li) detector and both annihilation quanta escape. For momentum conservation the photons in the 'double escape' event leave the Ge(Li) detector in opposite directions. In a pair of opposite NaI(Tℓ) quadrants, photons of energy $m_o c^2$ are detected 'simultaneously' and thus signify notice of a double escape event in the Ge(Li) detector. For a gamma ray energy E_γ the resulting spectrum consists of a peak with centroid at $E_\gamma - 2 m_o c^2$ imposed on a background which arises from range and bremsstrahlung losses. A

limitation of the pair spectrometer is the inability to detect a gamma ray with energy below the pair production threshold.

ELECTRONIC SYSTEM

A schematic diagram of the electronic circuitry is shown in figure 4·8. In brief, a gamma ray is detected by the pair spectrometer; the signals are amplified; the necessary logic conditions are established to ensure a 'correct' event; the signal from the Ge(Li) detector is made acceptable to a Nuclear Data 3300 multichannel pulse height analyzer.

More specifically, photons are detected in the NaI(Tℓ) crystals and the output of each quadrant is fed into an Ortec 113 preamplifier and Canberra 1418 amplifier. The voltage signal is then fed into a single channel analyzer with a 10% pulse height window set to detect events corresponding to 511 keV. The fast outputs of the single channel analyzers are fed to a dual coincidence gate in order to 'AND' opposite quadrants.

The Ge(Li) counter is connected to a Tennelec TC 130 FET preamplifier from which the resultant voltage signal is proportional to the total charge collected in the detector. The signal is amplified by a Tennelec TC 200 amplifier and

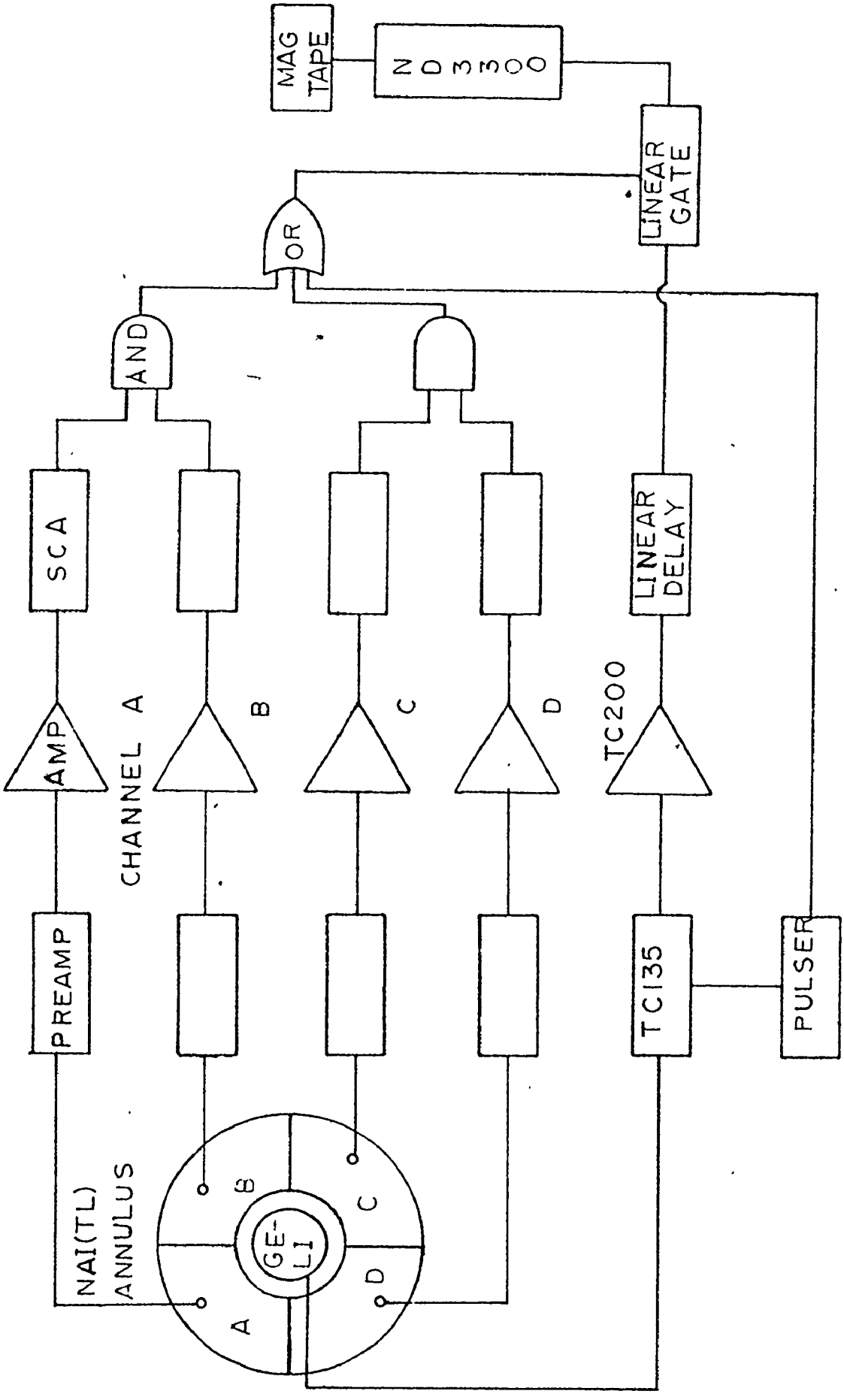

Figure 4.8 An overall schematic of the detection system

fed into an Ortec 427 delay amplifier in order to place the signal from the Ge(Li) detector in time with the coincidence signal from the NaI(Tℓ) annulus. Opposite quadrant AND conditions are combined into an OR function at the enable input of a Canberra 1451 linear gate through which the delayed signal from the Ge(Li) detector is passed.

A voltage reference pulser, built from a design reported by Strauss et al. (1968) produces signals which were fed into the Ge(Li) preamplifier and which were used for stabilization. In order for the pulser events to be accepted by the logic, the 'OR' pulse from the NaI(Tℓ) quadrants is 'OR ed' with a logic signal from the voltage reference pulser. This final condition is then used in the linear gate to select appropriate events from the Ge(Li) channel. The output of the linear gate is fed into a 4096 channel analogue to digital converter of a Nuclear Data 3300 multichannel analyzer. Stabilization is attained with circuits in the analyzer using the voltage reference signals.

EXPERIMENTAL PROCEDURE

Isotopes of silicon, chromium, and nickel were studied in this experiment. Each sample was irradiated in the through tube facility to obtain gamma ray spectra for

both thermal and keV neutron capture. For the former the sample alone was irradiated and for the latter, the sample was surrounded by a layer of ^{10}B. The samples were placed one at a time in the through tube irradiation position for 100-600 megawatt hours (M.W.H.) depending on the count rate which ranged from 2000 to 30000 pair events per minute. Spectra were accumulated for 24 hour periods and stored on magnetic tape; when sufficient data were accumulated for one sample, the stored spectra were summed in preparation for subsequent analysis. After irradiation the samples were stored for approximately one week so that most activation products had decayed sufficiently to allow dismantling of the assembly.

All the samples had purities greater than 99% and were cylindrical in shape. The Cr N was obtained from Alpha Inorganics, Montreal, and the ^{10}B from USAEC, Oak Ridge. The ^{10}B had an isotopic composition of ^{10}B - 92·4% ; ^{11}B - 7·6%. Powdered samples were contained in 1 - 2 mm walled cylindrical capsules with 1·2 or 1·9 cm O.D. and 5·1 cm in length. Samples not surrounded by ^{10}B were centred by means of a carbon spacer. Specifications for the different samples and the ^{10}B layer associated with each are given in table 1.

TABLE 1

Sample Specifications

		Sample					^{10}B Filter		
ample	Form	Density (g/cm^3)	Weight (gm)	Diameter (cm)	Length (cm)	Irrad: Time (MWH)	Thickness (cm)	Density (gm/cm^3)	Neutron Spectrum Peak keV
Si	crystal	2.348	12.2	2.1	1.5	214.3		- (thermal sample)	
Si	crystal	2.348	21.7	2.1	2.5	637.4	1.20	1.06	∿ .7
Ni	sintered	6.44	16.6	1.27	2.1	122.8		- (thermal sample)	
Ni	sintered	6.44	16.6	1.27	2.1	599.9	1.27	1.29	∿1.1
Cr	Cr N powder	2.93	7.0	.8	4.7	155.1		- (thermal sample)	
Cr	Cr N powder	2.96	26.5	1.5	4.7	419.1	1.22	1.06	∿ .7

The large amount of capture in the ^{10}B combined with the nature of the reaction led to sample temperatures the order of 600^{o}C. Heat dissipation was difficult due to the isolation of the sample in the carbon holder and to the insulation caused by the evacuation of the through tube facility; this, both sintered the boron, making dismantling of the samples difficult, and made choices of certain samples impossible.

As shown in figure 4.2 a thin sheet of cadmium was placed on the outside of the through tube prior to its use in this experiment. However, this layer was sufficiently thin that in a short time, the $^{113}Cd(n,\gamma)^{114}Cd$ reaction had proceeded at such a rate as to render the cadmium ineffective in absorbing thermal neutrons. Thus the present experiment was conducted with virtually no cadmium absorbing thermal neutrons and this led to the problem outlined in the previous paragraph.

CHAPTER 5

DATA ANALYSIS

The yield curves obtained for each group of transitions, characterized by a given final state, can provide information about partial and total radiation widths. As shown previously in a schematic way (figure 1·2), each primary transition has a corresponding emission spectrum appearing as a set of resonance multiplets. In order to analyze the yield curves for radiation widths, the gamma ray spectrum must be first corrected for background and detector efficiency. Secondly, a model function, which will be used in the analysis of the yield curves, must be determined for each resonance which leads to observable transitions to final states.

The generation of the model function proceeded via the following steps.

1) A resonance shape was calculated with the use of published values for resonance energy and neutron width; it was determined using the Breit Wigner formula (equation 2·15) with a constant Γ_γ. If published values were not available, energy centroids and resonance widths were computed from the observed data.

2) The resonance shape was multiplied by the flux incident upon the sample (flux distribution times boron filter absorption) and corrected for sample transmittance.

3) The probability spectrum for each resonance was then convolved with the Gaussian response function of the detector.

4) These model functions were then used in least squares analyses of the yield curves at each primary gamma ray energy for the appropriate resonances.

To present the technique of analysis quantitatively, the case of $^{28}Si(n,\gamma)^{29}Si$ will be examined in detail. Three resonances of ^{28}Si at 29, 67 and 173 keV with neutron widths, < 1, 2·2 and 23 keV respectively were treated together and, assuming a common Γ_γ, the radiation cross section computed. The result is illustrated in figure 5·1A. Next, the neutron flux and the effect of sample transmission were included and the result of these factors leads to the curve shown in figure 5·1B. Finally, the effect of finite detector resolution, in this case 12 keV @ 8·5 MeV, was included and this is shown in figure 5·1C. The gamma ray spectrum in figure 5·1C is that which would be observed if all three resonances had the same partial radiation width for the neutron widths specified.

Figure 5.1

This diagram presents the operative factors which contribute to an observed gamma ray spectrum when ^{28}Si is illuminated with reactor spectrum neutrons, filtered by 1.2 gm/cm^2 of ^{10}B. (A) shows the $^{28}Si(n,\gamma)$ cross section under the assumption all resonances have the same Γ_γ. (B) is the (n,γ) reaction rate anticipated when the flux $\Phi(E)$ and the self shielding effects for a typical sample (2.1 cm diameter x 2.5 cm long) are included. (C) is curve (B) with the effect of finite detector resolution (12 keV) included.

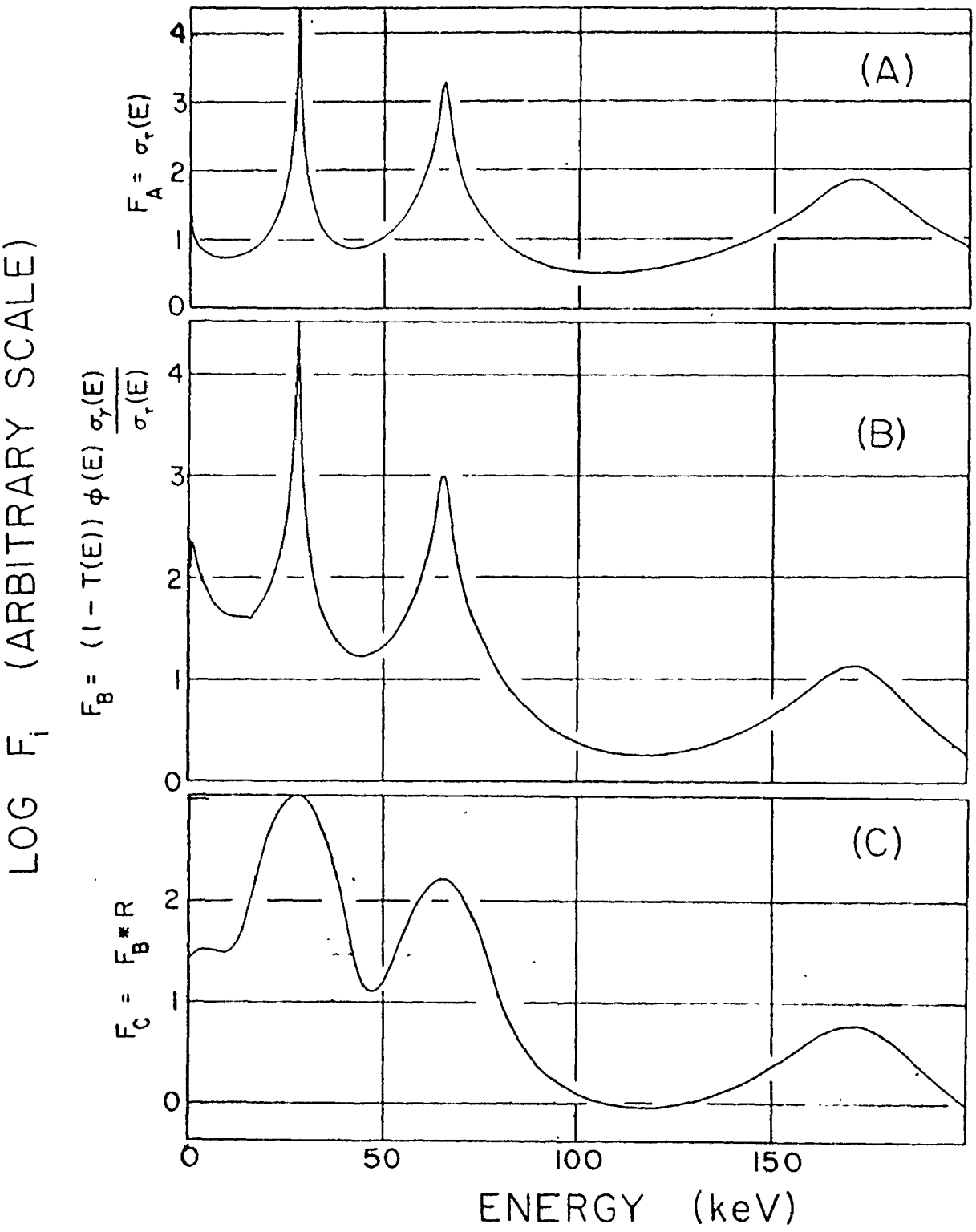
LOG F_i (ARBITRARY SCALE)
$F_A = \sigma_r(E)$
$F_B = (1 - T(E))\,\phi(E)\,\frac{\sigma_\gamma(E)}{\sigma_r(E)}$
$F_C = F_B * R$
(A)
(B)
(C)
0
1
2
3
4
0
50
100
150
ENERGY (keV)

The diagrams in figure 5·1 illustrate the formation of a spectrum for three resonances in ^{28}Si. In the actual analysis a model function for each resonance is calculated. As described in chapter 2 contributions from interference effects due to other resonances are neglected. Thus one can consider the problem to reduce to that of fitting the generated model functions to the observed resonance multiplets. Each amplitude so obtained is proportional to $\Gamma_{\gamma i}$.

In order to generate the model function for each resonance, the formula given in equation 2·14 was used. Here the intensity of gamma radiation to a final state is proportional to $\Gamma_{\gamma i}$ and this quantity is left as a linear, free parameter. Evaluation of equation 2·14 requires knowledge of the sample transmittance

$$T(E) = \int_r \exp\ (-\ N\sigma_T\ (E)\ r)\ P(r)dr\ ,$$

where r must be taken over the entire sample. This integral was determined by the use of the mean chord method and the compilation of Case et al. (1953). For a thin sample with mean chord t

$$1 - T(E) = 1 - \exp\ (-\ N\sigma_T\ (E)\ t)$$
$$\approx N\sigma_T(E)\ t\ .$$

The flux impinged upon the sample is that transmitted by the

^{10}B filter as given in equation 3·3. The Breit-Wigner resonance shape yields a calculated probability spectrum $s_c(E)$ when corrected for sample transmittance and the neutron flux irradiating the sample.

The model function $s_m(E)$ is the convolution of this calculated spectrum $s_c(E)$ and the detector response $r(E)$, where the functions are energy dependent. Thus,

$$s_m(E) = \int_{-\infty}^{\infty} r(E')\ s_c\ (E-E')\ dE' \quad .$$

This convolution of the response function represents a large computational effort; therefore, substitution of multiplication for convolution via the fast Fourier transform τ was developed. Then,

$$S_m = \tau\ (s_o(E)) \ ;\ R = \tau(r(E)) \ ;\ S_c = \tau(s_c(E)) \text{ and}$$

$$S_m = R \cdot S_c \quad .$$

The inverse transform is taken to obtain $s_m(E)$.

Due to the complexity of generating even an individual resonance spectrum, resonance parameters were difficult to obtain by standard non-linear techniques. Rather, estimates of the parameters were made and an error surface evaluated by varying the quantities in question and the minimum was sought. Energy centroids for resonances were found using the

first moment; then E_R remained fixed while Γ_n was varied. Figure 5·2 shows how $\chi^2/_f$, the normalized weighted residual squared, varies with Γ_n for the 67 and 173 keV resonances of ^{28}Si. Although the minimum in these curves appears to be 'sharp', the error in the resolution function associated with the detector provides large uncertainties.

As mentioned earlier a spectrum for each resonance observed in transitions to final states was generated. The amplitude of each of these resonances for a particular transition is proportional to $\Gamma_{\gamma i}$. These amplitudes were found by fitting model functions to the data using least squares techniques. When the value of Γ_n was less than 1 keV, the value of $\Gamma_{\gamma i}$ obtained by the ~~data~~ fitting routine was insensitive to changes in Γ_n, i.e. for 10 eV $< \Gamma_n <$ 1 keV, the value of $\Gamma_{\gamma i}$ may vary 10%. Thus, values of $\Gamma_{\gamma i}$ can be obtained without too large an error for an unknown Γ_n when Γ_n is much less than the resolution width.

Before analysis the data were corrected for detector efficiency and background was subtracted. Nitrogen, in the form of melamine, was used as a gamma ray source for intensity calibration of the pair spectrometer. Known intensities and energies for nitrogen capture gamma rays (Be 71) were used to obtain a relative efficiency curve as shown in figure 5·3.

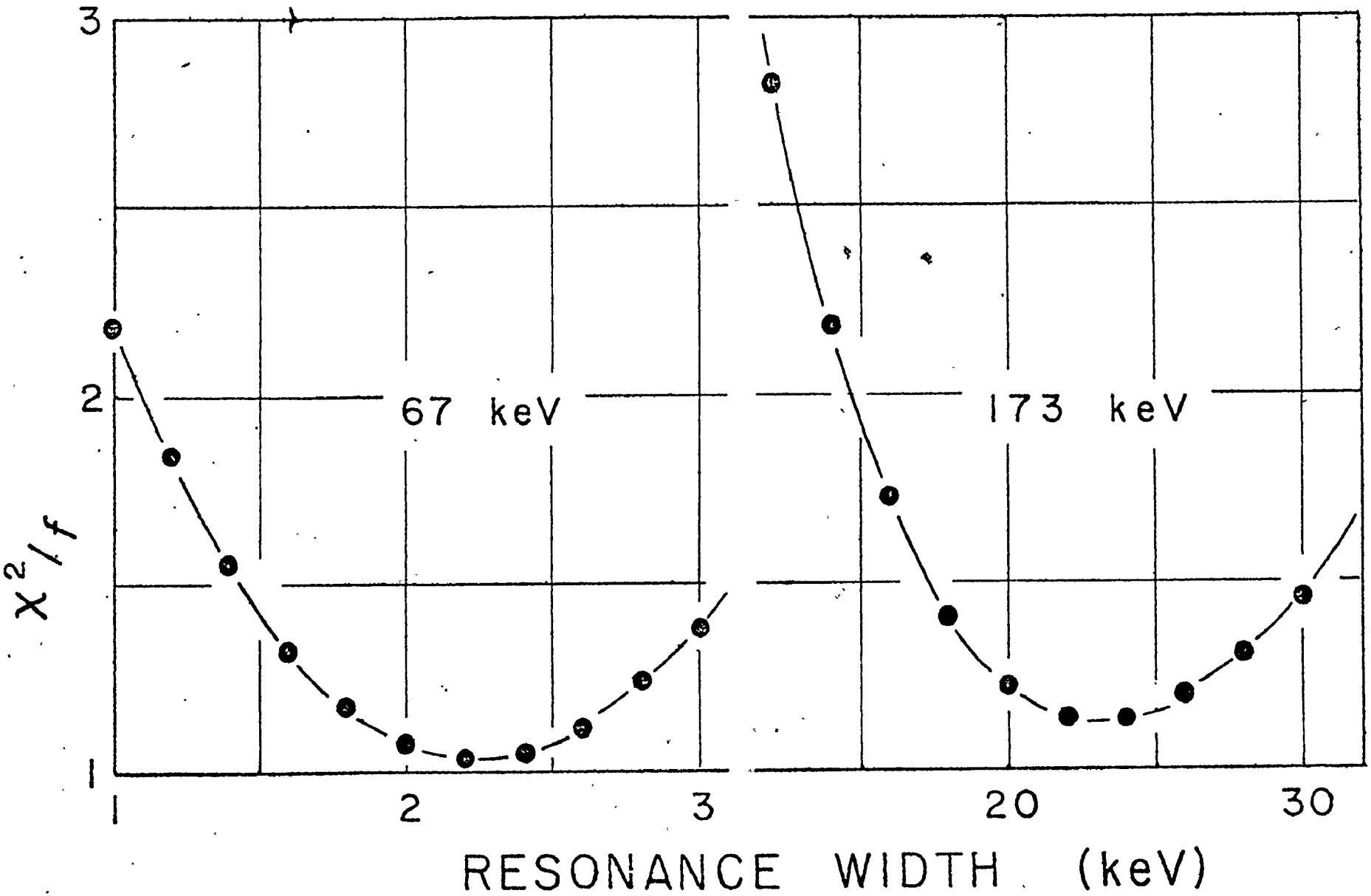

Figure 5.2 The agreement of fit achieved when equation 2·14 is computed using a single level Breit-Wigner resonance shape and the result convolved with the detector resolution. The normalized residual χ^2/f has a well defined minimum with an ordinate at that point in goo agreement with the expectation value of 1. The assignment of error in resonance width wa extracted from curves such as these.

Figure 5.3 A relative efficiency curve for gamma ray detection in the pair productive mode for the Ge(Li) - NaI(Tℓ) spectrometer.

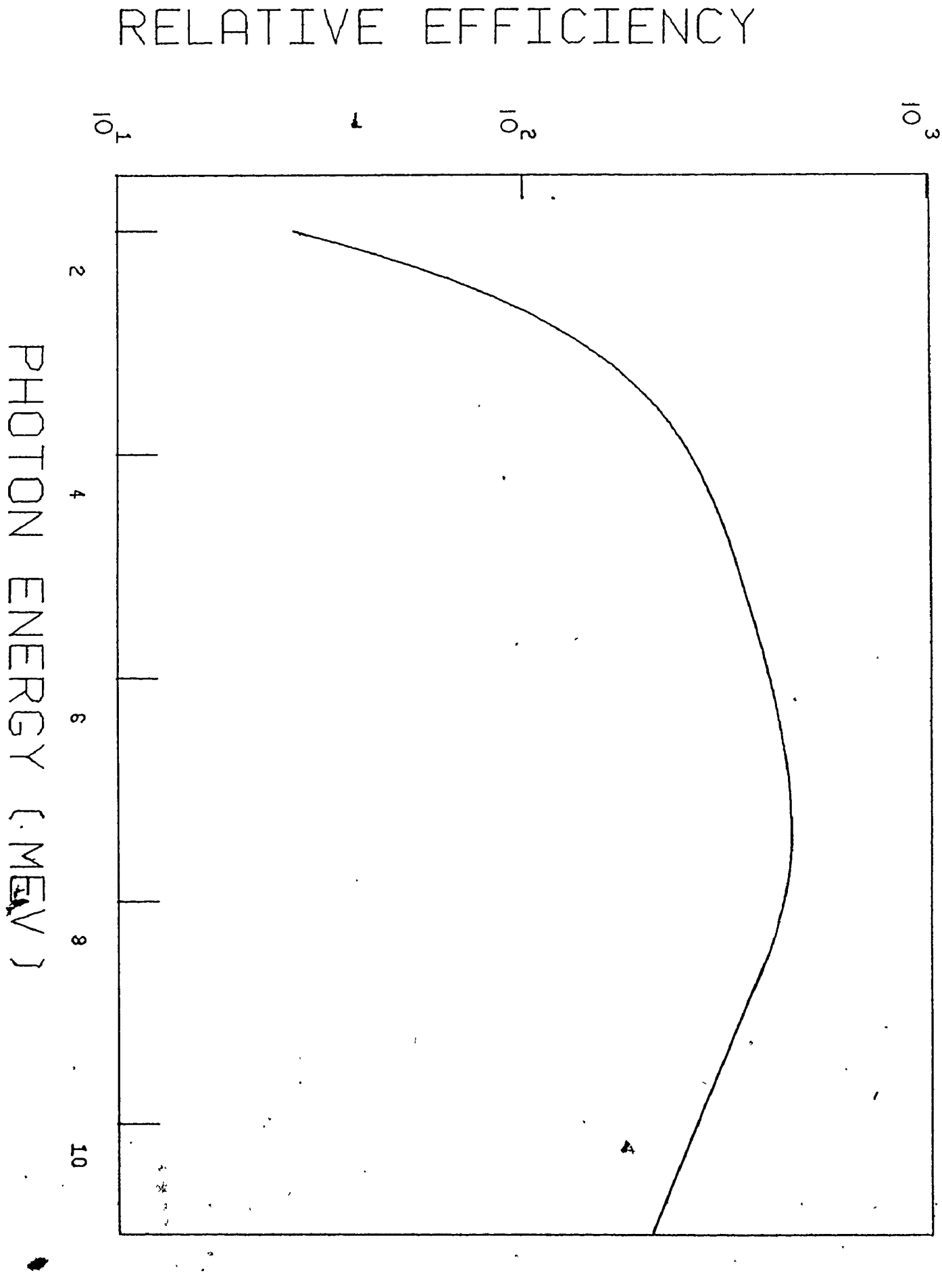

Figure 5.4 A typical nitrogen thermal neutron capture spectrum used to obtain the relative efficiency curve in figure 5.3.

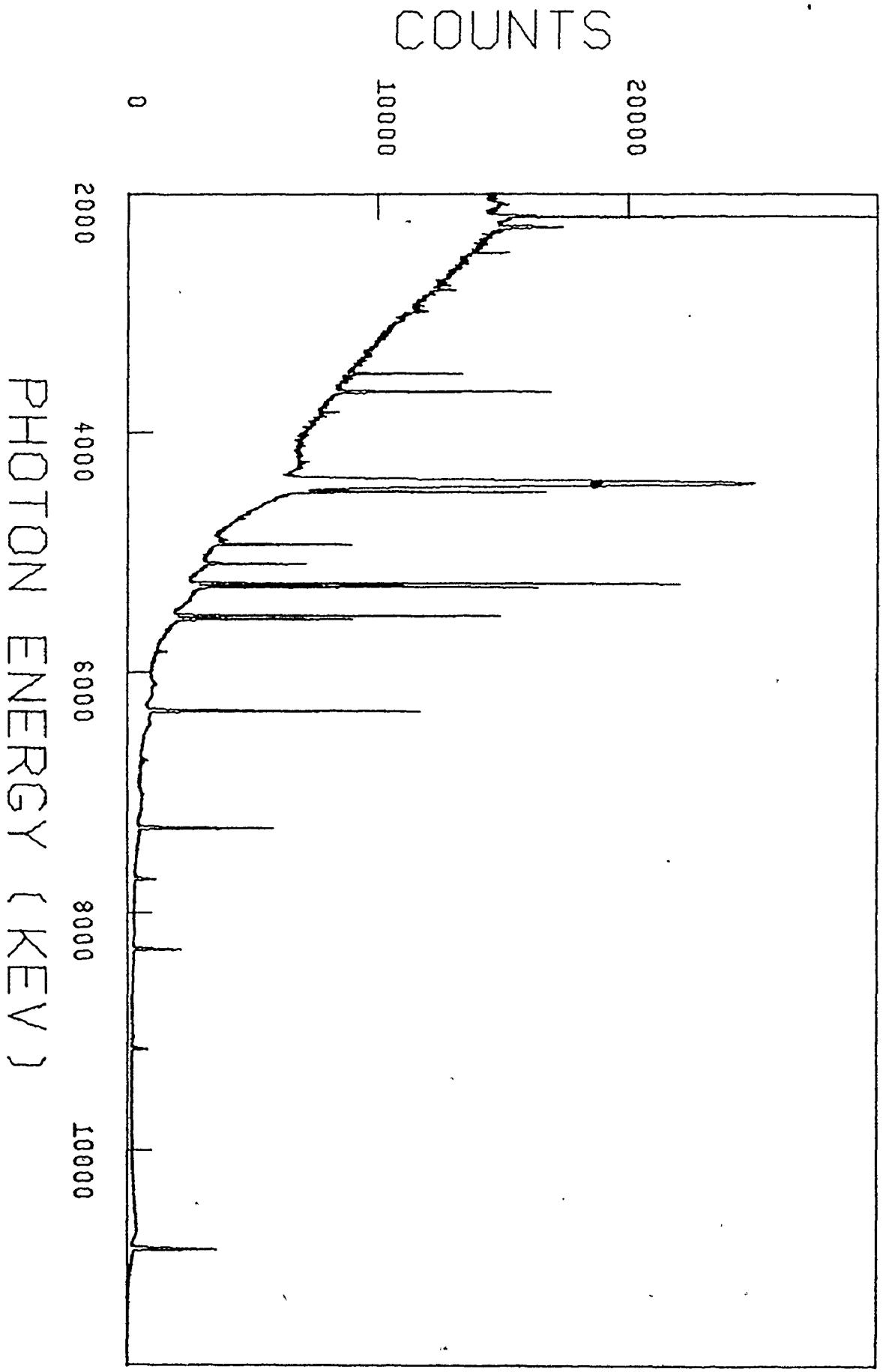

In figure 5·4 is shown the nitrogen capture spectrum.

Fitting the background of a gamma ray spectrum followed a four step process. 1) Throughout the spectrum, each point whose nearest neighbours were within one standard deviation was labelled as a background point. 2) A least squares polynomial fit was performed on these labelled points to obtain an estimate of the background. 3) A better representation of the background was obtained by choosing all the points below the estimate evaluated in step 2) and also those points within one standard deviation above the estimate. 4) A new least squares polynomial fit was performed on these points to obtain a final estimate for the background of the spectrum. This final background was subtracted from the data in preparation for analysis.

It should be pointed out that the difference between the photon energy of a transition to a given final state following resonance neutron capture and that for the corresponding transition following thermal neutron capture is the centre of mass kinetic energy of the neutron captured. Thus resonance energies which were measured in the present work are quoted in centre of mass energies. Energies may be transformed from the laboratory system to the centre of mass system by the following formula

$$T_{cm} = T_{lab} / (1 + \frac{m_n}{M})$$

where m_n is the mass of the neutron and M is the mass of the target. The resonances in ^{28}Si quoted here at 67 and 173 keV are measured in the centre of mass system; they correspond to resonances at 67·7 and 180 keV as observed by Allen and Macklin (1973) which, when transformed to the centre of mass system, become 65·4 and 174·4 keV.

It should also be noted that in this work the resonance energies are determined by a measurement of the difference in centroids between the resonances in the yield curve and the thermal peak measured with the system having the same gain. The resonance energies so determined do not, therefore, depend on an absolute measurement of the total transition energy.

CHAPTER 6

EXPERIMENTAL RESULTS

In this study resonance capture for silicon, chromium and nickel isotopes was conducted. In this work we measured relative partial radiation widths (table 3) for transitions to final states from neutron capture in resonant states. The normalization of partial radiation widths was such that measurements are not only comparable for transitions from the same resonant state but also for transitions from different resonant states. While relative measurements were obtained, attempts have been made to put the radiation widths in absolute units (eV) by normalizing the results to previous data. Values quoted for chromium and nickel isotopes were normalized from published total radiation widths (St 71); the absolute values given for the silicon isotopes were obtained by normalizing the sample size and irradiation time of the silicon isotopes to those of ^{52}Cr. The errors quoted in table 3 are those obtained for relative radiation widths; for comparison to absolute values, the measurements may have much larger systematic errors. Resonance values listed for silicon are centre of mass energies determined in this work, while the energies listed

for chromium and nickel are from data measured in the laboratory system (BN 73, St 71, Ga 71).

Gamma ray spectra for both thermal and keV neutron capture are shown for silicon, chromium and nickel in figures 6·1A, 6·1B; 6·2A, 6·2B; 6·3A, 6·3B respectively. Background lines occur in neutron capture spectra from two processes, neutron capture (n,γ) and inelastic scattering (n,n'). Gamma ray peaks from sources other than the sample assembly have been reduced by the collimation in the through tube. A spectrum of this background, in figure 6·4, shows gamma peaks for neutron capture in aluminum and hydrogen. The aluminum peak is from capture in the through tube material. The hydrogen peak is from capture in the pool water. This is direct radiation from pool water outside the tube at its ends and/or radiation reflected down the through tube. Background lines also arise from the carbon of the sample assembly, the aluminum of the chain used to lower the assembly and the boron used to surround the sample in keV neutron irradiations. A spectrum obtained by irradiating a sample of ^{10}B in a carbon assembly is shown in figure 6·5. A list of the energies of the background lines which occur is given in table 2. Only in the case of silicon irradiations did inelastic scattering peaks appear which were due to

Figure 6.1A The thermal neutron capture spectrum obtained for silicon.

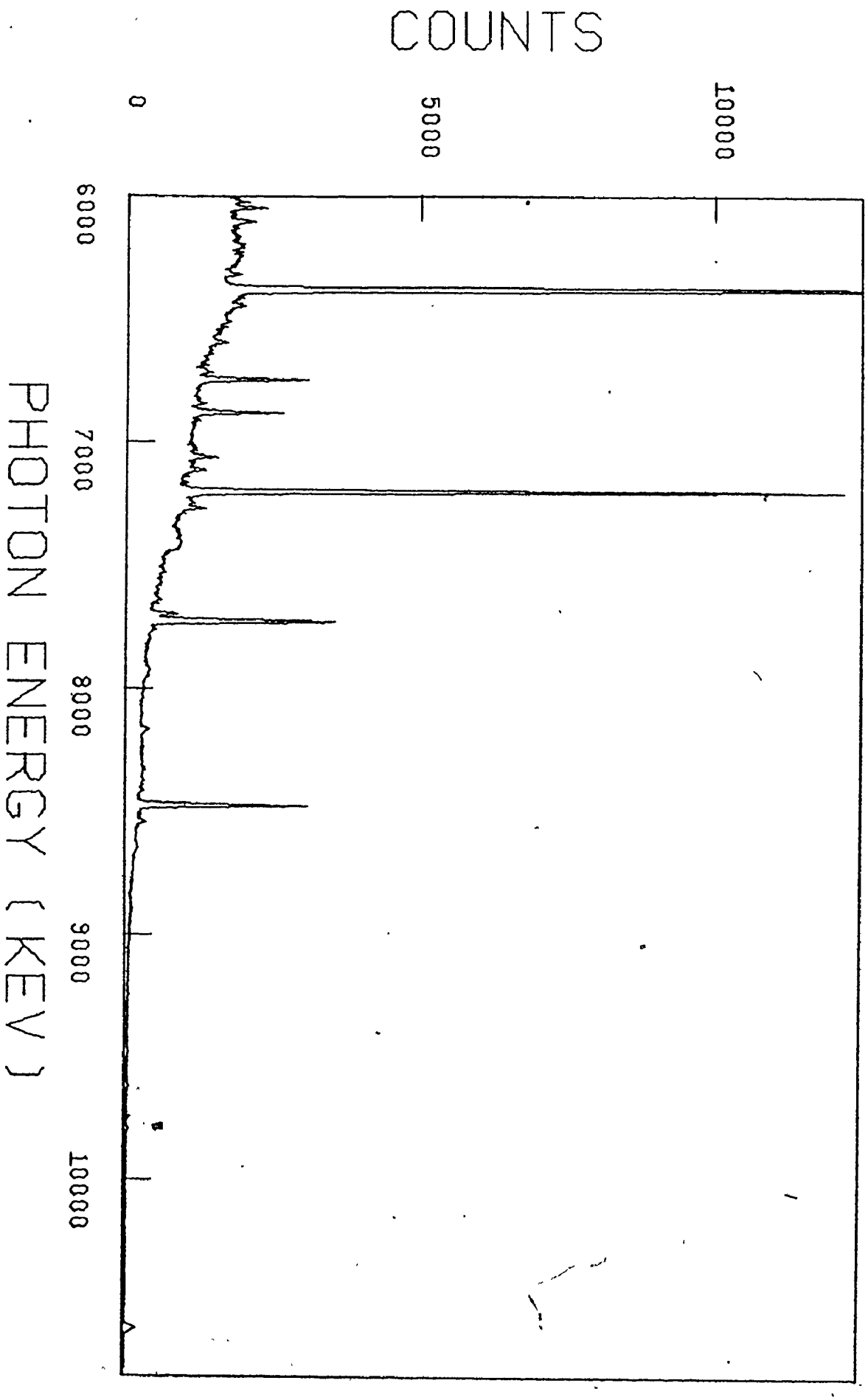

Figure 6.1B The keV neutron capture spectrum obtained for silicon.

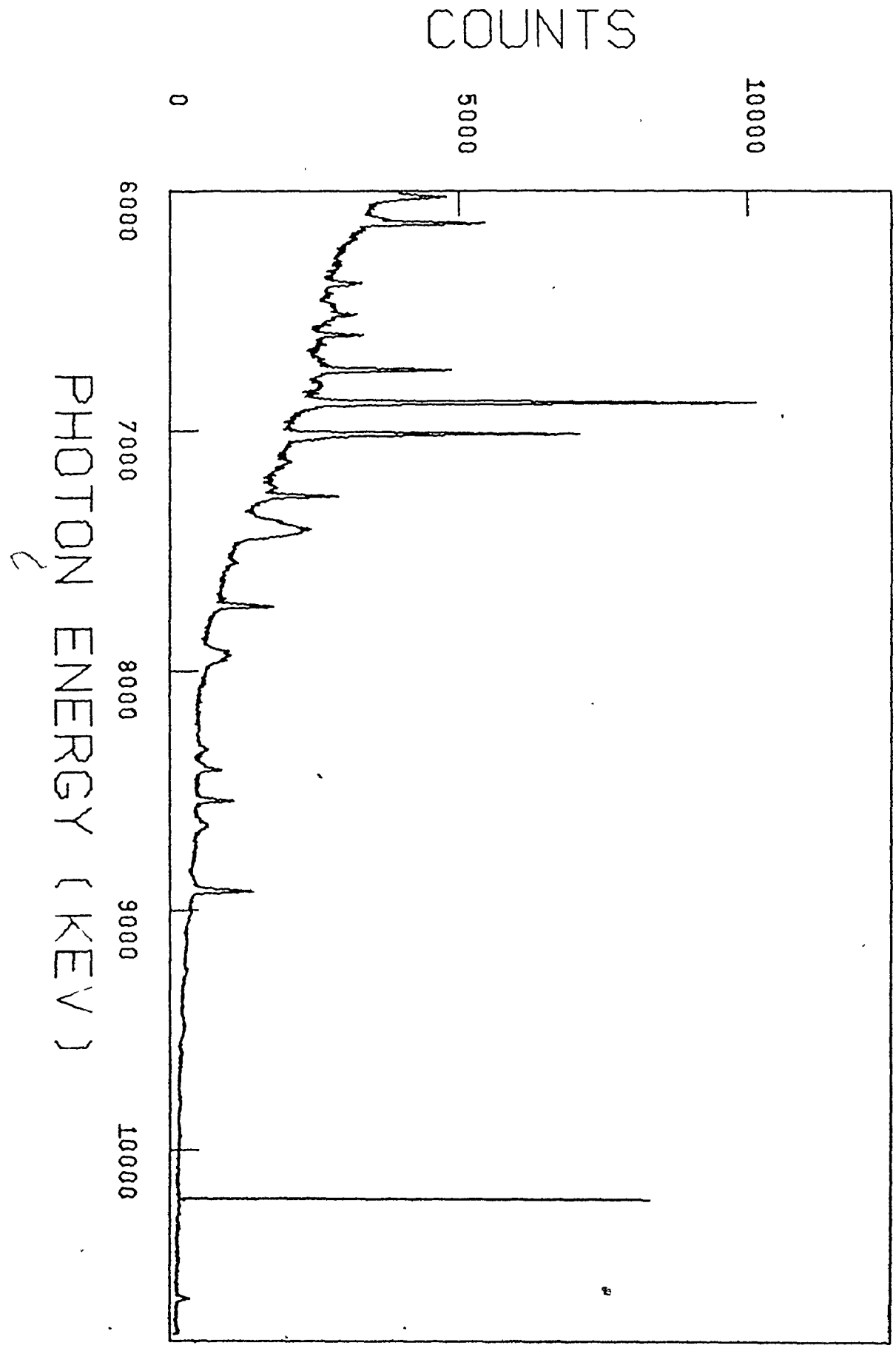

Figure 6.2A The thermal neutron capture spectrum obtained for chromium.

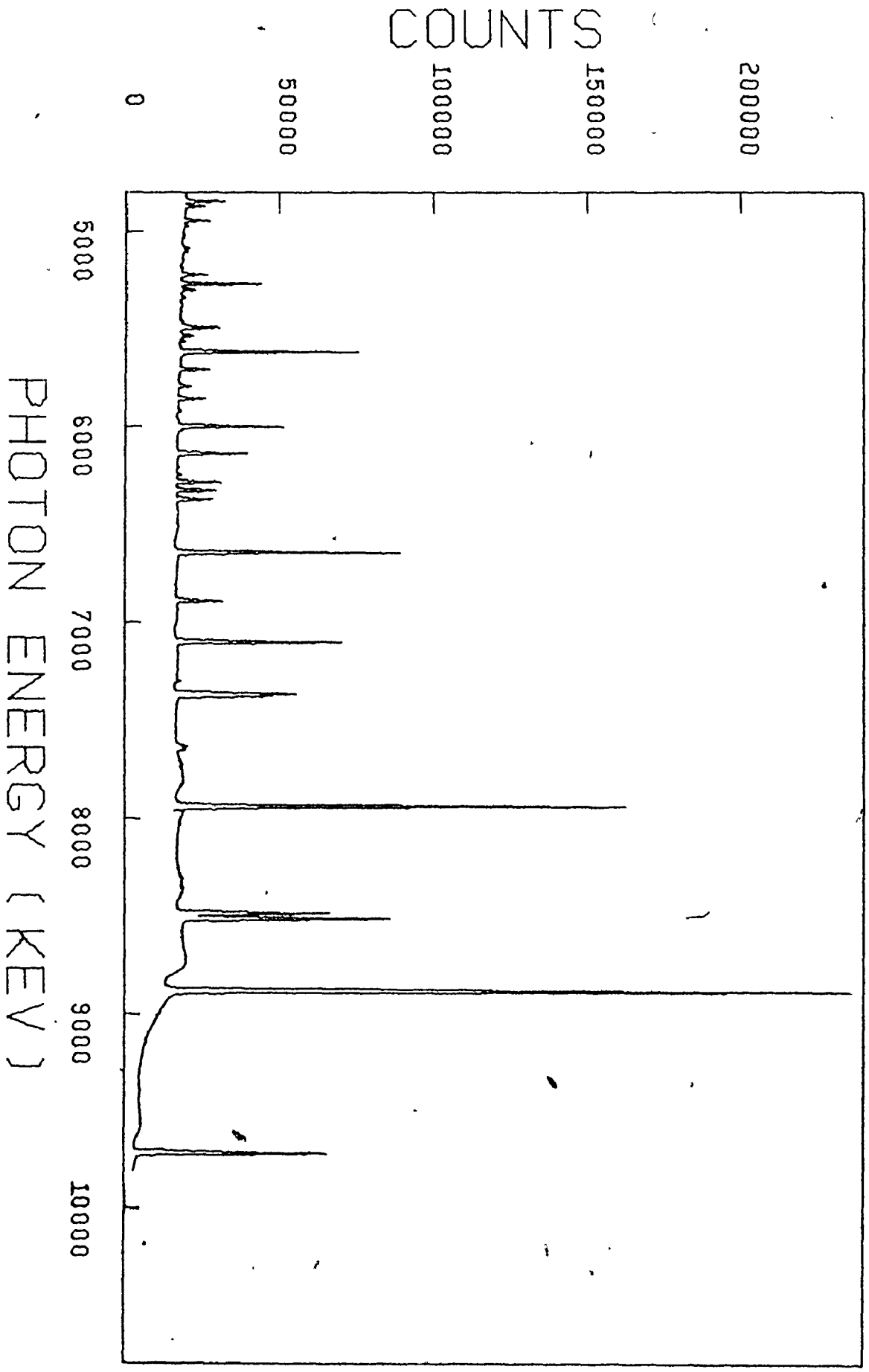

Figure 6.2B The keV neutron capture spectrum obtained for chromium.

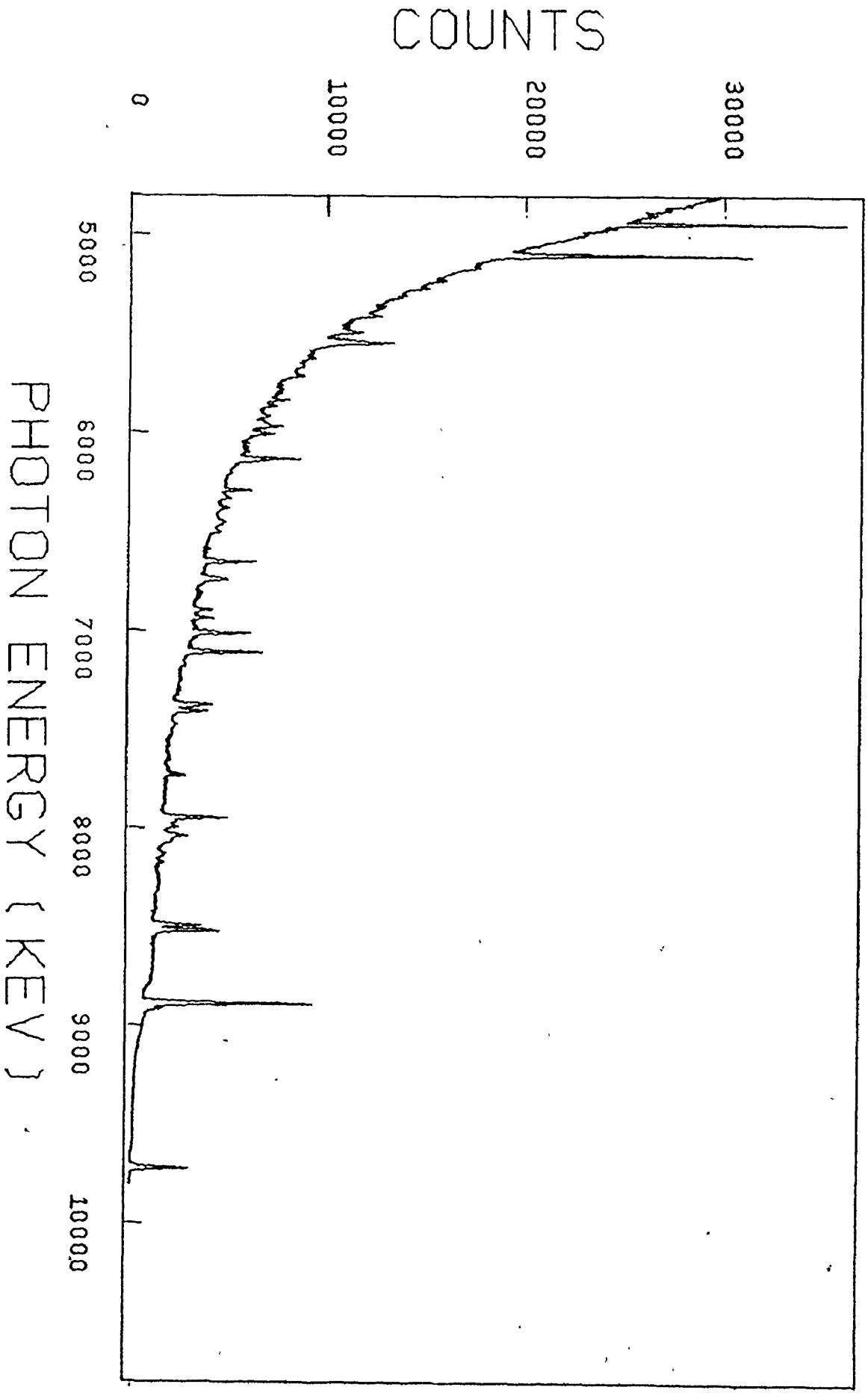

Figure 6.3A The thermal neutron capture spectrum obtained for nickel.

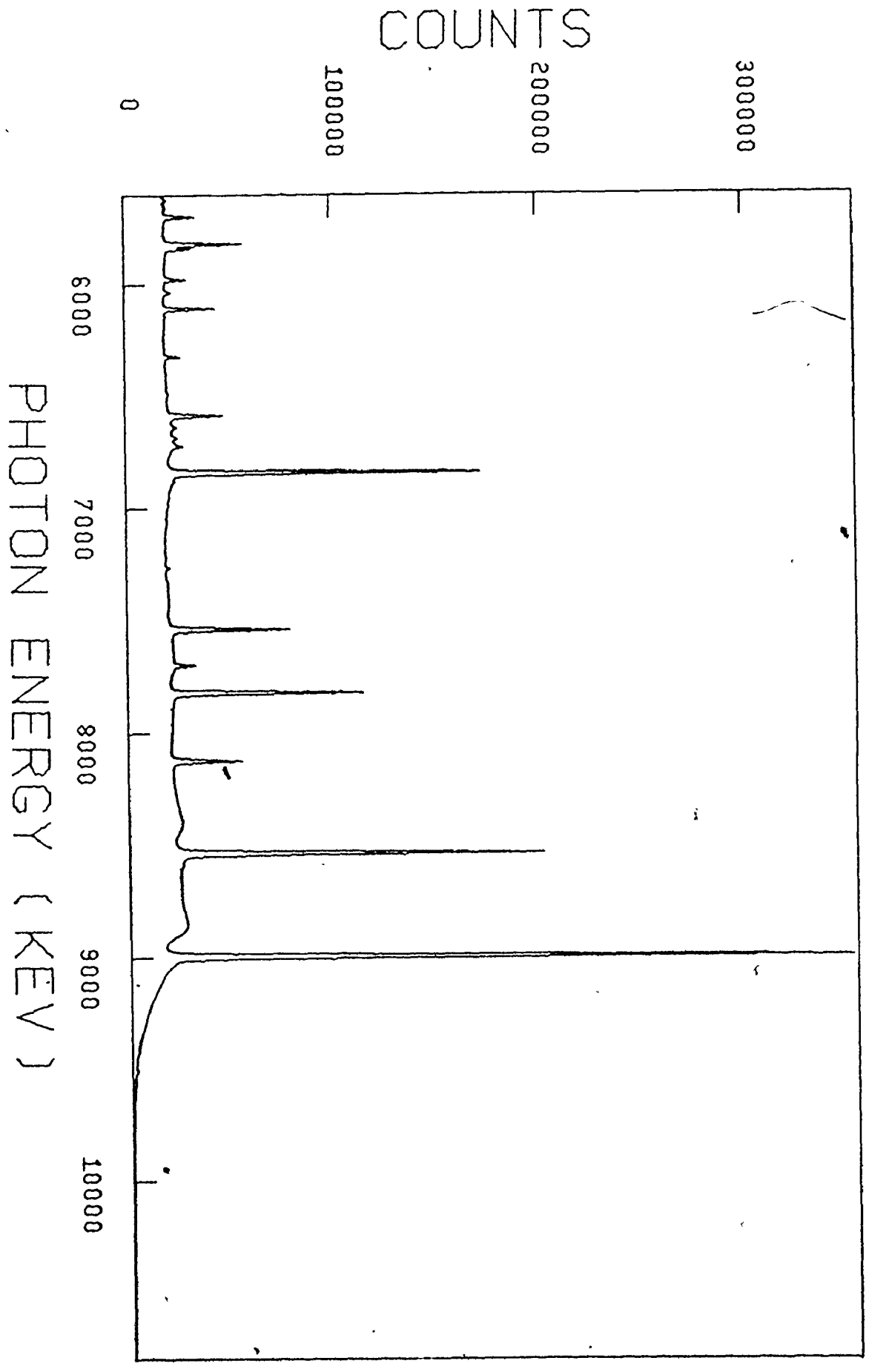

Figure 6.3B The keV neutron capture spectrum obtained for nickel.

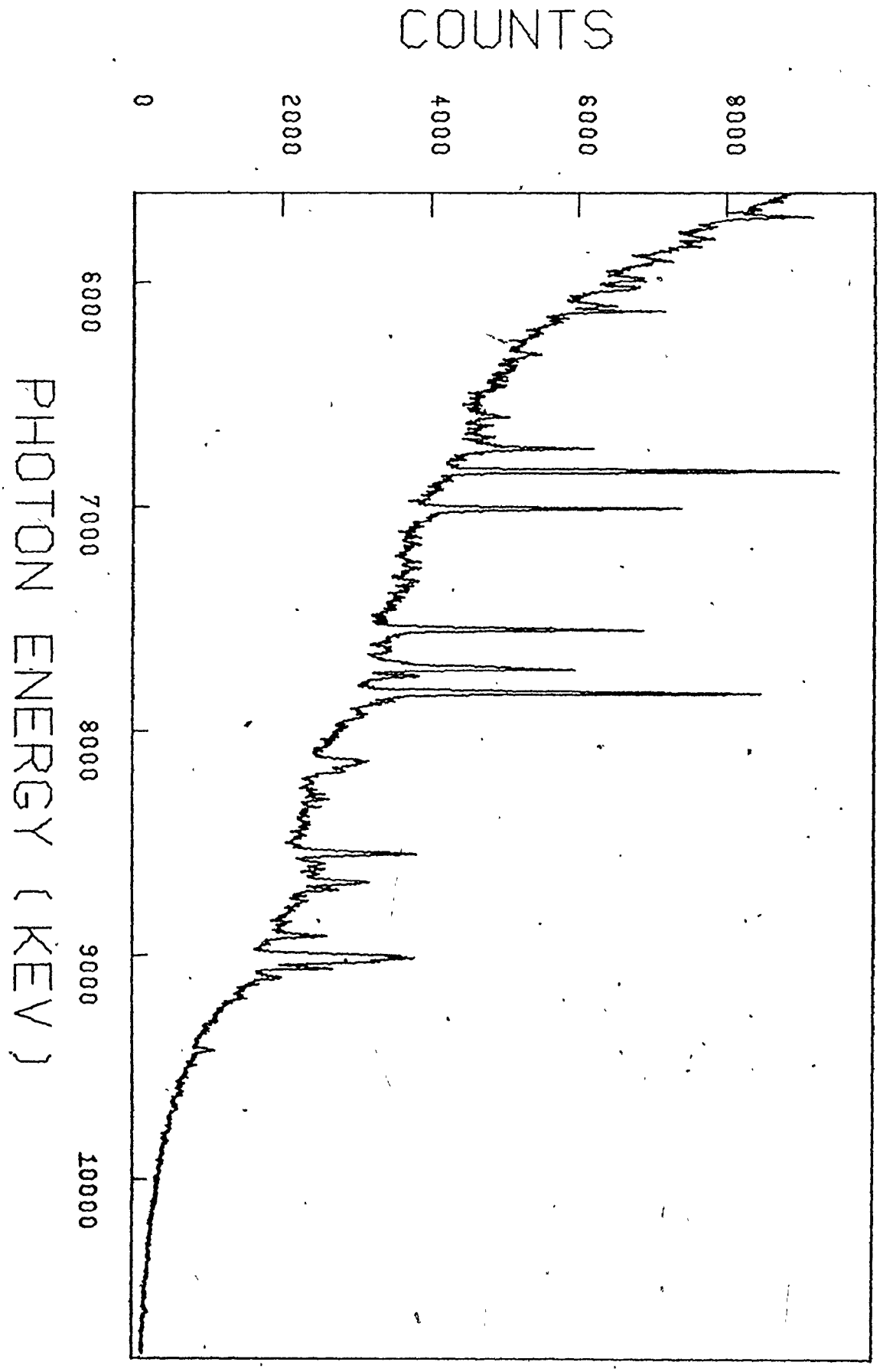

Figure 6.4 The background observed in the through tube with no sample present. Normalized to 100 MWH.

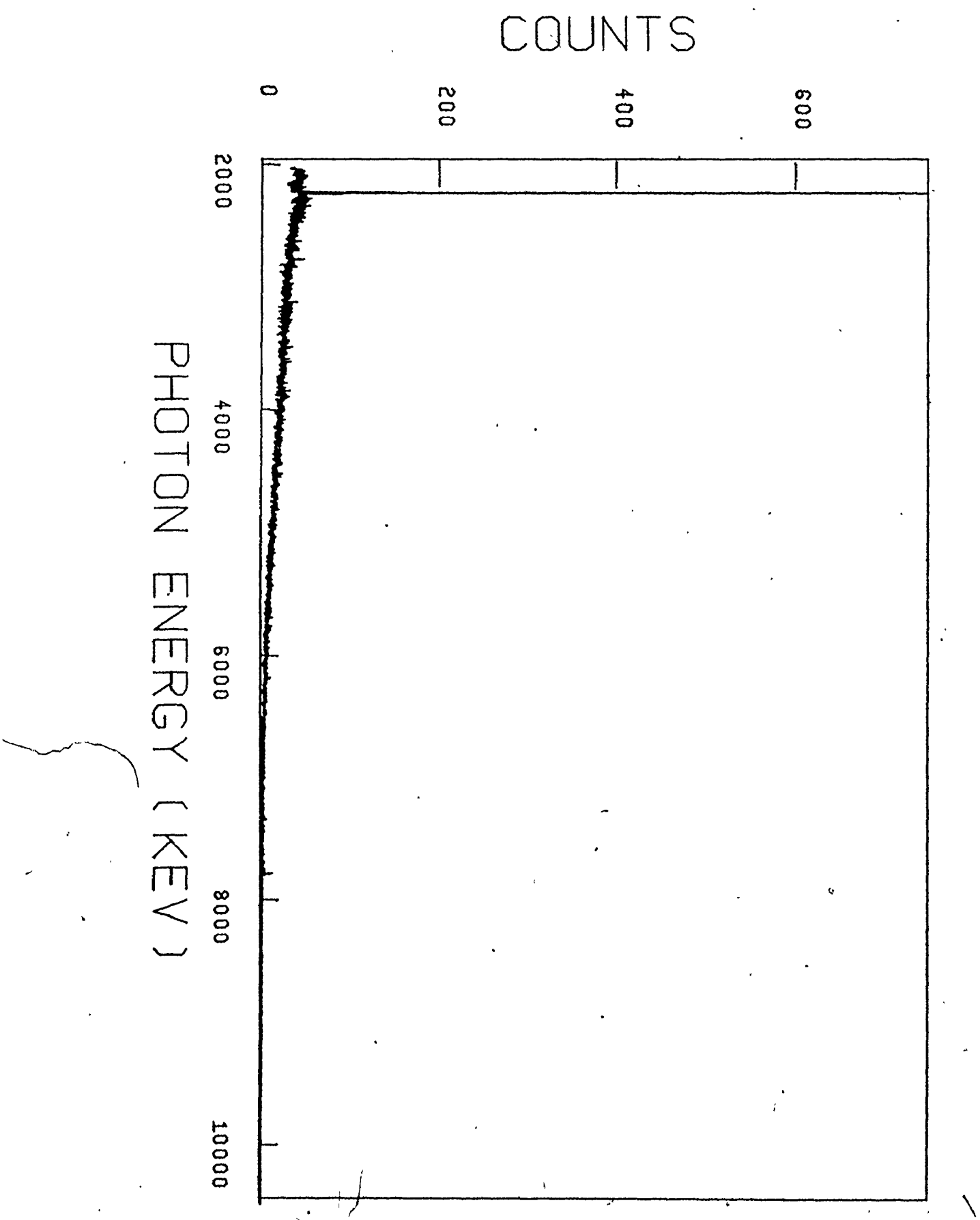

Figure 6.5 The spectrum obtained for irradiation of ^{10}B in a carbon sample assembly. Normalized at 100 MWH.

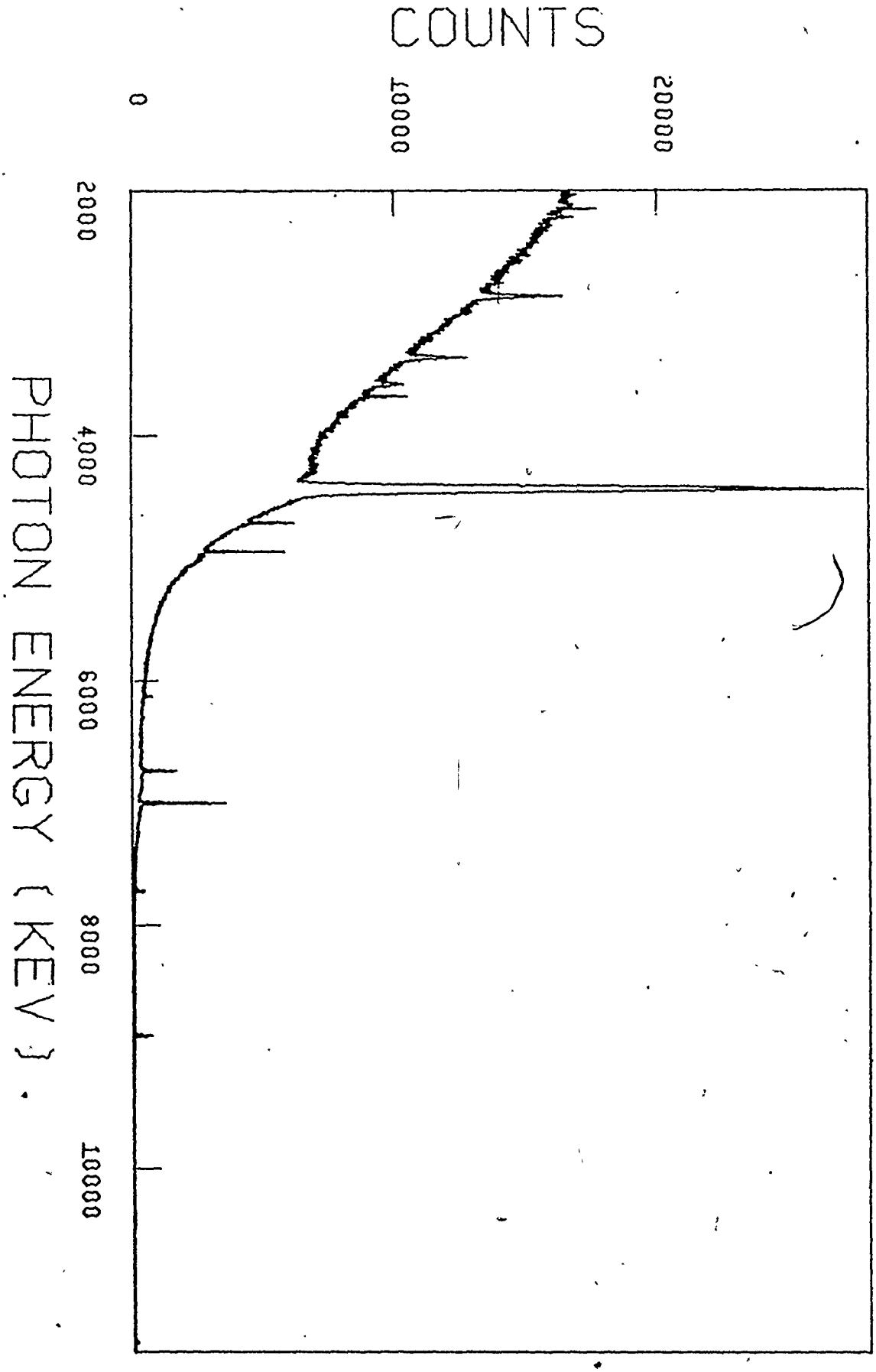

TABLE 2

Background Gamma Peaks[a]

Reaction	Gamma Ray Energy (keV)	Reference
$^{27}Al(n,\gamma)^{28}Al$	7723.8	(Ra 71)
$^{12}C(n,\gamma)^{13}C$	4945.2 3683.9	"
$^{12}C(n,n')^{12}C$	4433.	(La 61)
$^{12}C(\alpha,\gamma)^{16}O$	6130.	"
$^{11}B(n,\gamma)^{12}B$	3368.	"
$^{10}B(n,\gamma)^{11}B$	11447. 8916. 7006. 6739. 4711. 4444.	(Th 67)
$^{10}B(n,n')^{10}B$	3584. 2868. 2151.	(La 61)
$^{1}H(n,\gamma)^{2}H$	2223.	(Ra 71)

[a] A list of some of the prominent gamma ray peaks which appeared in the background during neutron irradiation.

scattering in the target itself.

The differences in the characteristics between the thermal and keV capture spectra can be seen in figure 6·6. Some of the principal features are: 1) The thermal capture spectrum (curve A) has a flat background with increasing energy while the corresponding keV capture spectrum (curve B) has a steep sloping background which decreases with increasing energy. 2) There is an absence of any thermal capture primary gamma rays from the sample surrounded by ^{10}B in the keV neutron capture spectrum (curve B). 3) The overall lower background in the keV capture spectrum compared to the thermal capture spectrum, especially above the $^{12}C(n,n')^{12}C$ gamma ray peak at 4·4 MeV.

Silicon

In figure 6·7 is shown the yield curve for the transition to the $1/2^+$ ground state of ^{29}Si following capture by ^{28}Si, for which the thermal line is at 8471.8±1 keV (Ly 67). The yield curve exhibits maxima at 67 and 173 keV. No transition from the 29 keV resonance was observed.

In figure 6·8 can be seen the variation in gamma ray yield for the transition to the $3/2^+$ first excited state in ^{29}Si at 1273 keV. This transition is observed to have resonances at 29 and 67 keV. Any contribution of the

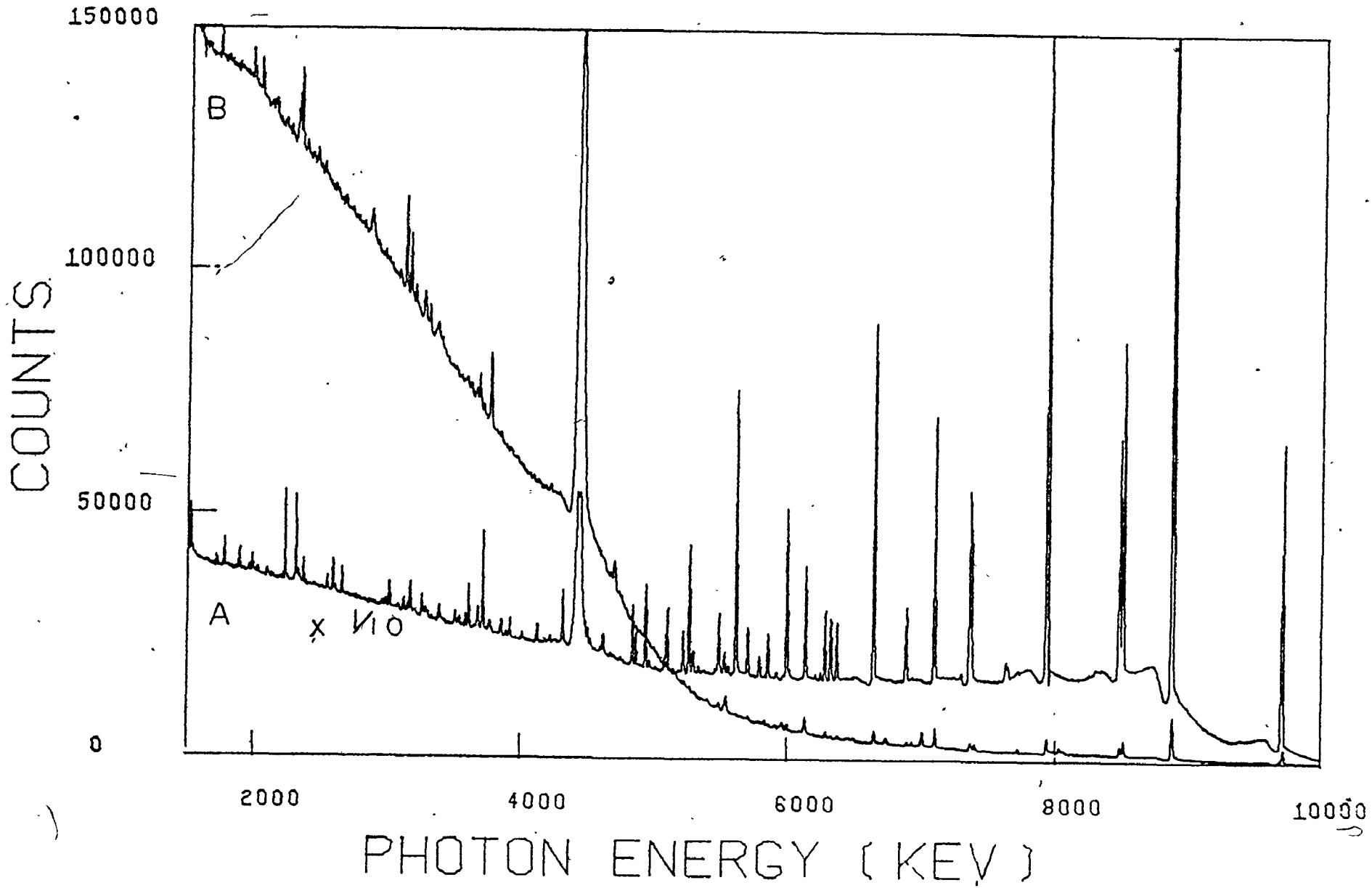

Figure 6.6 The thermal (curve A) and keV (curve B) neutron capture spectra obtained for chromium.

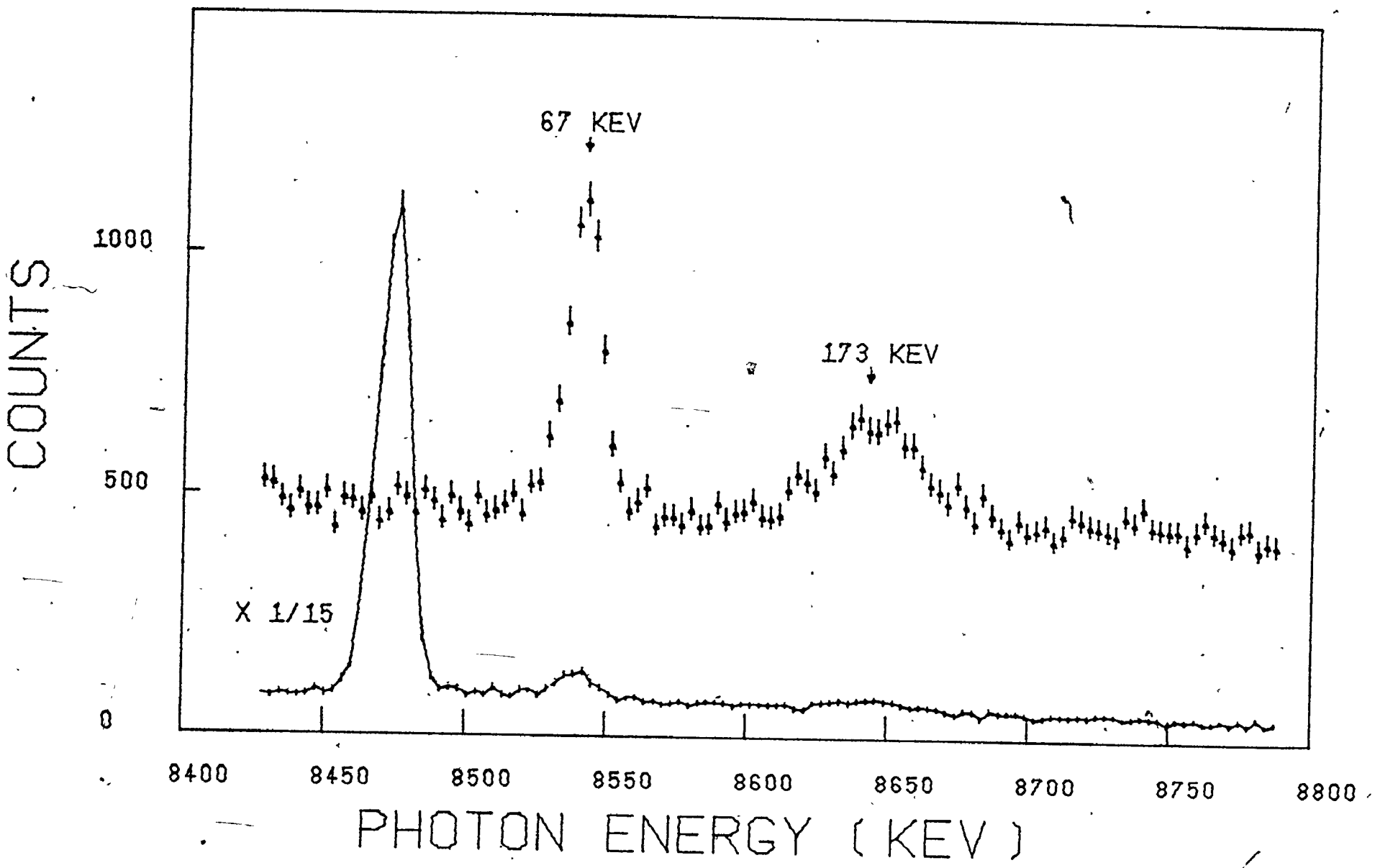

Figure 6.7 The solid curve indicates the thermal neutron capture gamma ray spectrum for $^{28}Si(n,\gamma)^{29}Si$ in the region of the 8472 keV ground state transition. The points show the spectrum obtained when the boron filter is used and here the 67 and 173 keV resonances are clearly evident.

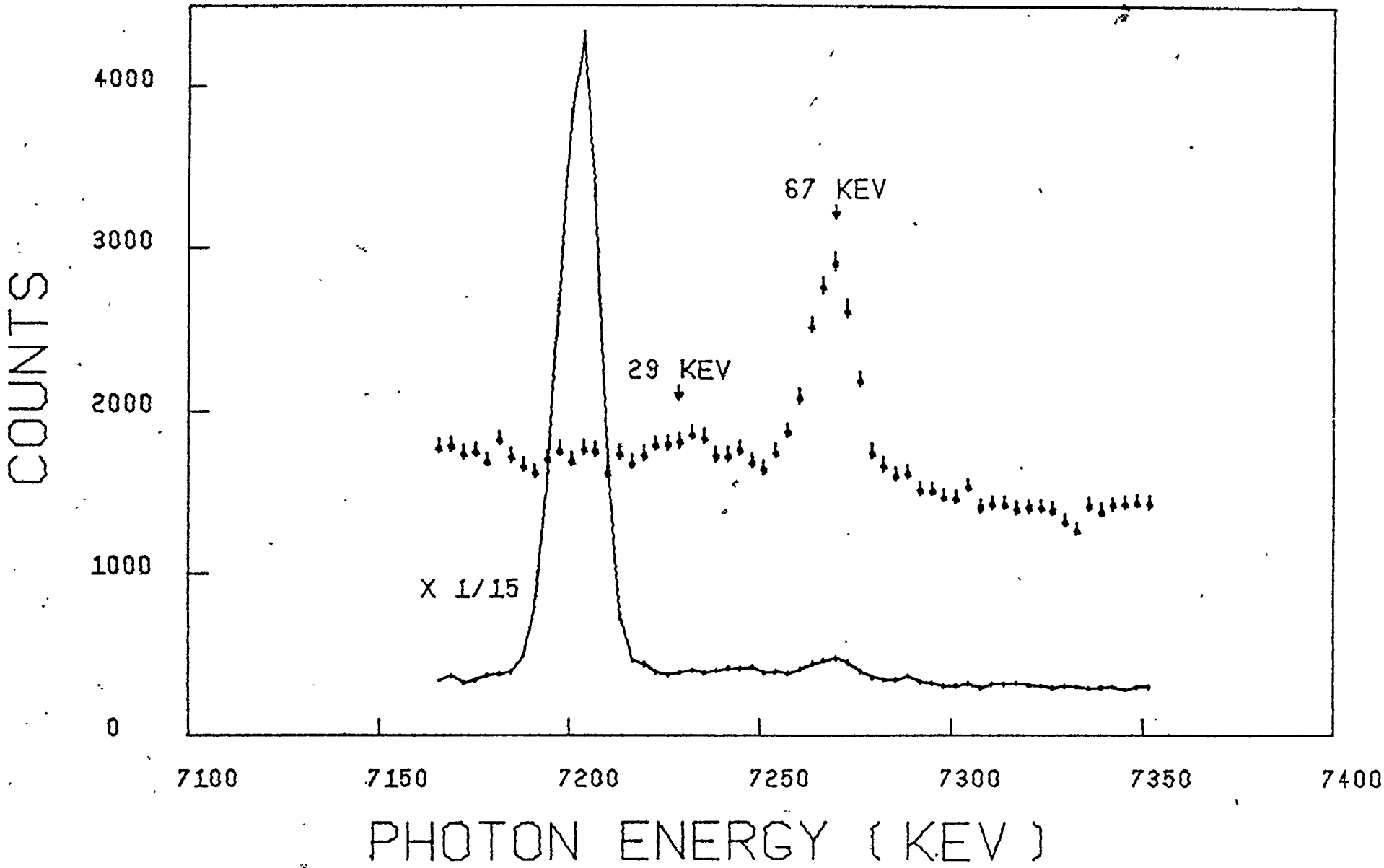

Figure 6.8 The solid curve is the thermal capture spectrum and shows the $^{28}Si(n,\gamma)^{29}Si$ transition to the 1273 keV first excited state. The points representing the yield curve when a boron filter is used, show the 29 and 67 keV resonances.

transition from the 173 keV resonance cannot be ascertained due to interference in this region from neutron inelastic scattering (Ni 72).

The resonance spectrum for the transition to the $5/2^+$ state at 2028 keV in ^{29}Si, as shown in figure 6·9, indicates the presence of the 67 and an 85 keV resonance. Interference from $^{28}Si(n,n')^{28}Si$ transitions (Di 70) occurs in the region near a possible transition from the 29 keV resonance. A peak is observed at the correct energy. Identification as a transition from the 29 keV state cannot be conclusive, since it is possible that the inelastic peak reported at 6481 keV (Di 70) may be an unresolved doublet. No significant contribution from the 173 keV resonance was observed.

The yield curves for the transitions to the ground state and first two excited states at 2236 and 3498 keV in ^{30}Si, both $J^\pi = 2^+$, were also determined. The yields for the two excited states exhibit resonances at 16 ± 1 and 35 ± 1 keV. The spectrum for the first excited state is shown in figure 6·10. No measurable intensity was observed for the decay of the 35 keV resonance to the ^{30}Si ground state.

Only one transition to the ground state in ^{31}Si

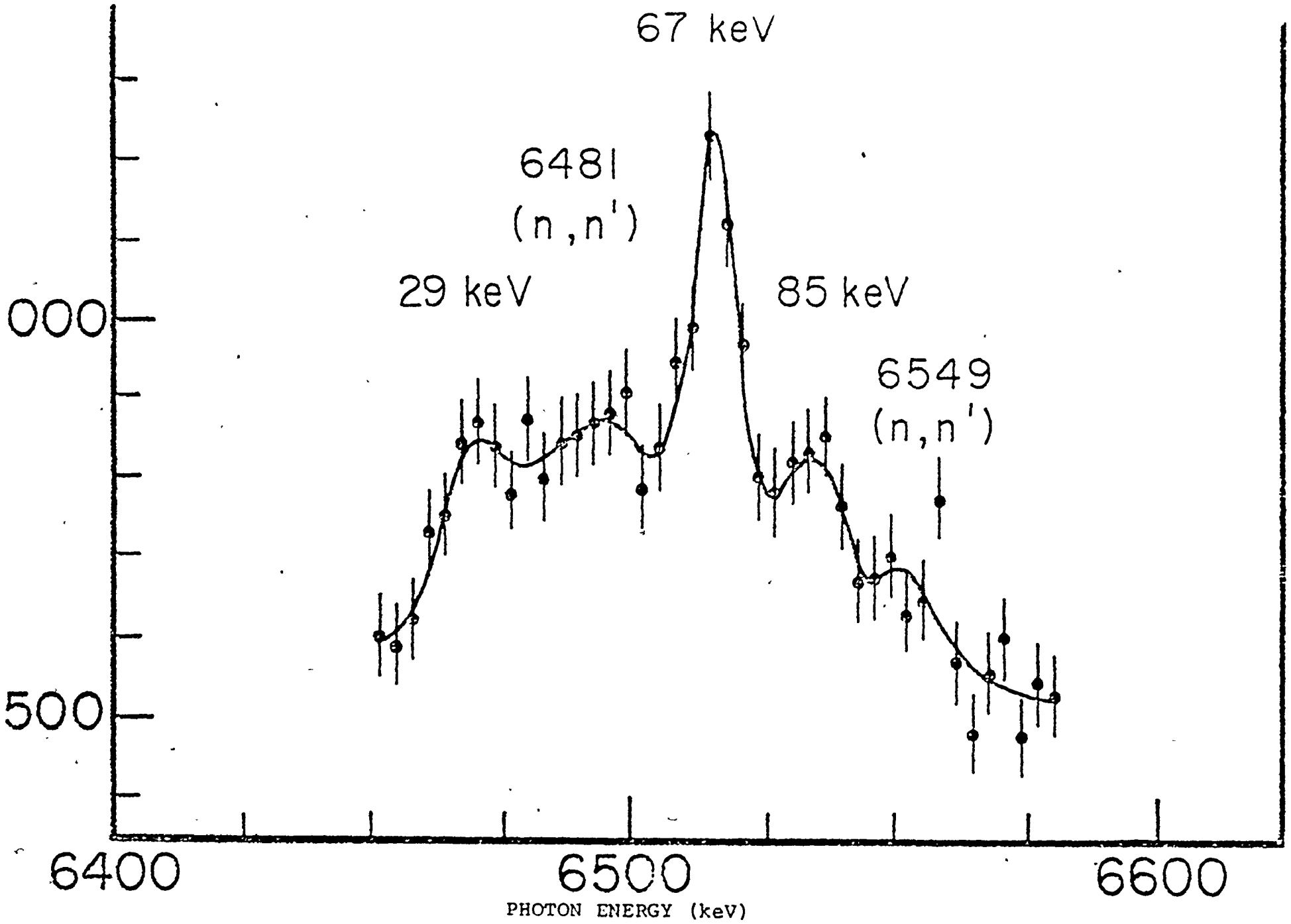

Figure 6.9 The keV neutron capture spectrum for the transitions to the $^{5}/_{2}^{+}$ state at 2028 keV in ^{29}Si is shown. Note the interference due to gamma rays following inelastic scattering from ^{28}Si.

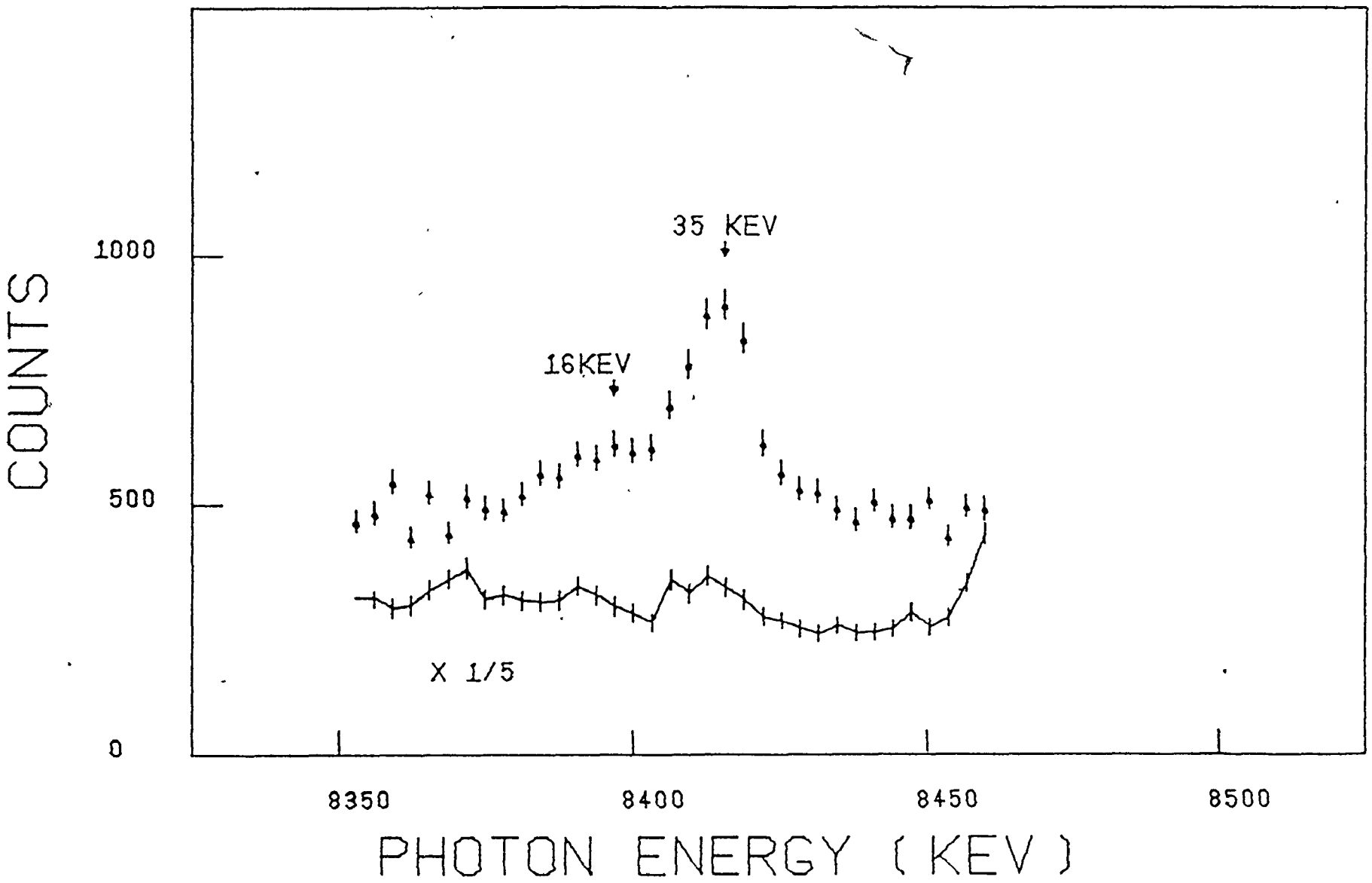

Figure 6.10 The yield curves for the transitions to the first excited state in the $^{29}Si(n,\gamma)^{30}Si$ reaction. Thermal capture (solid curve), keV capture (points).

was observed and this was from a single resonance at 2·2 keV.

Resonance parameters determined from the yield curves for the silicon isotopes are given in table 3A. The errors quoted for the observed neutron widths include uncertainties in the resolution function. Partial radiation widths are quoted in eV and given as a function of a $g\Gamma_{\gamma i}$. As mentioned previously the results of Si were normalized for sample sizes and irradiation times to ^{52}Cr results.

Chromium

Yield curves were obtained for transitions to the first and second excited states at 749 ($^3/_2^-$) and 777 ($^1/_2^-$) keV in ^{51}Cr for a single resonance at 5·64 keV in ^{50}Cr. No yield curve was detected for a transition to the $^7/_2^-$ ground state for which the Q-value is given as 9263·9 keV (ND 70). Resonance spectra were also obtained for transitions to levels in ^{51}Cr at 1899, 2890, 3126, 3767, 3771 and 4040 keV.

In figure 6·11 is shown the spectrum for transitions to the $^3/_2^-$ ground state in ^{53}Cr following capture in ^{52}Cr. Maxima were observed corresponding to resonances at 1·6, 22·9, 27·6, 50·2, 96·2, 121·4, 141·3, 194 ± 1 and 235·8 keV. Also a broad, unresolved maximum was observed from 280 to 380 keV in the resonance spectrum of transitions

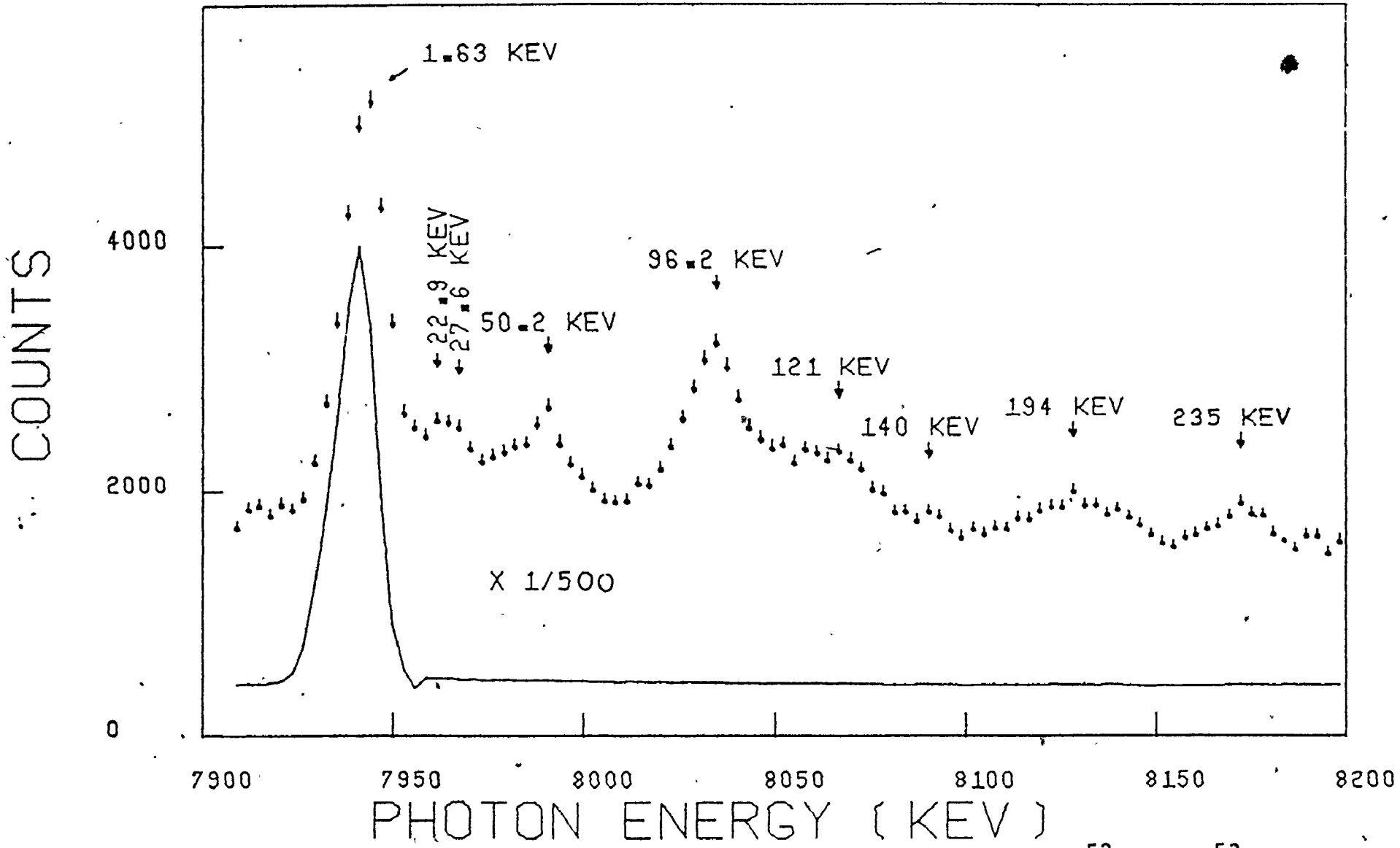

Figure 6.11 The yield curves for the transitionsto the ground state in the $^{52}Cr(n,\gamma)^{53}Cr$ reaction. The solid curve shows the thermal neutron capture in the region of the 7939 keV transition. The points represent the keV neutron capture spectrum with several resonances indicated.

to the ground state. Yield curves were obtained for transitions to levels in ^{53}Cr at 564, 1006, 1539, 1973, 2147, 2320 and 2667 keV. In figure 6·12 is shown the yield curve for the transition to the 1539 ($^{7}/_{2}^{-}$) level in ^{53}Cr with maxima corresponding to resonances at 48·3, 50·2, 96·2 and possibly 65 ± 1 keV. A resonance was detected at 194 ± 1 keV in a transition to the ground state and its width was evaluated at 15 ± 2·5 keV utilizing the method outlined in chapter 5 and shown in figure 5·2 for ^{28}Si.

Yield curves were obtained for transitions to the ground state and to levels at 835, 2620, 2829, 3074, 3395, 3437, 3720, 3854, 3925, 4011 and 4872 keV in ^{54}Cr for resonance capture in ^{53}Cr. A single gamma peak was observed in each yield curve with an energy centroid of 5.0 keV. This corresponds to transitions from the resonances at 4·185, 5·67, 6·74 and 8·18 keV (BN 73). A weighted resonance energy and neutron width were calculated from the parameters given for the four resonances (BN 73) and these values were used in yield curve analysis.

No keV neutron yield curves were obtained for resonance capture in ^{54}Cr although some transitions were observed in thermal capture. The partial radiation widths obtained from the yield curves of $^{50,52,53}Cr$ are shown in table 3B.

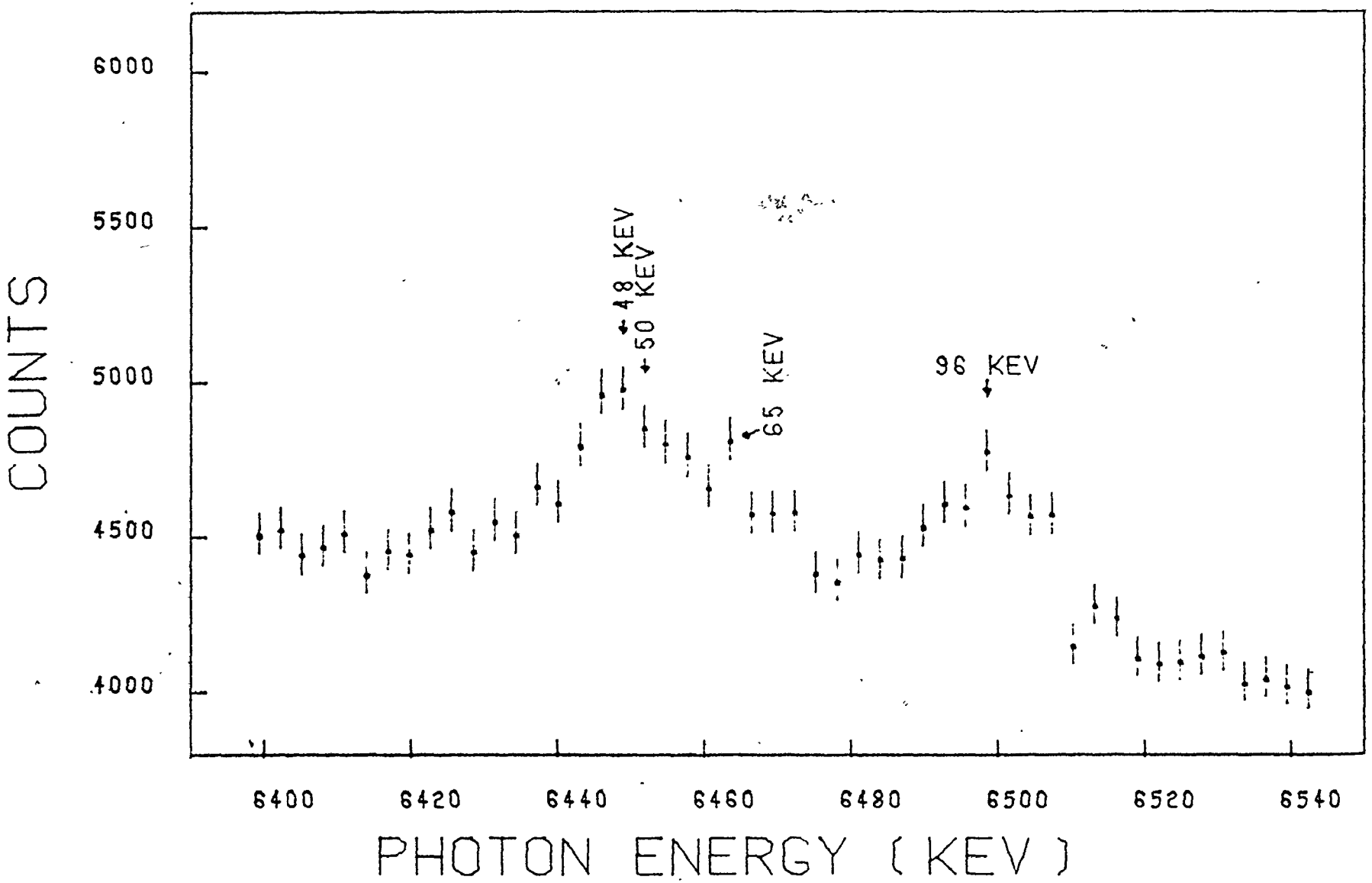

Figure 6.12 The keV neutron capture spectrum for the transitions to the $(^{7}/_{2}^{-})$ state at 1539 keV in ^{53}Cr is shown.

Nickel

In figure 6·13 is shown the yield curve for the transitions to the $^{3}/_{2}^{-}$ ground state in ^{59}Ni following neutron capture by ^{58}Ni. Maxima in the yield curve correspond to resonances at -28·5 (bound level), 15·5, 21, 32, 39, 63, 108, 137 and 193 keV. A spectrum of transitions to the first excited state 341 ($^{5}/_{2}^{-}$) keV is shown in figure 6·14. No transition to the first excited state is observable in the thermal capture spectrum for ^{58}Ni. Maxima occur in the spectrum corresponding to resonances at 21, 26, 32, 39, 63, 94, 117, and 137 keV. Spectra are given in figures 6·15 and 6·16 for transitions to the second and third excited states of ^{59}Ni respectively. A resonance at 83 keV occurs in a transition to the 471 ($^{1}/_{2}^{-}$) keV second excited state as well as others listed above. Resonances at 83, 147 and 231 keV as well as others listed above occur in the transitions to the 878 ($^{3}/_{2}^{-}$) keV third excited state. Yield curves were also obtained for transitions to levels in ^{59}Ni at 1303, 1737, 2421, 2900, 3036 and 3186 keV.

For resonance capture in ^{60}Ni the transitions to the $^{3}/_{2}^{-}$ ground state are shown in figure 6·17. Maxima in the yield curve correspond to resonances at 12·4, 28·7, 43·1,

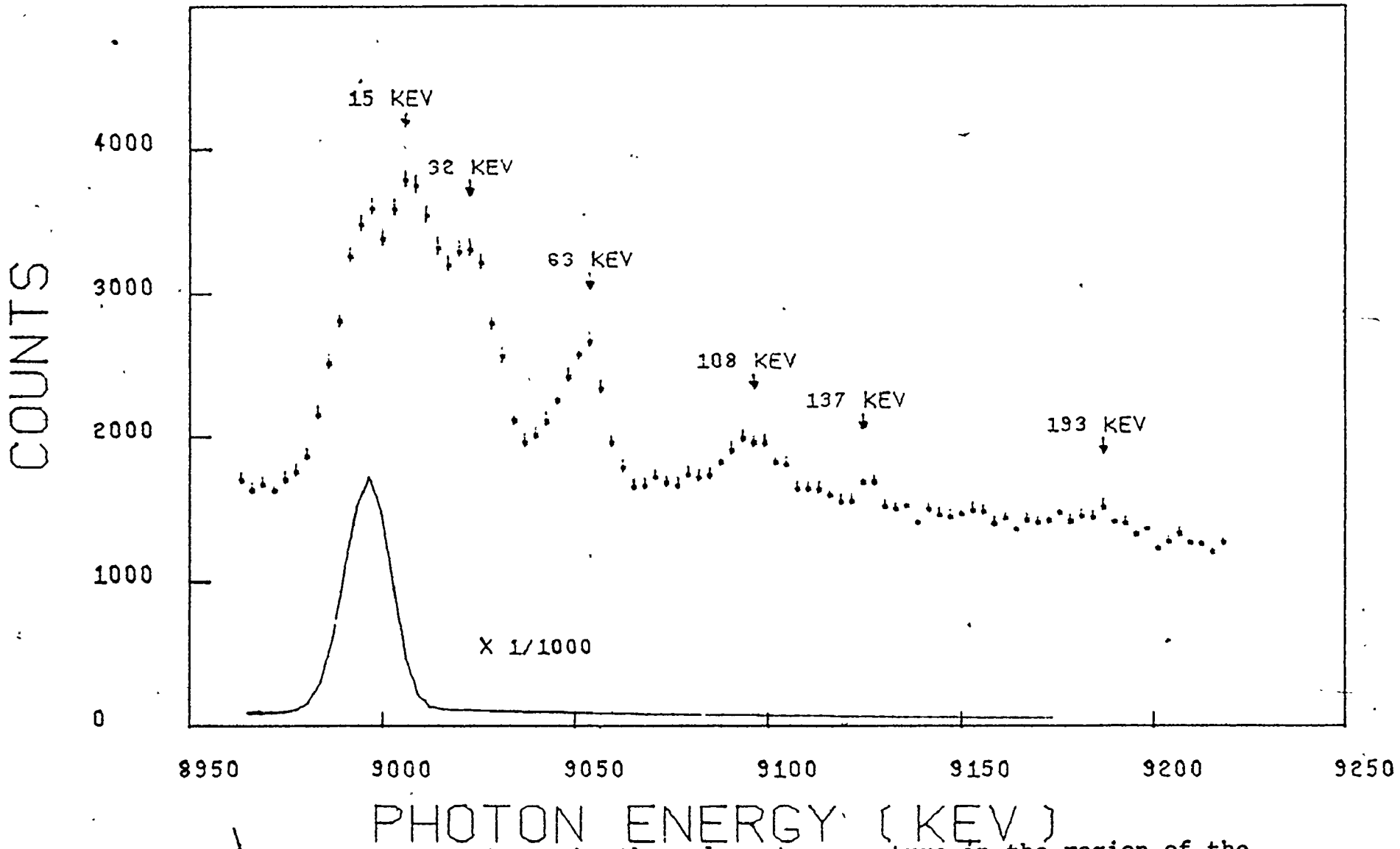

Figure 6.13 The solid curve shows the thermal neutron capture in the region of the 8999 keV transition to the ground state in the ^{58}Ni (n,γ) ^{59}Ni reaction. The points show the spectrum obtained when the boron filter is used. Several resonances are indicated

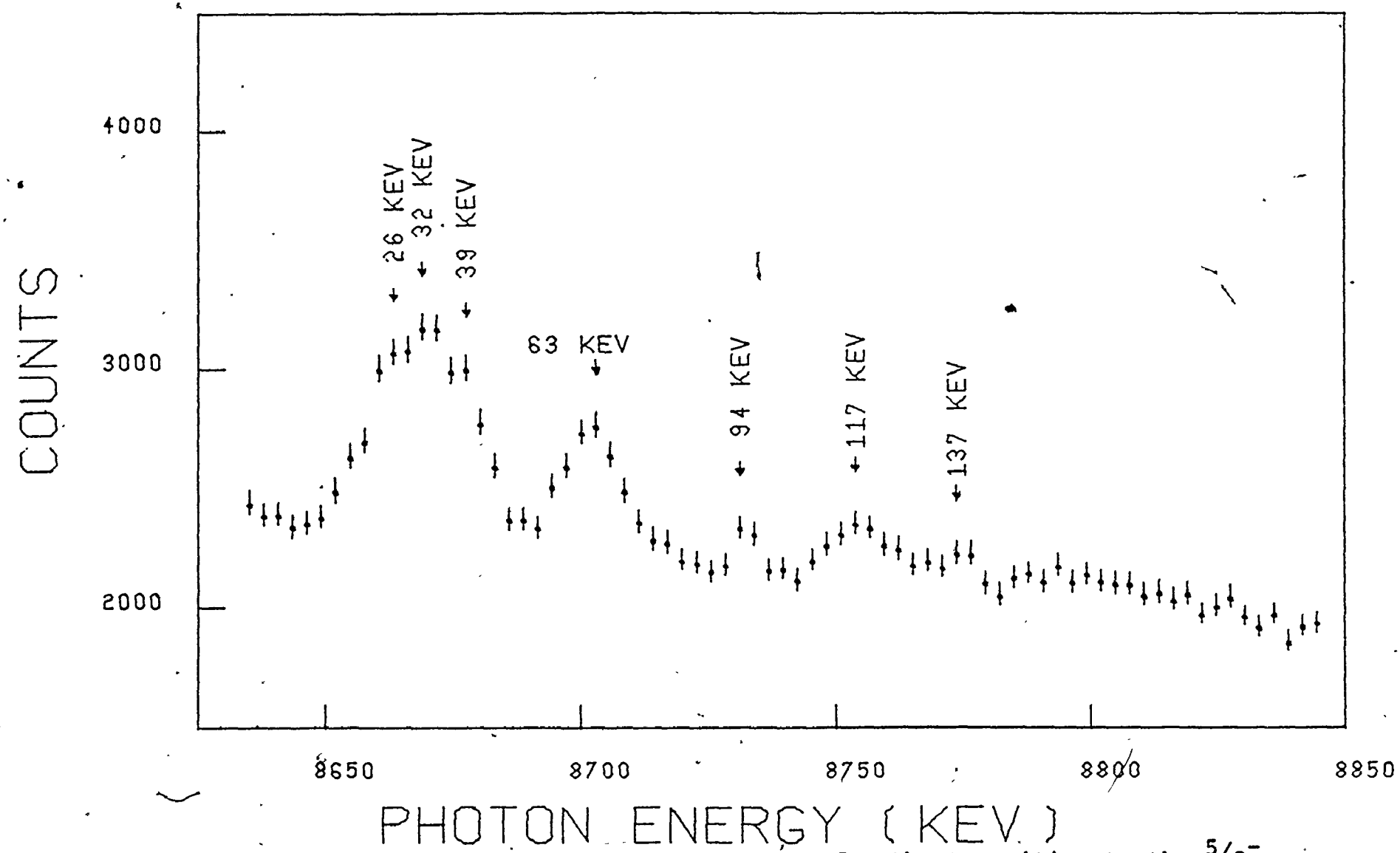

Figure 6.14 The keV neutron capture spectrum for the transitions to the $5/2^-$ first excited state at 341 keV in ^{59}Ni is shown.

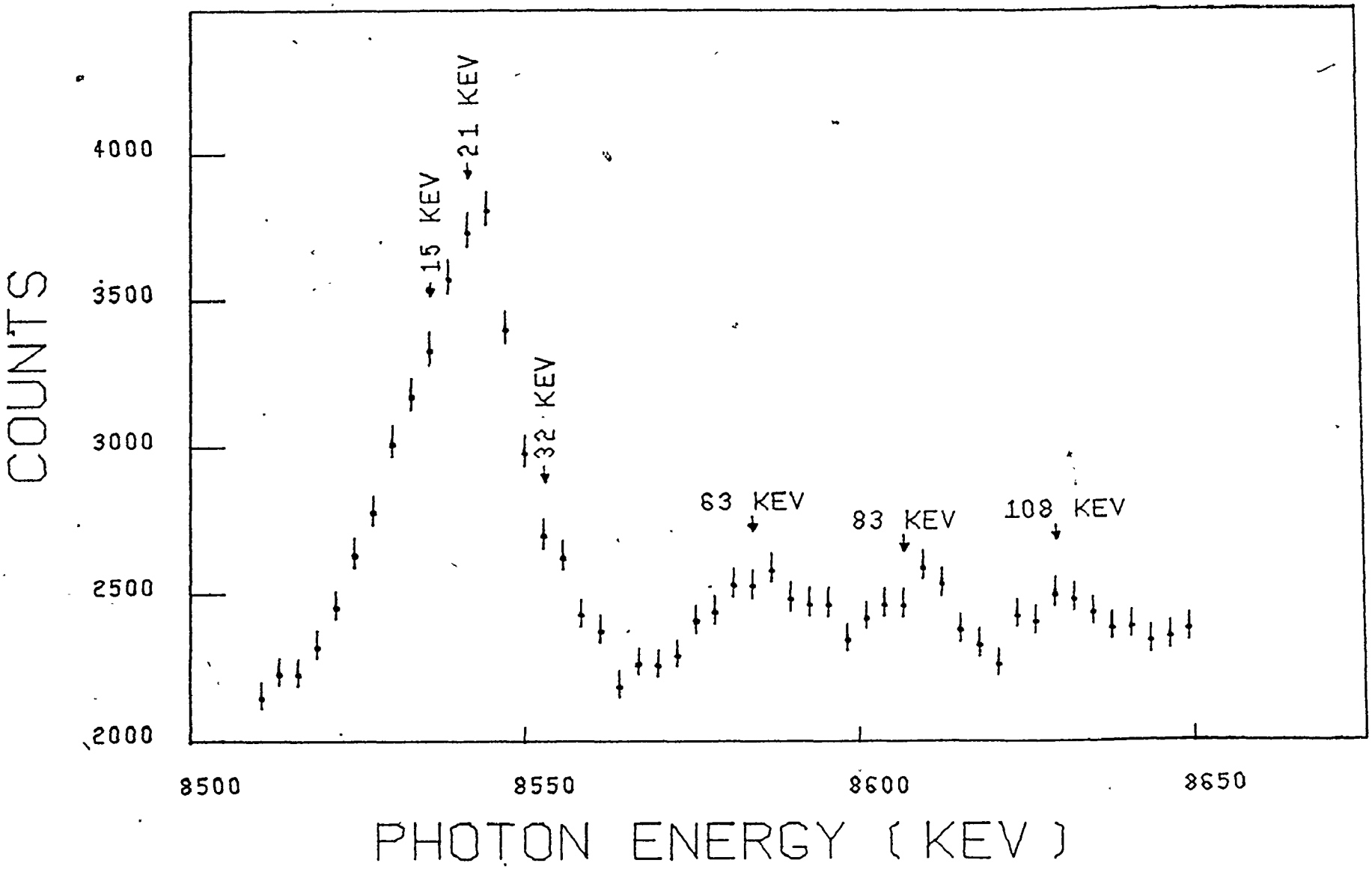

Figure 6.15 The yield curve for the transitionsto the $1/2^-$ second excited state at 471 keV in ^{59}Ni for keV neutron capture is shown.

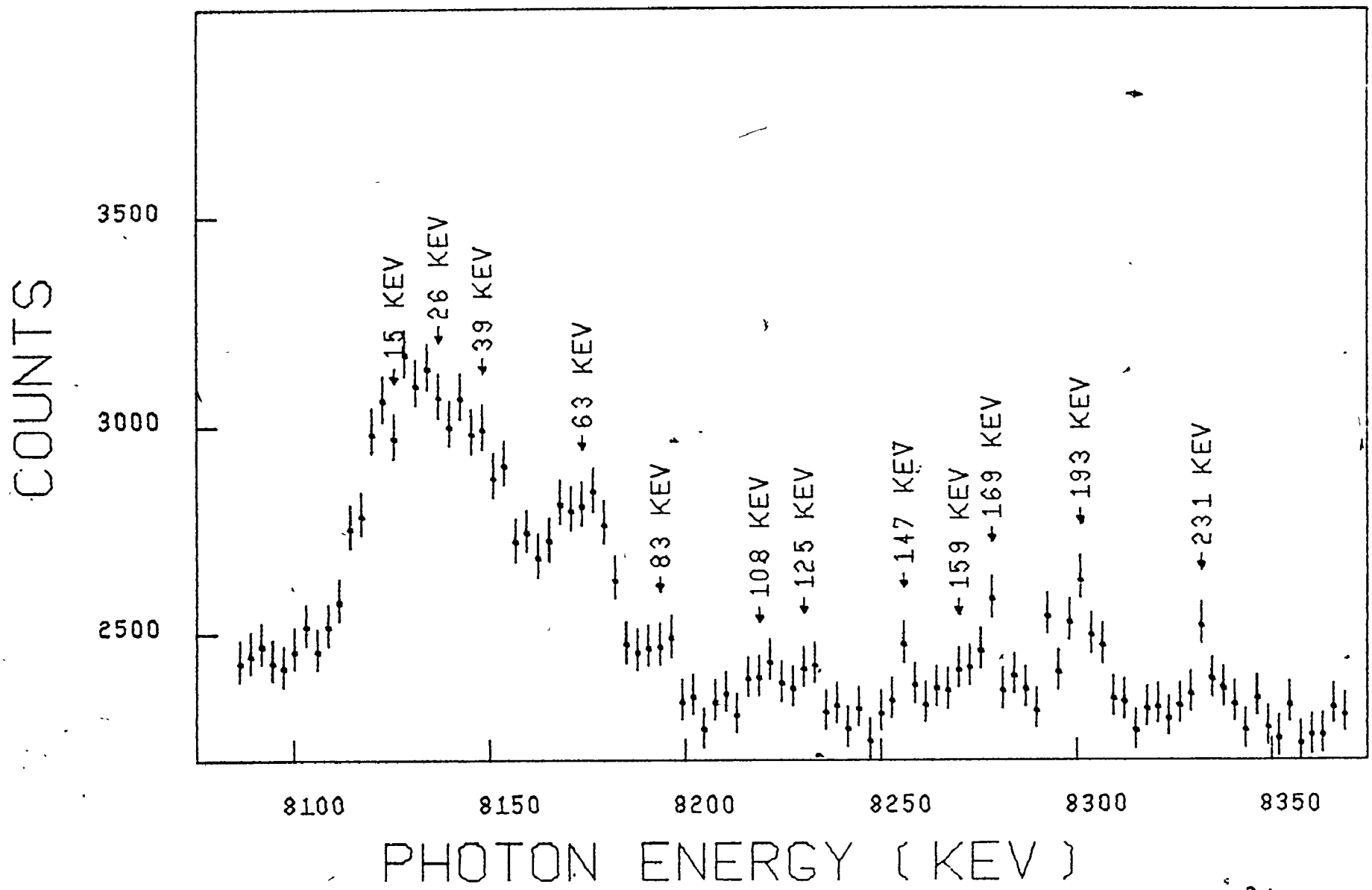

Figure 6.16 The keV neutron capture spectrum for the transitions to the $3/2^-$ third excited state at 878 keV in ^{59}Ni is shown.

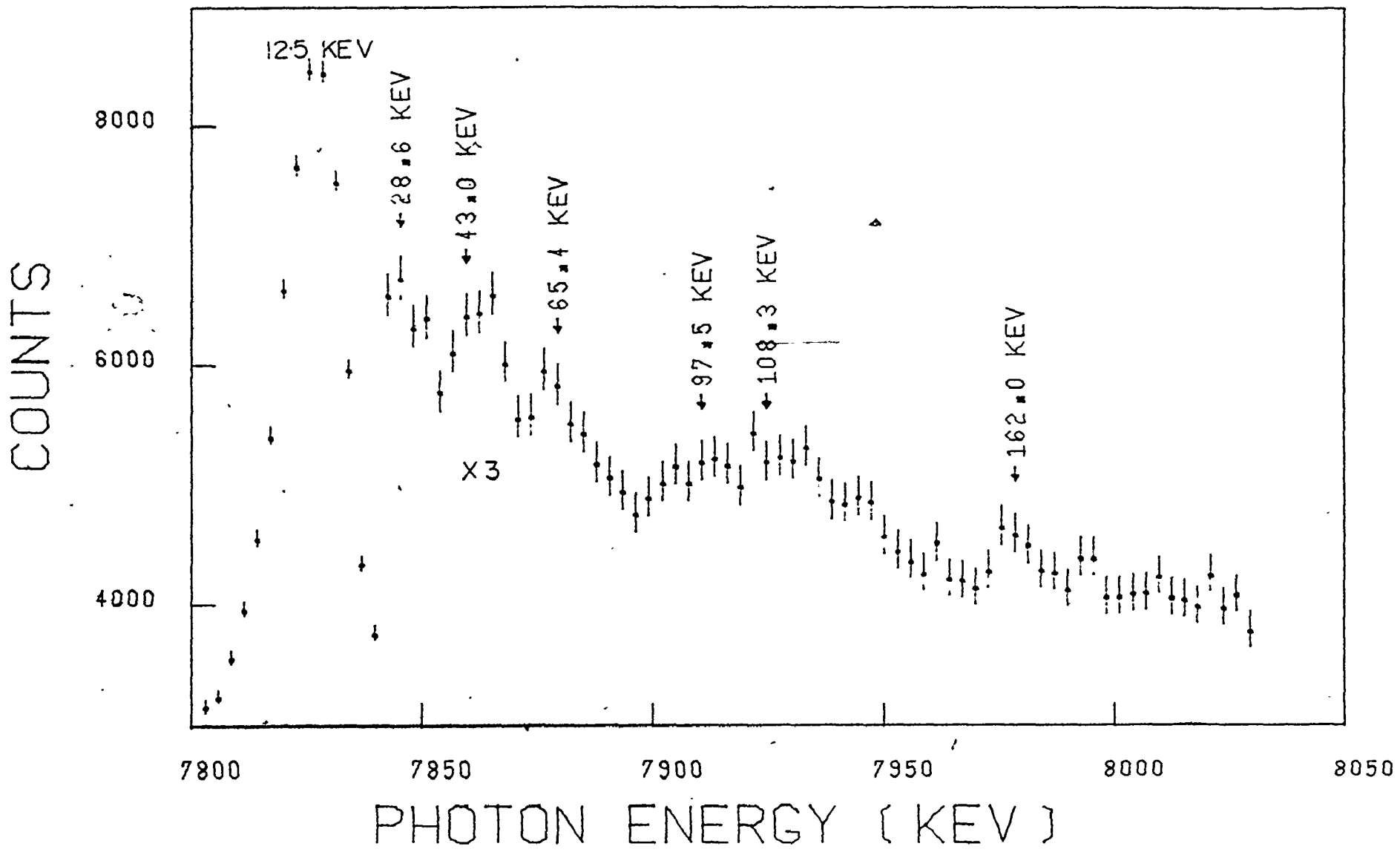

Figure 6.17 The keV neutron capture spectrum for the transitions to the ground state in the $^{60}Ni(n,\gamma)^{61}Ni$ reaction is shown.

65.3, 97.7, 109.5 and 162.0 keV. Other spectra were observed for transitions to levels in ^{61}Ni at 283 and 2124 keV. No transitions were observable in resonance capture to the first excited state 67 ($^{5}/_{2}^{-}$) keV as was the case for capture in ^{58}Ni. Only resonances between 12 and 65 keV could have produced observable transitions since large gamma ray peaks occurred at 7760 and 7833 keV due to resonance capture to other final states. Even a transition from resonance capture at 12.4 keV would have to be appreciable because of the 'tail' of the gamma peak at 7760 keV.

Yield curves were observed for transitions to the 0+ ground state and the 2+ 1172 keV first excited state of ^{62}Ni after neutron capture in ^{61}Ni. Only a single gamma peak was observed in each yield curve corresponding to resonances at $\sim$7.5 keV.

Yield curves were obtained for transitions to the $^{1}/_{2}^{-}$ ground state and to the second and third excited states in ^{63}Ni at 156 ($^{3}/_{2}^{-}$) and 519 ($^{3}/_{2}^{-}$) keV for neutron capture in ^{62}Ni.

No transitions for capture in ^{64}Ni were observed in keV neutron capture although some transitions were detected in thermal neutron capture. The partial radiation widths determined from the yield curves obtained for nickel are shown in table 3C.

TABLE 3A

Summary of Resonance Capture Results Obtained for Silicon[a]

$Si(n,\gamma)^{29}Si$

Final State (keV)	J_f^π	Photon Energy (keV)	Thermal Capture Intensity	29 keV Resonance	54 keV Resonance	67 keV Resonance	86 keV Resonance	173 keV Resonance	Sum of Partial Widths
0	1/2+	8472	2.7[b]	<0.001	<0.008	0.250±0.008	<0.01	1.28±0.05	1.53
73	3/2+	7200	10	0.015±0.003	<0.034	0.45±0.09	<0.06		0.47
28	5/2+	6446	0.2	0.021±0.009	<0.035	0.22±0.04	0.12±0.04	<0.10	0.23<I<0.47
27	3/2+	6047	0.7	<0.018	<0.012	0.22±0.08	<0.02	<0.26	0.22<I<0.49
35	3/2-	3539	64						0.49[c]
82	1/2-	2092	20						0.025[c]
Width (keV) assuming $\Gamma_n \sim \Gamma$				<1	<1	2.2±1	<1	23±2	

$(n,\gamma)^{30}Si$

Final State (keV)	J_f^π	Photon Energy (keV)	Thermal Capture Intensity	16 keV Resonance	35 keV Resonance	
0	0+	10610	0.26	0.092±0.06	<0.015	0.09
2237	2+	8376	0.028	0.031±0.004	0.44±0.03	0.47
3498	2+	7112	0.23	0.066±0.008	0.12±0.03	0.19
Width (keV) assuming $\Gamma_n \sim \Gamma$				∿1.5	∿1.5	

$Si(n,\gamma)^{31}Si$

Final State (keV)	J_f^π	Photon Energy (keV)	Thermal Capture Intensity	2.2 keV Resonance
0	3/2+	6589	0.018	0.011±0.001
Width (keV) assuming $\Gamma_n \sim \Gamma$				<1

[a] These values are proportional to $g\,\Gamma_\gamma$ and are given in eV.

[b] Photons/100 neutron captures in ^{28}Si.

[c] The observation of these transitions, which are dominant in thermal capture, is made difficult here because of the low energy of the primary transition. By observing the secondary, one obtains a summed value for all resonances.

TABLE 3B

Summary of Resonance Capture Results Obtained for Chromium[a]

$^{50}Cr(n,\gamma)^{51}Cr$

Final State (keV)	J_f^π	Photon Energy (keV)	Thermal Capture[b] Intensity	5.64 keV Resonance
0	7/2 -	(9264)	32	
749	3/2 -	8513	23	0.68±0 02
777	1/2 -	8485	12 2	0.44±0.04
1899	3/2 -	7363	3.6	0 31±0.05
2890	3/2 -	6372	6.8	0.10±0.01
3126	3/2 -	6136	3.6	0.22±0.01
3767	1/2-,3/2-	5495)	3 6	0.30±0.02
3771	3/2 -	5491)		
4040	1/2 -	5222	2.3	0.16±0 01
4637	3/2 -	4625	1.2	< 06
5260	1/2-,3/2-	4022	8	< 05

$^{52}Cr(n,\gamma)^{53}Cr$

Final State (keV)	J_f^π	Photon Energy (keV)	Thermal Capture[b] Intensity	1.43 keV Resonance	22.9 keV Resonance	27.6 keV Resonance	48.3 keV Resonance	50 2 keV Resonance	65 keV Resonance	96 2 keV Resonance	121 4 keV Resonance	141 3 keV Resonance	194 keV Resonance	235.8 keV Resonance
0	3/2 -	7939	55	0 095±0 030	0.12±0.03	0.11±0.03		0.66±0 05		5 44±0.20	2 11±0 21	1 70±0 37	5 66±0 73	3 00±0 52
564	1/2 -	7375	10 4	0.036±0 005	0.24±0.07	0.26±0.10		<0.11		1 15±0 41	<0.45	0 84±0 75	<1 2	<1.3
1006	(5/2 -)	6933		0.029±0 002	<0.03	<0.04	0.12±0.05	<0 13						
1539	(7/2 -)	6400		<0 004	<0.03	<0.03	0.16±0.20	0 19±0.05	0.29±0.06	1 79±0 15	<0.17	<0 29	<0.45	<1.6
1973		5966		0 030±0 006	<0.09	0.24±0.06		<0 15		<0 68	<0 38			
2147		5792		0 010±0 008	0.09±0.06	<0.10				<0 49	<0 53	<0.29		
2320	3/2 -	5619	13.9	0 013±0 006	<0.	<0.10		0.20±0 13						
2667	1/2 -	5270	5 1	0 023±0 015	<0.19	<0.24		<0 33						

$^{53}Cr(n,\gamma)^{54}Cr$

Final State (keV)	J_f^π	Photon Energy (keV)	Thermal Capture[b] Intensity	5.03 keV Resonance
0	0+	9717	22	0 58±0 02
835	2+	8884	44	1.29±0.04
2820	2+	7101	5.9	0 42±0.01
2829	0+	6886	1.6	0.094±0.004
3074	2+	6642	7.1	0.28±0 01
3395		6322	1 0	0 07±0 01
3537	2+	6287	1.3	0 15±0 01
3720	1+,2+	5997	3 6	0 15±0 01
3854		5857	1 0	0 07±0 01
3925		5792	-	0 05±0 02
4011		5706	9	0 095±0.01
4872	1+,2+	4846	1 2	0 05±0 04

[a] These values are proportional to a Γ_γ and are given in eV.

[b] Photons/100 neutron captures.

TABLE 3C

Summary of Resonance Capture Results Obtained for Nickel[a]

$^{58}Ni(n,\gamma)^{59}Ni$

Final State (keV)	J_f^π	Photon Energy (keV)	Thermal Capture[b] Intensity	-28.5 keV Resonance	15.5 keV Resonance	21 keV Resonance	26 keV Resonance	32 keV Resonance	39 keV Resonance
0	3/2 -	8999	49	3.02±0.12	0.26±0.02	0.21±0.03	<0.11	0.86±0.05	0.26±0.06
341	5/2 -	8658		<0.09	<0.02	0.10±0.02	0.11±0.05	0.32±0.07	0.20±0.05
471	1/2 -	8533	21	<0.88	0.19±0.02	0.20±0.04	<0.09	0.11±0.04	<0.07
878	3/2 -	8121	4.8	<0.07	0.09±0.01	<0.04	0.19±0.02	<0.07	0.37±0.03
1303	1/2 -	7697	1.7		<0.02	0.25±0.03	<0.07		
1737	(≤5/2)	7258	.4	0.24±0.07	<0.01	<0.04	<0.01	<0.07	<0.05
2421	3/2-,1/2-	6579	2.4	<0.88	0.06±0.01	<0.04	<0.11	<0.09	<0.10
2900	3/2 -	6105	2.1	<0.88	<0.04				<0.08
3036	1/2-,3/2-	5964		<0.57	<0.03	0.09±0.03	<0.12	0.12±0.06	<0.10
3186	1/2 -	5817	3.3	<2.6	0.02±0.01	<0.08	0.08±0.03	<0.11	0.31±0.09

$^{60}Ni(n,\gamma)^{61}Ni$

Final State (keV)	J_f^π	Photon Energy (keV)	Thermal Capture[b] Intensity	12.5 keV Resonance	28.6 keV Resonance	43.0 keV Resonance	65.4 keV Resonance	86.3 keV Resonance	97.5 keV Resonance
0	3/2 -	7820	39	1.68±0.04	0.70±0.11	1.03±0.26	1.65±0.46	<0.70	1.36±0.98
283	1/2 -	7537	23.2	1.06±0.02	0.23±0.05	0.56±0.12	0.70±0.22	0.65±0.36	1.77±0.53
1101	3/2 -	6719	2.0				<0.66	<0.88	<1.7
2124	1/2 -	5695	6.7	0.36±0.02	0.09±0.07	<0.14	0.47±0.29	<0.60	

$^{61}Ni(n,\gamma)^{62}Ni$

Final State (keV)	J_f^π	Photon Energy (keV)	Thermal Capture[b] Intensity	7.55 keV Resonance
0	0 +	10599		0.24±0.03
1172	2 +	9417		0.78±0.08

$^{62}Ni(n,\gamma)^{63}Ni$

Final State (keV)	J_f^π	Photon Energy (keV)	Thermal Capture[b] Intensity	454 keV Resonance
0	1/2 -	6838	76	1.69±0.07
88	5/2 -	6750		<0.04
156	3/2 -	6683	1.3	0.11±0.03
519	3/2 -	6320	3.9	0.12±0.03

[a] These values are proportional to $g\,\Gamma_\gamma$ and are given in eV.

[b] Photons/100 neutron captures.

63 keV Resonance	83 keV Resonance	94 keV Resonance	108 keV Resonance	117 keV Resonance	125 keV Resonance	137 keV Resonance	147 keV Resonance	159 keV Resonance	169 keV Resonance	193 keV Resonance	231 keV Resonance	Sum of partial widths
2.33±0.11			2.89±0.26		<0.29	1.00±0.35		<0.69	<0.57	2.65±0.71		13.5
1.09±0.08		0.25±0.12	<0.44	1.22±0.20	<0.44	0.40±0.26		<0 62	<0.50	< 0.61		3.7
0.69±0.14	0.42±0.13		0.98±0.39									2.6
1.06±0.08	0.11±0.08		0.15±0.15		0.22±0.22	<0.28	0.26±0.26	0 98±0.55	1.32±0.47	4.43±0.61	3.41±0.79	12.6
1.22±0.11												1.5
0.58±0.08			<0.20		<0 24	0.89±0.30		<0.59	<0.49	<0.62		1.7
< <0.16												0.1
0.39±0.18			<0.44									0.4
1.35±0.23			<0 41		<0.49							1.6
0.40±0.11			2.19±0.30		1.01±0.33							4.0

108.3 keV Resonance	162.0 keV Resonance	Sum of partial widths
3.25±1.28	2.92±1.90	12.6
2.10±0.64		7.1
<3.5		—
		0.9

CHAPTER 7

DISCUSSION

SILICON ISOTOPES

^{28}Si

Neutron capture resonances were observed at 29 ± 2, 67 ± 1, 85 ± 1 and 173 ± 1 keV as shown in table 3A. These are centre of mass energies and correspond to 30, 69, 88 and 179 keV in the laboratory system. Resonances have previously been observed at 195 keV by Fields et al. (1951), at 55 and 188 keV by Newson et al. (1959), at 181 keV by Lane et al. (1962) and at 38 and 68 keV by Lundberg and Berqvist (1970). A resonance at approximately 65 keV appears in data previously presented (Fe 51, La 62). More recently Allen and Macklin (1973) determined resonances at 15.14, 15.29, 31.74, 38.82, 55.6, 67.7, 70.84, 86.98, 180.6 keV. Of these, the authors assign 31.74 to ^{29}Si. However, total cross section measurements by Good and Harvey (1972) on the separated isotopes ^{29}Si and ^{30}Si indicate that the 15.29 and 38.8 keV resonances belong to ^{29}Si. Moreover, they do not report observing the 31.74 keV resonance for the targets used. The results obtained here agree with those of Good and Harvey and indicate that the resonances at

31.74, 67.7, 86.98 and 180.6 keV belong to ^{28}Si.

The errors quoted for the observed neutron widths include uncertainties in the resolution function. Only the 173 keV resonance for ^{28}Si is observed to have a neutron width well outside the limits imposed by the detector resolution. The 23 ± 2 keV value obtained is lower than the 60 keV quoted by Newson et al. (1959) and compares favourably to the 32.5 keV value quoted by Lane et al. (1962) when their value is corrected for self absorption effects. It is in good agreement with the 28 ± 6 keV result given by Allen and Macklin (1973). In figure 5·2 is shown the variation in χ^2/f with neutron width obtained when fitting the data for the 67 and 173 keV resonances of ^{28}Si associated with the ground state transition. The 2.2 ± 1 keV value obtained for the 67 keV resonance compares favourably to the 1.5 ± .3 keV width reported by Newson et al. (1959) and that obtained by previous investigators (Fi 51, La 62). The value determined here may indicate a small unresolved contribution from the 54 keV resonance rather than the true neutron width. Upper limits for contributions from the 54 keV resonance are given in table 3A. Because of the finite detector resolution the neutron widths of the 29 and 85 keV resonances are given only the limit ≤ 1 keV.

Capture of an s-wave neutron by ^{28}Si leads to

states in ^{29}Si with spin and parity $J_c^\pi = {}^1/_2{}^+$. These might be expected to decay predominantly via M1 radiation to any final state of spin ${}^1/_2{}^+$ and ${}^3/_2{}^+$. The resonance capture spectrum for transitions to the ${}^5/_2{}^+$ state at 2028 keV shows maxima at 67 and 85 keV (figure 6.9). Deexcitation via E1 radiation is more probable than E2 (En 66b); thus, both the 67 and 85 keV resonances were considered to be p-wave with $J_c^\pi = {}^3/_2{}^-$. The presence of large p-wave resonances is plausible, since the silicon nuclei lie near the maximum in the peak of the p-wave strength function. A p-wave assignment for the 67 keV resonance agrees with the results of Kenny et al. (1974).

The deduction of the capture spin of the 29 keV resonance is more difficult. As previously pointed out, there is interference in the detection of keV capture transitions to the ${}^5/_2{}^+$ state at 2028 keV due to the presence of $^{28}Si(n,n')^{28}Si$ reaction gamma rays (figure 6.9). If a transition from the 29 keV resonance is present, as indicated, then, it is the result of p-wave capture with $J_c^\pi = {}^3/_2{}^-$. A resonance was observed at 31 ± 2 keV in a 3570 ± 2 keV transition to the ${}^3/_2{}^-$ state at 4935 keV. Additional information could not be extracted because of the proximity of the $^{10}B(n,n')^{10}B$ gamma peak at 3584 keV.

The well established interference between resonance and potential scattering for the 173 keV resonance establishes $\ell=0$ and $J_c^\pi = 1/2^+$ for this state (La 62). It is interesting to note that the partial width for decay of this state by M1 radiation to the $1/2^+$ ground state is approximately five times stronger than for corresponding E1 decay of the 67 keV resonance.

Data presented by Kenney et al. (1974) would indicate a resonance at 38 keV with a strong transition to the first excited state and a moderate transition to the ground state. From the data obtained here (figures 6.7, 6.8, 6.9) no transitions were observed at these energies. Interestingly enough Kenney et al. report no information on the presence of a resonance at 29 (31.7) keV. The relative strength of the transitions for the 67 keV resonance are in agreement with the data of Lundberg and Berqvist (1970) and Kenney at al. (1974) with one exception, i.e. the transition to the ground state. The value observed here (table 3A) is about 60% of that reported by either of the above. The reason for the discrepancy is not clear. There is agreement with Kenney et al. that there is no measurable transition to the 3067 keV ($5/2^+$) state for the 67 keV resonance; whereas, Lundberg and Berqvist report a moderately strong transition.

The intensity distribution present in thermal neutron capture (Ly 67), where transitions to the 6382 ($1/2^-$) and 4935 ($3/2^-$) keV levels dominate, is not observed in keV neutron capture. Transitions to the 6382 keV level are not seen and to the 4935 keV level are barely observable. By measuring the intensities of the secondary gamma rays, i.e. transitions from the 6382 and 4935 keV levels to the ground state, one obtains the sum of the intensities of the resonance capture states decaying to the above levels. The intensities of the secondary gamma rays were corrected for detector efficiency and branching ratios, and converted to relative radiation widths. A list of summed partial radiation widths is given in table 3A. It shows that transitions to the 4935 and 6382 keV levels are relatively weak compared to the same transitions for thermal neutron capture. The difference between thermal and keV neutron capture intensities would suggest that thermal neutron capture is predominantly due to a negative resonance or hard sphere capture.

^{29}Si

Resonances were observed to occur at 16 ± 1 and 35 ± 1 keV and correspond to previously measured values of 15.3 and 38.8 keV (Al 73, Go 73). The yield curves for

the transition to the ground state (0+) and the first two excited states at 2236 (2+) and 3498 (2+) keV in ^{30}Si were determined. The yield curve for the first excited state is shown in figure 6.10.

Capture of an s-wave neutron in ^{29}Si results in states with $J_c^\pi = 0^+$ or 1^+. Since the 16 keV resonance decays to both the $J^\pi = 2^+$ excited states and the $J^\pi = 0^+$ ground state it is probable that this state is characterised by $J_c = 1$, since both spin states would be accessible by either E1 or M1 radiation. The decay of the 35 keV resonance to the 2236 (2^+) keV level is at least 3 times stronger than any other transition observed in ^{30}Si. This might indicate that the deexcitation is E1 radiation. If this were so, the resonance would be p-wave with $J_c^\pi = 1^-$ or 2^-. The data presented by Kenney et al. (1974) are in agreement with the intensity pattern observed here. Their value for the resonance energy, 26 ± 5 keV, does not agree with the 35 ± 1 keV determined in the present work (figure 6.10) nor with recent total cross section results (Go 73).

^{30}Si

Only the yield curve for the ground state transition was observed with keV neutron capture in ^{30}Si. The resonance energy, 2.24 keV (Go 73), was used to fit the single peak

observed. Any possible contribution from the resonance at 4.98 keV was obscured because of the finite gamma ray detector resolution.

CHROMIUM ISOTOPES

^{50}Cr

Capture of an s-wave neutron by ^{50}Cr leads to states in ^{51}Cr with spin and parity $J_c^{\pi} = 1/2^+$. These are expected to decay to final states of spin $1/2^-$ or $3/2^-$ by E1 radiation on the basis of the systematics in this mass region. Transitions to levels in ^{51}Cr reported here (table 3B) are, then, most probably due to s-wave capture in the resonance at 5.64 keV (St 71). Any detection of possible capture in the p-wave resonance at 5.49 keV (St 71) is masked by the resolution of the gamma ray detector. The distribution of partial radiation widths reported here (table 3B) agrees with the distribution previously reported by Allen et al. (ND 73) and show good correlation to the distribution of intensities from thermal capture as shown in the same table.

As shown in figure 7.1 a gamma peak with a large width is observed in the yield curve for the transitions to the 3767 ($1/2,3/2$) and/or 3771 ($3/2^-$) keV levels of ^{51}Cr at 5542 keV. Analysis with parameters previously reported (St 71)

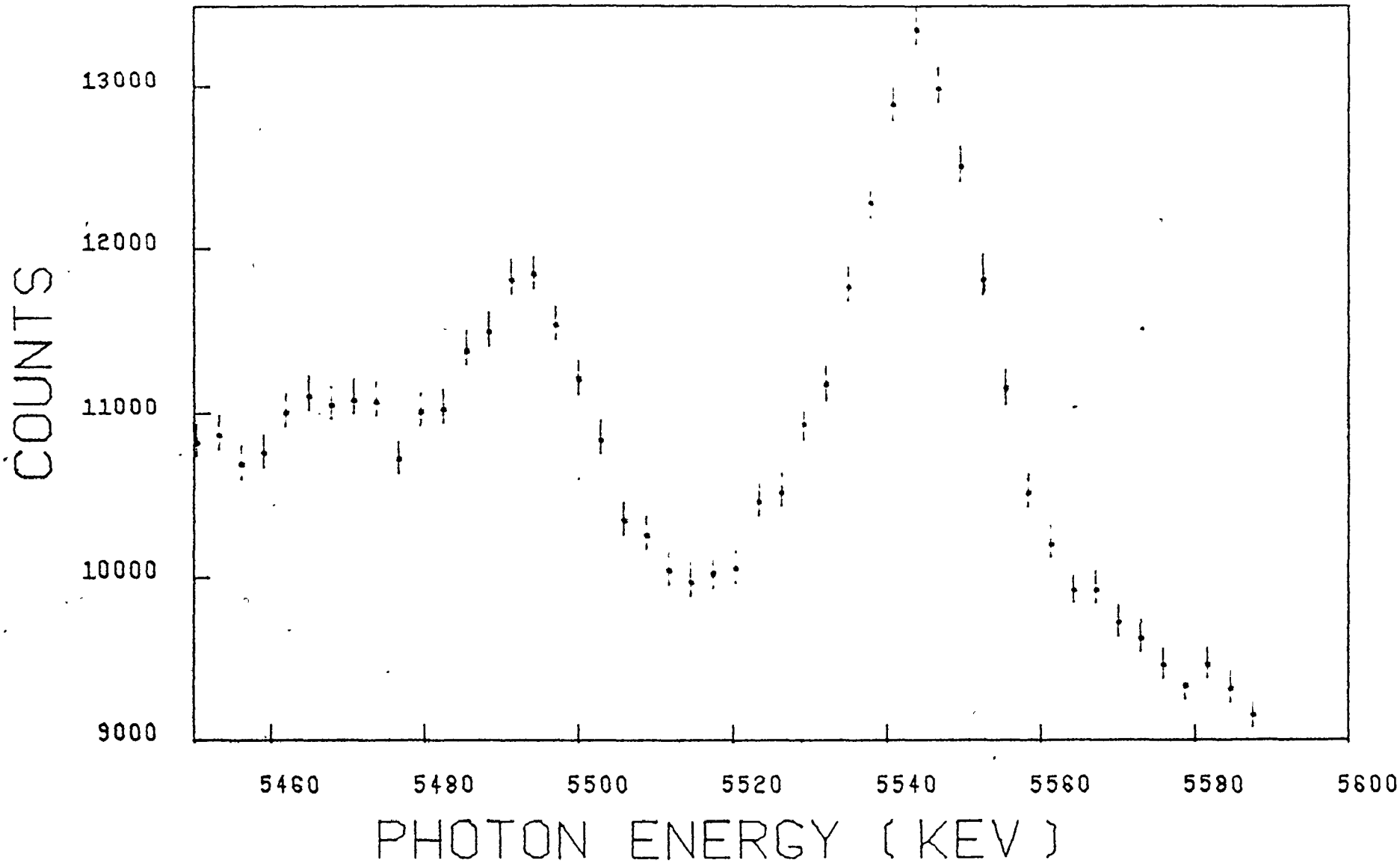

Figure 7.1 The yield curve for keV neutron capture corresponding to transitions to the 3767 ($^1/_2$, $^3/_2$) and 3771 ($^3/_2^-$) keV levels in ^{51}Cr. Note the large, broad maximum at ∿ 5543 keV.

for resonances in ^{50}Cr failed to achieve a satisfactory fit. It seems possible that a few resonances of energy near 50 keV from transitions to both levels of 3767 and 3771 keV could contribute to the maximum observed in the yield curve.

^{52}Cr

The yield curve for the transitions to the $^{3}/_{2}^{-}$ ground state in ^{53}Cr after neutron capture in ^{52}Cr is shown in figure 6.11. The curve reveals resonances of energies previously reported (St 71) and in addition indicate a peak at 194 keV with a width of 15 ± 2.5 keV. Two narrow resonances have been previously reported at 197 and 199 keV (BN 66); more recent tabulations (St 71, BN 73) list no resonances near 194 keV. Although no clear maxima are observed in the region between the 27.6 and 50.2 keV resonances, the continuum above background suggests possible contributions from resonances at 33.9, 34.3, and 48.3 keV (BN 73). Similarly in the region between 96.2 and 123.2 keV possible contributions are present due to resonances at 106, 112, 113, and 118 keV (BN 73). Due to the large width the resonance at 194 keV is most likely s-wave capture.

The resonance spectrum for transitions to the 1539 ($^{7}/_{2}^{-}$) level in ^{53}Cr, as shown in figure 6.12, exhibits maxima corresponding to resonances at 48.3, 50.2 and 96.2 keV.

A maximum was also observed at 65 ± 1 keV; no resonance has been previously reported at this energy (BN 73). The 1539 keV level has been reported to have $\ell_n = 3$ and a possible spin of $7/2^-$ (ND 70). Since the resonances at 50.2 and 96.2 keV are s-wave (BN 73) it would seem that gamma deexcitation to this level is either E3 ($7/2^-$) or M2 ($5/2^-$), or that p- or d-wave resonances are present near the 50.2 and 96.2 keV s-wave resonances. While the 48.3 keV resonance has been reported and is p-wave (BN 73), no resonances have been reported near the 96.2 keV resonance (BN 73).

The distribution of intensities in keV neutron capture agree with data reported by Allen et al. (ND 73) with the exception of the transition to the 1006 keV level. Contributions from other isotopes in the Allen et al. data would account for the discrepancy. The only correlation between thermal and keV neutron intensities is that the ground state transition contributes more than half of the total observed intensity.

In table 4 there is a comparison of the total radiation widths measured in this experiment for certain resonances and those by Steiglitz et al. (1971). The total radiation widths quoted for this experiment were obtained

TABLE 4

Total Radiation Width for $^{50,52,53}Cr$

Isotope	Resonance (keV)	Γ_γ (eV) Steiglitz et al. (1971)	Present Data A	Present Data B
^{52}Cr	50·2	1·16 ± 0·2	0·84 ± 0·28	1·28±0·43
	96·2	4·80 ± 0·8	5·51 ± 0·68	8·40±0·98
	141·3	2·07 ± 0·3	1·67 ± 0·59	2·55±0·89
^{50}Cr	5·64	3·10 ± 0·25	1·45 ± 0·06	2·22±0·10
^{53}Cr	5·03	13·09 ± 1·05[a]	6·43 ± 0·14	9·80±0·22

A Normalized for ^{52}Cr resonances only.

B Normalized for all the resonances listed.

a The sum of the total radiation widths for 4·18, 5·67, 6·78, 8·18 keV resonances from the data of Steiglitz et al. (1971).

by taking the sum of the partial radiation widths determined for transitions from a particular resonance to different final states, as given in table 3B. There is fairly good agreement when comparing values of the total radiation widths for ^{52}Cr alone. The reason for the larger discrepancies when $^{50,53}Cr$ resonances are considered is not known. A possible answer is that significantly different fractions of the total intensity are measured for different resonances.

^{53}Cr

Capture of an s-wave neutron by ^{53}Cr leads to states in ^{54}Cr with spin and parity 1^- or 2^-. These would then predominantly decay to final states of spin 0^+, 1^+, 2^+, 3^+ by dipole radiation. The four s-wave resonances at 4.18(1^-), 5.67(2^-), 6.74(1^-) and 8.18(2^-) keV probably contributed to the maximum in the yield curves for transitions to the levels in ^{54}Cr (table 3B) which occurred at 5 keV. The distribution of partial radiation widths determined here agrees with that reported by Allen et al. (ND 73) with the exception of the ground state transition. It was determined here to be half as strong as the transition to the first excited state (table 3B) rather than one-sixth as strong as reported by Allen et al. (ND 73). The errors reported for the partial

radiation widths determined here may be larger than quoted in table 3B since the value of the neutron flux used in calculations was averaged over the range of 4 to 8 keV while the flux varies by a factor of two in this region. That is, if one of the maxima observed was largely due to a contribution by the resonance at 4.18 or 8.18 keV rather than by all four resonances its partial width would be significantly different than that quoted.

NICKEL ISOTOPES

^{58}Ni

Capture of an s-wave neutron by ^{58}Ni leads to states in ^{59}Ni with spin and parity $J_c^{\pi} = 1/2^+$. These would then predominantly decay to final states $1/2^-$ and $3/2^-$ by E1 radiation. Yield curves for transitions to the ground state and the first, second and third excited states are shown in figures 6.13, 6.14, 6.15, 6.16. From these and the listing of partial radiation widths determined (table 3C) it can be seen that a large number of closely spaced resonances occur in the region 0-40 keV. A list of resonances for ^{58}Ni is given in table 5. While only resonances at -28.5, 15, 21, 26, 32 and 39 keV were analyzed, several other resonances may have been present and have contributed to the intensity but were not observable due to resolution effects. Thus

TABLE 5

Resonance Parameters for ^{58}Ni [a]

E_o(keV)	$g\Gamma_n$ (eV)	J	ℓ
-28.5		1/2	0
6.9			(1)
13.3			(1)
13.7			(1)
15.5	1200	1/2	0
19.0			(1)
20.0			(1)
21.2			(1)
26.1			(1)
26.7			(1)
32.4		(3/2)	(1)
34.2			(1)
36.1			(1)
39.6			(1)
47.8		(3/2)	(1)
52.0		(3/2)	(1)
54.7			(1)
58.6			(1)
60.1			(1)
61.8			(1)
63.0	3600	1/2	0
66.4			(1)
68.8			(1)
69.8			(1)
78.0			(1)
81.1			(1)
83.1	110		0
89.8			(1)
92.3			(1)
94.5			(1)
97.0			(1)
101.1			(1)
105.3			(1)
107.7	1400	1/2	0
110.7			(1)
117.5			(1)
120.3		1/2	0
125.0	700	1/2	0
137.0	1760	1/2	0
140.5	3460	1/2	0
147.5	175		>0
159.5	6000	1/2	0

(cont'd)

E_o (keV)	$g\Gamma_n$ (eV)	J	ℓ
169·0	750	1/2	0
183·5	250		>0
193·0	3500	1/2	0
207·0	6800	1/2	0
215·0	260		>0
231·0	6000	1/2	0
243·0	250	1/2	0
247·5	360		>0

[a] A partial list of resonance parameters for ^{58}Ni from BNL-325 Neutron Cross Sections (BN 73).

partial radiation widths, given in table 3C, may have larger errors than quoted if other resonances have contributed to the yield curves.

The yield curve for the transition to the 341($5/2^-$) keV first excited state (figure 6.14) exhibits maxima corresponding to resonances previously determined to be p-wave as shown in table 5. However, one resonance at 137 keV appears which has been assigned as s-wave (Ga 71). An s-wave capture state decaying to a $5/2^-$ state would require M2 radiation. Other explanations are possible: the assignment of the 137 keV resonance could be incorrect or another near by p-wave resonance could be present and thereby account for the capture. The maximum at $\sim$ 63 keV cannot definitely be assigned to the 63.2 keV s-wave resonance due to several p-wave resonances in the 60-66 keV region (table 5) which may be responsible for the capture. It is also possible that in transitions to other levels, where the resonance at 63 keV is most likely due to s-wave capture followed by E1 radiation, close lying p-wave resonances may contribute.

The spin of the 1737 keV level in ^{59}Ni has been previously reported as $\leq 5/2$ (ND 68). Partial radiation widths were measured for transitions from the -28.5, 63.2

and 137 keV resonances (table 3C). These are s-wave resonances, thus, the spin of the 1737 keV level would be limited to $^{3}/_{2}$ or $^{1}/_{2}$ to allow for dipole radiation.

The limited data previously reported (Aℓ 69, ND 73) on the distribution of relative intensities agrees with the partial radiation widths determined here for both ^{58}Ni and ^{60}Ni. Comparison of the results presented in table 3C shows a poor correlation between thermal and keV neutron capture gamma ray intensity distributions. A possible explanation for this is that the -28.5 keV resonance contributes most of the cross section at thermal energies and that the positive resonances are ineffectual. This view is supported by Garg et al. (1971) who found that the negative resonance accounts for 90% of the cross section at thermal energies.

No comparison of total radiation widths measured here to previous data was attempted since much of the intensity in what appears to be s-wave resonances may have been contributed by close lying p-wave resonances. Normalization of radiation widths to absolute values was performed by comparing ^{60}Ni values and correcting for isotopic abundance. This was also done for ^{61,62}Ni values as well.

^{60}Ni

The yield curve for transitions to the ground state in ^{61}Ni after neutron capture in ^{60}Ni is presented in figure 6.17. Besides the resonances noted others may be present. In the region above the 108 keV resonance there may be contributions from p-wave resonances at 121, 124, 130 and 140 keV (BN 73). A maximum occurs at 183 keV. There is a large s-wave resonance reported at 187 keV, however, this energy value is too far removed from that of 183 keV for a satisfactory fit to be achieved. No other resonance is reported in this energy region (BN 73).

A comparison of the total radiation widths measured here and the data, presented by Steiglitz et al. (1971) is given in table 6. It shows excellent agreement. As mentioned previously the uncertainty in the total radiation widths as measured here might be higher than quoted due to the error caused by unobservable transitions. Comparison of the thermal and keV capture intensities (table 3C) shows a good correlation in contrast to the $^{58}Ni(n,\gamma)^{59}Ni$ distributions.

^{61}Ni

Only one maximum was observed in the yield curves

TABLE 6

Total Radiation Widths for ^{60}Ni

Resonance (keV)	Γ_γ (eV) Steiglitz et al. (1971)	Present Data
12·5	3·30 ± 0·3	3·11 ± 0·05
28·6	1·10 ± 0·1	1·02 ± 0·15
43·0	1·73 ± 0·18	1·60 ± 0·32
65·4	2·43 ± 0·26	2·82 ± 0·58

corresponding to the transitions to the ground and first excited states for $^{61}Ni(n_{keV},\gamma)^{62}Ni$. In table 7 are listed three s-wave resonances which occur near the energy corresponding to the maxima in the yield curves. Since the J value for the 7.15 keV resonance is 1, it is most probable that this resonance contributes to the ground state transition since the gamma radiation would be E1, while gamma radiation from the J=2 resonances at 7.55 and 8.73 keV would be quadrupole. The transition to the 1172 (2+) first excited state may be due to contributions from any or all of the three resonances.

^{62}Ni

Only a single maximum was observed for transitions from the $^{62}Ni(n,\gamma)^{63}Ni$ reaction corresponding to the s-wave resonance at 4.54 keV. No transitions were observed to the $5/2^-$ first excited state in ^{63}Ni at 87 keV.

Compound versus Direct Reaction for ^{52}Cr, $^{58,60}Ni$.

Resonance capture spectra measurements on ^{169}Tm and ^{163}Dy at Brookhaven (Be 68, Mu 70) have revealed correlations between the total radiation and reduced neuton widths for these isotopes and these have been interpreted in terms of intermediate structure. Similarly resonances

TABLE 7

Resonances in ^{61}Ni[a]

E_o (keV)	2g Γ_n (eV)	J	ℓ
7.15	50	1	0
7.55	225	2	0
8.73	7.5	2	0

[a] A partial list of resonances in ^{61}Ni (BN 73).

of Ni and Cr have also shown such correlations (St 71). Correlation coefficients of $\rho\ (\Gamma_\gamma, \Gamma_n{}^o)$ were calculated for ^{52}Cr, $^{58,60}Ni$ s-wave resonances. These calculations were performed using the formula

$$\rho(\chi,y) = \frac{\mathrm{cov}(\chi,y)}{\sqrt{\sigma_\chi^2 \cdot \sigma_y^2}}$$

$$= \frac{\sum_i (\chi_i - \bar{\chi})(y_i - \bar{y})}{\sqrt{\sum_i (\chi_i - \bar{\chi})^2 \sum_i (y_i - \bar{y})^2}} ,$$

and the values obtained are given in table 8. Significant correlation occurred for total and partial radiation widths of ^{52}Cr and ^{60}Ni but not for ^{58}Ni.

In the correlations, the total radiation widths were obtained by summing the $\Gamma_{\gamma i}$'s listed in table 3 for the resonances used. These resonances were: 50, 96, 121, 140, 190, 230 keV for ^{52}Cr; 15, 63, 108, 125, 137, 159, 169, 193 for ^{58}Ni; 12, 28, 43, 65, 86, 98, 108 keV for ^{60}Ni. The correlation between partial radiation widths and reduced neutron widths was calculated for transitions to levels where all or most of the $\Gamma_{\gamma i}$'s were measured for the above resonances. These were the ground state transitions for ^{52}Cr and ^{58}Ni and the ground state and second excited state for ^{60}Ni.

TABLE 8

Correlation Coefficients

Isotope	Correlation[a]	p	Confidence Level[b] %	Confidence Level[b] (90%)	No. of Resonances
^{52}Cr	Γ_γ/Γ_n^o	·591	86·5	·680	6
	$\Gamma_{\gamma_o}/\Gamma_n^o$	·596	86·5	·680	6
^{58}Ni	Γ_γ/Γ_n^o	·216		·560	8
	$\Gamma_{\gamma_o}/\Gamma_n^o$	·117		·560	8
^{60}Ni	Γ_γ/Γ_n^o	·682	92·3	·610	7
	$\Gamma_{\gamma_o}/\Gamma_n^o$	·632	90·5	·610	7
	$\Gamma_{\gamma_2}/\Gamma_n^o$	·576	88·3	·610	7
$^{52}Cr^{60}Ni$	Γ_γ/Γ_n^o	·597	96·3	·410	13

[a] Correlations were taken between the total radiation width Γ_γ and the reduced neutron width Γ_n^o ; correlations were also taken between partial radiation widths $\Gamma_{\gamma i}$ and Γ_n^o where i = o represents the ground state transition and i = 2 that of the second excited state.

[b] Confidence levels refer to the level above which there is probability of correlation for sets of random numbers, e.g. a 90% confidence level gives the value above which there is a 10% probability for sets of random number to correlate.

In order to calculate confidence levels, pairs of random numbers were sampled from a Porter-Thomas distribution i.e a χ^2 distribution with one degree of freedom, and a correlation coefficient calculated for a variety of sample sizes. Many correlations were computed (10^5) and histograms made. Then, 90% confidence levels for the coefficients found for ^{52}Cr, $^{58,60}Ni$ which are given in table 8. In figure 7.2 is shown two such histograms for 6 and 13 pairs of random numbers used in the determination of confidence levels.

Partial radiation widths for transitions to the same final state should follow a Porter-Thomas distribution for a compound nuclear reaction, that is, have one degree of freedom. The partial radiation widths used were for the same resonances as listed previously for correlation coefficients. The estimation of ν was made using the formula

$$\langle \nu \rangle = \frac{n-3}{n} \left\langle \frac{2}{\sigma^2} \right\rangle - \frac{2}{n}$$

as described by Lycklama et al. (1969), where n is the number of elements in the distribution to be tested and σ^2 is the variance. Bias in $\langle \nu \rangle$ is the order of 3% (Ly 69) and the error in the estimate is given by (Ly 69)

$$\Delta\nu = \langle \nu \rangle \cdot \sqrt{\frac{2}{n}} .$$

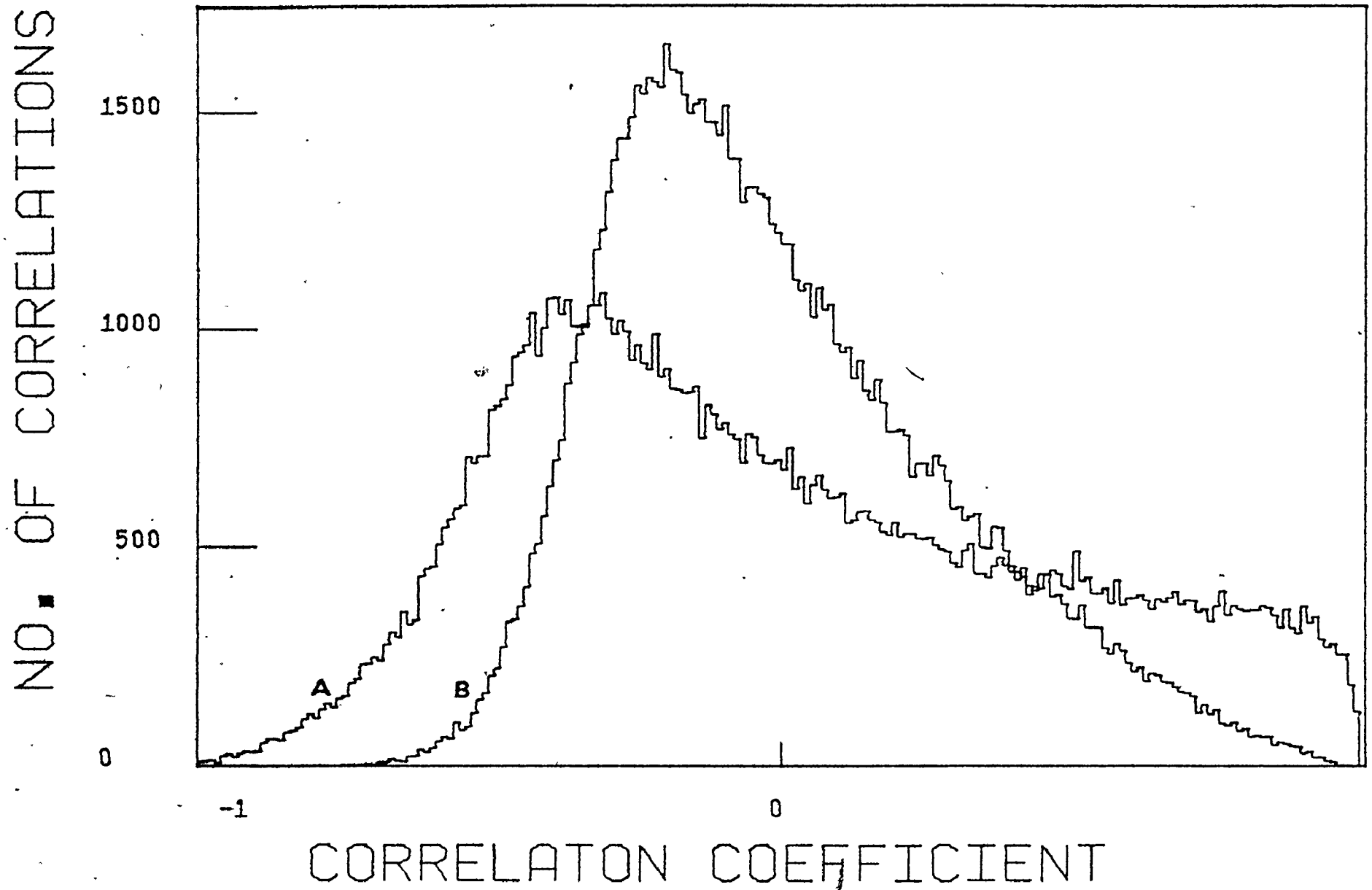

Figure 7.2 Histograms . - number of correlations vs. correlation coefficient. A 100,000 coefficients were calculated for each histogram for 6 (diagram A) and 13 (diagram B) pairs of random numbers sampled from a Porter-Thomas distribution.

TABLE 9

Estimates of the Number of Degrees of Freedom ν

Isotope	Final State	No. of Partial Widths	ν	$\Delta\nu$
^{52}Cr	ground	6	1·96	1·13
^{58}Ni	ground	8	1·58	·79
	4th	8	.46	.23
	[a]ground & 4th	16	1·30	.41
^{60}Ni	ground	7	3·08	1·65
	2nd	7	2·29	1·22
	[a]ground & 2nd	14	4·21	1·59

[a] Sets of partial radiation widths were normalized to a mean of 1·00 before combination for an estimate of ν.

The estimate in ν and errors are listed in table 9.

Estimates in ν gave values of 1.30 ± 0.41 for ^{58}Ni and 4.21 ± 1.59 for ^{60}Ni. These would suggest a value close to unity for ^{58}Ni suggesting that ^{58}Ni $(n_{keV},\gamma)^{59}$Ni is a compound reaction and the value of $\nu > 1$ for ^{60}Ni would indicate that the ^{60}Ni$(n_{keV},\gamma)^{61}$Ni reaction is not a compound but a direct mechanism. A value of ν, 1.96 ± 1.13 was determined for ^{52}Cr but interpretation is difficult because of the small sample size.

Groshev and Demedev (1967) compared (n_{th},γ) and (d,p) strengths for $\ell=1$ transitions in ^{53}Cr, ^{59,61}Ni. The results showed a good correlation existed and suggested that neutron capture proceeded through a direct mechanism as did the (d,p) reaction for these isotopes. A comparison of (n_{keV},γ) and (d,p) strengths was carried out here and the results are shown in table 10. Both thermal and keV neutron intensities are shown normalized to the (d,p) strengths for comparison. Correlation coefficients are given for the (n,γ) and (d,p) strengths. For ^{52}Cr and ^{60}Ni isotopes both thermal and keV neutron capture intensities reveal a correlation to (d,p) strengths; however, for ^{58}Ni a correlation exists for thermal capture but not for keV neutron capture.

The results of the correlation, $p(\Gamma_\gamma,\Gamma_n^o)$, testing for possible resonance channel capture, the estimate of ν

TABLE 10

Comparison of (n,γ) and (d,p) Strengths

Isotope	Final State (keV)	I_γ/E_γ^3 Thermal[a]	I_γ/E_γ^3 KeV Neutron[b]	(d,p) $(2J+1)S$[c]
^{52}Cr	0	2.0	3.7	2.3
	564	.5	.5	.79
	2320	1.4	.1	1.1
	2667	.6	-	.12
Correlation Coefficient[d] (90% confidence level - .73)		.68	.68	
^{58}Ni	0	2.3	1.1	2.75
	471	1.2	.3	1.25
	878	.3	1.4	.32
	1303	.1	.2	.54
	2421	.3	.03	.03
	2900	.3	.1	.02
	3036	-	.4	.05
	3186	.6	1.2	.05
Correlation Coefficient (90% confidence level - .55)		.82	.26	
^{60}Ni	0	1.5	1.8	1.58
	283	1.0	1.1	1.22
	1101	.1	-	.14
	2124	.7	.3	.34
Correlation Coefficient (90% confidence level - .73)		.70	.74	

[a] Intensity formed by taking values in table 3, dividing by E_γ^3 and normalizing to (d,p) strengths.

[b] Intensity formed by taking the sum of s-wave partial widths to the same final state, dividing by E_γ^3 and normalizing to (d,p) strengths.

[c] (ND 68, ND 70)

[d] Correlations of (n,γ) intensities to (d,p) strengths.

and the (n,γ)(d,p) correlations suggest that the $^{52}Cr(n,\gamma)^{53}Cr$ and $^{60}Ni(n,\gamma)^{61}Ni$ reaction in the keV region predominantly act through a direct mechanism while $^{58}Ni(n,\gamma)^{59}Ni$ is predominantly a compound reaction in this region. The anomalous high energy gamma emissions (Gr 58) and the (n,γ)(d,p) correlations (Gr 67) for ^{52}Cr and ^{60}Ni thermal neutron capture have been interpreted as indicating a direct reaction mechanism. Thus, thermal and keV neutron capture results convey a consistent picture. However, thermal neutron capture by ^{58}Ni reveals anomalous high energy gamma spectra (Gr 58) and (n,γ)(d,p) correlation (Gr 67) also indicating a direct mechanism, but in keV neutron capture the results of the $p(\Gamma_\gamma, \Gamma_n^o)$ correlation, the estimate of ν and the (n,γ)(d,p) correlation indicate a compound reaction. A possible explanation for this dichotomy is that thermal neutron capture results are dominated by the resonance at -28.5 keV and the (n,γ)(d,p) correlation obtained from these results is due to this single resonance; whereas, the results of keV neutron capture take into account many resonances and these resonances together show no correlation.

CHAPTER 8

CONCLUSIONS

The results obtained in this work have shown that the dispersive method can be used to obtain measurements of $\Gamma_{\gamma i}$ in the keV resonance region. Total radiation widths can be estimated from the sum of $\Gamma_{\gamma i}$ for a given resonance when there is good sensitivity for measuring a large fraction of the gamma deexcitation intensity. Besides radiation widths the method results in isotopic identification of resonances, measurement of neutron widths when appreciable compared to detector resolution, identification of primary transitions in gamma ray cascades and possible spin identification of both resonant states and excited levels.

The study of resonant capture in silicon has resulted in identification of the spin and parity of the 85 keV resonance to be $J^{\pi} = {}^{3}/_{2}^{-}$. In addition, it has been possible to make isotopic assignment of the 32 keV resonance to ^{28}Si, and the 38 keV resonance to ^{29}Si. The decay properties of the 16 keV resonance in ^{29}Si suggest that it most likely has a spin of 1.

Results of resonant capture in chromium have revealed two new resonances at 65 ± 1 keV and 194 ± 1 keV in ^{52}Cr with the latter being due to s-wave capture and having a width of 15 ± 2.5 keV.

The possibility high multipole radiation after probable s-wave neutron capture has been observed for transitions to levels of high spin, 1539 ($^{7}/_{2}^{-}$) keV in ^{53}Cr and 341 ($^{5}/_{2}^{-}$) keV in ^{59}Ni.

From keV neutron capture results, studies were made of the distribution of radiation widths, and correlations of (n,γ) and (d,p) strengths, as well as, p (Γ_γ, Γ_n^o) for ^{52}Cr, $^{58,60}Ni$ isotopes. These have led to the interpretation that the $^{52}Cr\ (n_{keV},\gamma)^{53}Cr$ and $^{60}Ni\ (n_{keV},\gamma)^{61}Ni$ processes proceed through a direct mechanism and that $^{58}Ni(n_{keV},\gamma)^{59}Ni$ reacts through a compound mechanism.

There are several limitations in the method employed in this work which could be improved. The greatest of these is the resolution of the gamma ray detector. Detectors are available with resolution of ∿ 5 keV @ 8 MeV; this, in lieu of the 12 keV realized in this work, would result in an improvement in sensitivity and resonance identification. The reduction of background in the gamma ray spectra due to boron and carbon would also lead to greater sensitivity. This can be accomplished through an improved geometry, viz.,

no boron or carbon be in the view of the gamma ray detector. Also proper shielding of the sample assembly from thermal neutrons with the use of cadmium would reduce the $^{10}B(n,\alpha)^{7}Li$ reactions so that ambient temperatures at the sample would be lowered. This would allow a wider selection of isotopes to be studied. Implementation of pulse shape discrimination and rejection of events for which bremsstrahlung is detected by the pair spectrometer annulus (Ro 75) would improve signal to noise by a factor of $\sim$ 3 to 10.

The dispersive method has been shown to have greater efficiency in the keV resonance region for examination of resonance structure than conventional time of flight techniques. However, a dispersive system is not suited for detection of resonance structure when resonance spacing is less than detector resolution. While the study of isotopes with high level density is not possible with the dispersive method, sufficient resonances in these isotopes usually occur in the low energy region where a time of flight system has good efficiency. Thus, in this respect the methods are complementary.

REFERENCES

(Aj 60) F. Ajzenburg-Selove, ed. Nuclear Spectroscopy. A. New York (1960).

(Al 68) B. J. Allen, M. J. Kenney, R. J. Sparks. Nucl. Phys. A122, 220 (1968).

(Al 69) B. J. Allen, J. R. Bird, M. J. Kenney. AAEC/E200 (1969).

(Al 73) B. J. Allen, R. L. Macklin. Int'l. Conf. on Photonuclear Reactions and Applic. p. 271, (1973).

(Be 61) I. Berqvist, N. Starfelt. Nucl. Phys. 22, 513 (1961).

(Be 68) M. Beer, M. A. Lone, R. E. Chrien, O. A. Wasson, H. R. Muether. Phys. Rev. Lett. 20. 340 (1968).

(Be 70) G. B. Beard, G. E. Thomas. Nucl. Phys. A157, 520 (1970).

(Be 71) D. Bellman. Atomkernenergie 17, 145 (1971).

(BN 64) BNL-325 Neutron Cross Sections. Brookhaven Nat'l. Lab. Report, U.S. Gov't. Printing Office (1964).

(BN 66) ibid (BN 64) 2nd ed. (1966).

(BN 73) ibid (BN 64) 3rd ed. (1973).

(Bo 36) N. Bohr. Nature, London 137, 344 (1936).

(Bo 60) L. M. Bollinger. Slow Neutron Resonances. ibid (Aj 60) p. 429.

(Bo 67) A. P. Bogdanov, L. N. Bystrov, E. A. Rudak, E. I. Firsov. Sov. J. Nucl. Phys. 13, 129 (1967).

(Bo 70) L. M. Bollinger, G. E. Thomas. Phys. Rev. C2, 1951 (1970).

(Br 64) G. E. Brown. Nucl. Phys. 57, 339 (1964).

(Br 71) D. L. Broder, A. F. Gamalii, B. V. Zemstev, B. N. Nesterov, L. P. Kham'Yanov. Sov. J. Nucl. Phys. 13, 129 (1971).

(Ca 53) K. M. Case, F. de Hoffman, G. Placzek. Intro. to Theory of Neutron Diffusion. Vol. 1, U.S. Gov't. Printing Office (1953).

(Ch 67) R. Chrien, M. Reich. Nucl. Inst. & Meth. 53, 93 (1967).

(Co 72) S. Cochavi, W. R. Kane. Phys. Rev. C6, 1650 (1972).

(Co 74) A. H. Colenbrander, T. J. Kennett. Nucl. Inst. & Meth. 116, 251 (1974).

(Di 70) J. K. Dickens. Phys. Rev. C2, 990 (1970).

(En 66a) H. A. Enge. Intro. to Nuclear Physics. Addison-Wesley, Reading, Mass. p. 421 (1966).

(En 66b) ibid (En 66a) p. 259

(En 73) P. M. Endt, C. Vander Leun. Nucl. Phys. A214, 1 (1973).

(Er 68) P. I. C. Ernst. Master's Thesis, McMaster University (1968).

(Ew 64) G. T. Ewan, A. J. Tavendale. Nucl. Inst. & Meth. 26, 183 (1964).

(Fe 57) C. A. Fenstermacher, R. G. Bennett, A. E. Walters, C. K. Bockleman, H. L. Shultz. Phys. Rev. 107, 1650 (1957).

(Fe 63) H. Feshbach, L. Estrada. Ann. of Phys. 23, 123 (1963).

(Fi 51) R. E. Fields, M. Walt. Phys. Rev. 83, 479 (1951).

(Fi 66) H. J. Fiedler, L. B. Hughes, T. J. Kennett, W. V. Prestwich, B. J. Wall. Nucl. Inst. & Meth. 81, 263 (1970).

(Fo 58) J. D. Fox, R. L. Zimmerman, D. J. Hughes, H. Palevsky, M. K. Brussel, R. E. Chrien. Phys. Rev. 110, 1472 (1958).

(Ga 71) J. B. Garg, J. Rainwater, W. W. Havens, Jr. Phys. Rev. C3, 2447 (1971).

(Go 73) W. M. Good, J. A. Harvey. ORNL - 4844 (1973).

(Gr 56) L. V. Groshev, B. P. Adyasevich, A. M. Demidov. Proc. Int'l. Conf. on Peaceful Uses of Atomic Energy, Geneva, 2, 39 (1956).

(Gr 58) L. V. Groshev, A. M. Demidov, V. N. Lutsenko, V. I. Pelekhov. Sov. J. of At. Erg. 8, 127 (1958).

(Gr 67) L. V. Groshev, A. M. Demidov. J. Nucl. Phys. 4, 558 (1967).

(Ha 55) J. A. Harvey, D. J. Hughes, R. S. Carter, V. E. Pilcher. Phys. Rev. 99, 10 (1955).

(Ha 70a) J. A. Harvey. Expt'l. Neutron Resonance Spectroscopy. Academic Press, New York, p. 136 (1970).

(Ha 70b) ibid (Ha 70a) p.269

(Ho 69) R. W. Hockenbury, Z. M. Bartolome, J. R. Tatarczuk, W. R. Moyer, R. C. Block. Phys. Rev. 178, 1746 (1969).

(Hu 54) D. J. Hughes, J. A. Harvey. Nature 173, 942 (1954).

(IA 69) IAEA, Proc. Int'l. Symp. on Neutron Capture Gamma Ray Spectroscopy. (Studvisk, Aug. 1969), p. 105, STI/PUB/235.

(IA 70a) IAEA, Neutron Fluency Measurements. Tech. Rep. 107, p. 4 (1970).

(IA 70b) ibid (IA 70a) p. 29.

(IA 74) IAEA, 2nd. Int'l. Symp. on Neutron Capture Gamma Ray Spectroscopy. (Petten, June 1974).

(Ka 67) W. R. Kane, M. A. Mariscotti. Nucl. Inst. & Meth. 56, 189 (1967).

(Ke 58) T. J. Kennett, L. M. Bollinger, R. T. Carpenter. Phys. Rev. Lett. 1, 76 (1958).

(Ke 59) T. J. Kennett, L. M. Bollinger. Nucl. Phys. 12, 249 (1959).

(Ke 74) M. J. Kenney, P. W. Martin, L. E. Carlson, J. A. Biggerstaff. Aust. J. Phys. 27, 759 (1974).

(Ki 53) B. B. Kinsey, G. A. Bartholomew. Can. J. Phys. 31, 537 (1953).

(Ko 72) J. Kopecky, K. Abrahams, F. Stecher-Rasmussen. Nucl. Phys. A188, 535 (1972).

(La 55) H. H. Landon. Phys. Rev. 100, 1414 (1955).

(La 57) H. H. Landon, E. R. Rae. Phys. Rev. 107, 1333 (1957).

(La 60) A. M. Lane, J. E. Lynn. Nucl. Phys. 17, 586 (1960).

(La 61) Landolt-Bornstein. Numerical Data and Functional Relationships in Science & Technology. Gr. 1, Vol. 1, Energy Levels of Nuclei A=5-257, Springer-Verlag, Berlin (1961).

(La 62) R. O. Lane, A. J. Elwyn, A. Langsdorf Jr. Phys. Rev. 126, 1105 (1962).

(La 66) J. R. Lamarsh. Intro. to Nuclear Reactor Theory. Addison-Wesley, Don Mills, Ont. p. 172 (1966).

(Le 34) D. E. Lea. Nature 133, 24 (1934).

(Le 56) J. S. Levin, D. J. Hughes. Phys. Rev. 101, 1328 (1956).

(Lo 73) A. M. Lopez. Ph.D. Thesis, McMaster Univ. (1973).

(Lo 74) A. M. Lopez. Private Communication (1974).

(Lu 70) B. Lundberg, I. Bergvist. Physica Scripta 2, 265 (1970).

(Lu 74) M. Lubert, N. C. Francis, R. C. Block. Nucl. Phys. A230, 83 (1974).

(Ly 67) H. Lycklama, L. B. Hughes, T. J. Kennett. Can. J. Phys. 48, 1871 (1967).

(Ly 68) J. E. Lynn. The Theory of Neutron Resonance Reactions, Clarendon Press, Oxford (1968).

(Ly 69) H. Lycklama, T. J. Kennett, L. B. Hughes. Can. J. Phys. 47, 665 (1969).

(Mo 36) P. B. Moon, R. Tillman. Proc. R. Soc. 153, 421 (1936).

(Mu 70) S. F. Mughbaghab, R. E. Chrien, O. A. Wasson. Phys. Rev. Lett. 25, 1670 (1970).

(ND 67) Nuclear Data, A3, (1967).

(ND 68) Nuclear Data, B2, A=59-61, (1968).

(ND 70) Nuclear Data, B3, A=50-54, 58 (1970).

(ND 73) Nuclear Data, A11, (1973).

(Ne 59) H. W. Newson, R. C. Block, P. F. Nichols, A. Taylor, A. K. Furr, E. Merzbacher. Ann. Phys. 8, 211 (1959).

(Ni 70) L. Nichol, A. Lopez, A. Robertson, W. V. Prestwich, T. J. Kennett. Nucl. Inst. & Meth. 81, 263 (1970).

(Ni 71) L. W. Nichol. Ph.D. Thesis, McMaster Univ. (1971).

(Ni 72) L. W. Nichol, T. J. Kennett. Can. J. Phys. 50, 553 (1972).

(Po 56) C. E. Porter, R. G. Thomas. Phys. Rev. 104, 483 (1956).

(Ra 36) F. Rasetti, E. Segre, G. Fink, G. R. Dunning, G. B. Pegram. Phys. Rev. 49, 104 (1936).

(Ra 69) N. C. Rasmussen, Y. Hukai, T. Inouge, V. J. Orphan. MITNE - 85 (1969).

(Re 54) A. L. Recksiedler, B. Hamermesh. Phys. Rev. 96, 109 (1954).

(Ro 72) R. Robertson, T.J. Kennett. Nucl. Inst. & Meth. 98, 599 (1972).

(Ro 75) A. Robertson, G. C. Cormick, T. J. Kennett, W. V. Prestwich. Nucl. Inst. & Meth. (In Press).

(Ru 11) E. Rutherford. Phil. Mag. 21, 669 (1911).

(Se 58) R. E. Segèl. Phys. Rev. 111, 1620 (1958).

(St 68) M. G. Strauss, L. W. Sifter, F. R. Lenkazres, R. Brenner. IEEE Trans. Nucl. Sci. NS-15, 518 (1968).

(St 71) R. G. Steiglitz, R. W. Hockenbury, R. C. Block. Nucl. Phys. A163, 592 (1971).

(Th 67) G. E. Thomas, D. E. Blatchley, L. M. Bollinger. Nucl. Inst. & Meth. 56, 325 (1967)

(Th 75a) V. J. Thomson, A. M. Lopez, W. V. Prestwich, T. J. Kennett. Nucl. Inst. & Meth. 126, 263 (1975).

(Th 75b) V. J. Thomson, W. V. Prestwich, T. J. Kennett. Can. J. Phys. (In Press).

(Wa 52) B. E. Watt. Phys. Rev. 87, 1037 (1952).

(Wh 72) D. H. White, R. E. Howe. Nucl. Phys. A187, 12 (1972).